2019

Characterization of In-Vivo Damage in Implantable Cardiac Devices and the Lead Residual Properties

Anmar Mahdi Salih
Wright State University

CHARACTERIZATION OF IN-VIVO DAMAGE IN IMPLANTABLE CARDIAC DEVICES AND THE LEAD RESIDUAL PROPERTIES

A thesis submitted in partial fulfillment of the
requirements for the degree of
Master of Science in Biomedical Engineering

by

ANMAR MAHDI SALIH

B.S. in Medical Engineering, Al-Nahrain University, 2009

2019

Wright State University

WRIGHT STATE UNIVERSITY

GRADUATE SCHOOL

April 26, 2019

I HEREBY RECOMMEND THAT THE THESIS PREPARED UNDER MY SUPERVISION BY Anmar Mahdi Salih ENTITLED (Characterization of In-Vivo Damage in Implantable Cardiac Devices and the Lead Residual Properties**)** BE ACCEPTED IN PARTIAL FULFILLMENT OF THE REQUIREMENTS FOR THE DEGREE OF Master of Science in Biomedical Engineering.

_____

Tarun Goswami, D.Sc.
Thesis Director

_____

John C. Gallagher, PhD
Interim Chair, Department of
Biomedical, Industrial and
Human Factors Engineering

Committee on Final Examination:

_____

Caroline Cao, Ph.D.

_____

Ulas Sunar, Ph.D.

_____

Abdul Wase, M.D.

_____

Tarun Goswami, D.Sc.

_____

Barry Milligan, Ph.D.
Interim Dean of the Graduate School

ABSTRACT

Salih, Anmar Mahdi M.S.B.M.E. Department of Biomedical, Industrial, and Human Factors Engineering, Wright State University, 2019. Characterization of *In-Vivo* Damage in Implantable Cardiac Devices and the Lead Residual Properties.

Approximately, 92.1 million patients in the US suffer from cardiovascular diseases with an estimated healthcare cost of over $300 billion; out of which at least one million patients have Cardiac Implantable Electronics Devices (CIED). CIED represented by pacemakers, Implantable Cardioversion Defibrillator (ICD), and Cardiac Resynchronization Therapy (CRT) are exposed to in-vivo damage. These damages are complex and composed on multiple levels and present challenges while assessing their combined extent. Since 2004, more than one hundred recalls were reported for cardiac devices. ICD devices had the majority with 40.8% recalls, pacemaker recall percentage was 14.5%, CRT recall percentage was12.7%, leads recalls were 9.7%, and others (stents and LVAD) with 22.3% recalls. The objective of this research is to investigate the damage of the cardiac devices and the changes in the residual properties after *in vivo* implantation, such knowledge will lend insight into the common damage patterns, controlling the probability of failure in the design of future devices, and improve reliability. *In vivo* damage assessment was performed on 65 retrieved cardiac devices and 136 leads from different manufacturers (Medtronic, St. Jude Medical-Abbott and Boston Scientific). The examined damage

features were surface deformation, burnishing, pitting, scratching, discoloration, delamination, insulation defects, coil damage, and abrasion.

The results showed that the main damage mode observed was scratching, and the anterior side of the Pulse Generator (PG) was more exposed to damage than the posterior side. Additionally, the middle part of the lead was more exposed to damage than the proximal part. Tensile test was also performed on new and retrieved Medtronic 5076 CapSureFix Novus MRI SureScan leads. Load to failure showed a significant decrease after 18 months of in-vivo exposure (*P-value =0.0008*). Percentage elongation showed a significant decrease after 94 months of in-vivo exposure (*P-value<0.0001*). Ultimate tensile strength showed significant decrease after 73 months of in-vivo exposure (*P-value=0.0339*) and percentage elongation at 5N force showed significant decrease after 66 months of in-vivo exposure (*P-value =0.0037*). On the other hand, modulus of elasticity has direct proportion with the number of in-vivo months and showed significant increase (*P-value=0.0051*) after 73 months of in-vivo environment.

In conclusion, it can be inferred that the as received pulse generator had mainly scratches that were shallow, narrow and could not have affected the functionality of the devices. The as received leads had visible insulation defects, stretches, and coil damages that could have caused different types of failures and could have affected the functionality of the devices.

TABLE OF CONTENTS

LIST OF FIGURES

LIST OF TABLES

LIST OF ABBREVIATIONS

CIED	Cardiac Implantable Electronic Device
PM	Pacemaker
ICD	Implantable Cardioverter Defibrillator
CRT	Cardiac Resynchronization Therapy
CRT-P	Cardiac Resynchronization Therapy-Pacemaker
CRT-D	Cardiac Resynchronization Therapy- Defibrillator
LVAD	Left Ventricular Assist Device
PG	Pulse Generator
RV	Right Ventricle
RA	Right Atrium
LV	Left Ventricle
CS	Coronary Sinus
SEM	Scanning Electron Microscope
FTIR	Fourier-Transform Infrared Spectroscopy
SA Node	Sinoatrial Node
AV Node	Atrio-Ventricular Node
AF	Atrial Fibrillation
SSS	Sick Sinus Syndrome

HF	Heart Failure
EF	Ejection Fraction
SVC	Superior Vena Cava
ERI	Elective Replacement Interval
CPU	Central Processing Unit
RAM	Random Access Memory
ROM	Read Only Memory
ETFE	Ethylene Tetrafluoroethylene
PF	Passive Fixation
NASPE	North American Society of Pacing and Electrophysiology
BPEG	British Pacing and Electrophysiology Group
CVD	Cardiovascular Disease
MDT	Medtronic
SJM	St. Jude Medical
BSC	Boston Scientific
OTW	Over the Wire
HP	High Performance
ETR	Extra Tear Resistant
ASTM	American Society for Testing and Materials
UTS	Ultimate Tensile Strength

ACKNOWLEDGEMENTS

I would like to express my deepest appreciation to my thesis advisor professor Tarun Goswami for his continuous guidance and support. He continually and convincingly conveyed a spirit of adventure in regard to research, and an excitement in regard to teaching. Without his guidance and persistent help, this thesis would not have been possible.

I would like to thank my committee members Professor Caroline Cao for sharing her expertise regarding human factors and FDA; Professor Ulas Sunar for sharing his knowledge and expertise. And my sincere appreciation to Dr. Abdul Wase for providing us with the devices and allowing us to interrogate the cardiac devices in his clinic. And I would like to thank Wright State Anatomical Gift Program for providing us with the majority of the devices.

Finally, I would like to thank my family, especially my wife Farah and my mother Faeqah for their love and affection. I could not have done it without their support. And a special thanks to who I wish he can see me at this moment, my beloved father (may his soul rest in peace). I want to thank my two sisters and my brother for believing in me. I would like to thank all my friends who supported me and believed in me to pursue my dream and achieve a master's degree.

This thesis is dedicated to my beloved father, *Mahdi Salih (RIP)*

CHAPTER 1: INTRODUCTION

1.1 INTRODUCTION

A cardiac device is a medical electronic equipment located under the skin at the area of the chest or the abdomen to treat the abnormality in heart rhythm. It delivers electrical impulses to the heart via the lead [1]. There are several types of biomedical devices that can be used as a therapy to tachyarrhythmia and bradyarrhythmia like Implantable Cardioverter Defibrillator (ICD) and Pacemaker. These two devices have leads that are implanted either in the Right Ventricle (RV) or Right Atrium (RA) depending on patient's case. A single chamber pacemaker or ICD has one lead that passes through subclavian vein to the RA or RV, while the dual chamber PM or ICD has two leads, one implanted into the right ventricle and the other implanted into the right atrium. Another procedure requires a third lead implanted into the Coronary Sinus (CS) to provide Cardiac Resynchronization Therapy (CRT).

The market size of the cardiovascular devices is voluminous, and the number of implanted devices is increasing with time. According to Journal of the American College of Cardiology, the number of the dual chamber devices were around 520,000 in 2009 (pacemakers and ICDs) [3], and this number has increased to 1.14 million in 2016, and by 2023 it is projected to be 1.43 million [4]. The single chamber atrial implantation is declining, however; in the USA, physicians prefer to implant dual chamber pacemakers [5]. Age of the patients who receive PMs, ICDs, and CRTs devices range 65 ± 14 years

[3], although children also are candidates for such procedure. The hospital charges for cardiac devices implantation of CRT is around $110,000 [84].

1.2 MOTIVATION

Since 2004, more than one hundred recalls were reported for cardiac devices. ICD devices had the majority with 40.8%, pacemaker 14.5%, CRT 12.7%, leads 9.7%, and others (stents and LVAD) with 22.3% recalls [6]. Minimizing the risks of failure and reducing emergency visits are crucial. Therefore, there is a need to investigate retrieved cardiac devices to fully understand damage development and residual properties due to in-vivo exposure. Several studies [7, 8, 9, 10] were reported in this area; however, each with limitations. For instance, Jacobs et al. [7] performed electrical tests, optical microscopy and Scanning Electron Microscope (SEM) on the lead. This study [7] focused only on one manufacturer in their experiment. Wiggins et al. [8] used optical microscopy, SEM and Fourier-Transform Infrared Spectroscopy (FTIR) to determine the chemical degradation on the inner and outer insulation. However, their experiment included only 7 leads. In order to provide significant representation for damage development of the cardiac devices through in-vivo implantation, a comparison between multiple manufacturers, different damage features, and residual properties are needed. To the best of our knowledge, this is the original effort in which damage assessments of more than one hundred leads exposed to in-vivo environment for up to 16 years from multiple manufacturers was undertaken. In general,

this study involved thorough visual inspection, different types of damage, several types of lead failure, optical microscope inspection, mechanical testing and electrical tests.

In addition to investigating the damage assessments of cardiac devices, there is a need to investigate the residual properties of leads after being exposed to in-vivo environment. Long-term exposure may lead to catastrophic results depending upon the integrity of insulation. Several studies were conducted to evaluate the residual properties of the leads to estimate how their insulation degraded and predict the degradation process. For instance, Chan et al. [10], investigated three major cardiac device leads by immersing these leads in 0.9% normal saline solution for 10 days at room temperature, and performed tensile test to obtain their residual properties. Starck et al. [11] used 13 pacemaker leads from one manufacturer and categorized these leads into three groups depending on locking stylet-used to support the lead and inserted through the coil. All the above mentioned studies performed in-vitro experiments. In order to provide a realistic representation of the changes in residual properties of lead insulator inside the human body, there was a need to investigate retrieved cardiac devices that have been exposed to in-vivo environment for at least ten years. Tensile test, visual inspection (after and before the test), and optical microscope inspection (after and before the test) were performed to evaluate the degradation of the silicone insulation of Medtronic 5076 CapSureFix Novus MRI SureScan leads of different in-vivo implantation durations.

1.3 THESIS OUTLINES

This thesis is divided into five chapters. The second chapter provides a comprehensive review of cardiac devices. This chapter includes basic background information on cardiac devices, components, several lead design aspects, and types of battery materials. In addition, several case studies in cardiac device failure were discussed.

Chapter three presents investigation of retrieved cardiac devices. A thorough *in vivo* damage assessment investigation of retrieved devices was performed.

Chapter four focuses on the characterization of the residual properties of Medtronic 5076 CapSureFix Novus MRI SureScan lead with in vivo implantation devices.

Chapter five summarizes the finding of the thesis. In this chapter, the recommendation for future works was discussed. This thesis presents data that will be valuable to design of novel cardiac devices, materials, and at the same time improve longevity of in-vivo application.

CHAPTER 2: BACKGROUND

2.1 PACEMAKER

Pacemaker is a type of CIED that is located under the skin in the upper chest with lead implanted via the vein into the heart. More recently, leadless pacemakers are available (Micra-Medtronic) that are implanted directly into the RV via the Femoral veins. It delivers electrical impulses to the chambers of the heart via the leads [78]. Pacemakers are used to assist patients with sinus node dysfunction, first-, second-, third-AV block, syncope, and other diseases [15]. Three types of pacemaker are in use, single chamber, dual chamber, and triple chamber pacemaker.

2.1.1. Single Chamber Pacemaker

This type of pacemaker has only one lead which is implanted either in the right ventricle or the right atrium [16]. This type is used when there is dysfunction of Sino-Atrial (SA) node commonly referred to as sick sinus syndrome, Atrio-Ventricular (AV) node, and bundle of His (part of the conductive system of the heart which delivers impulses from atrioventricular node to the apex of the heart) [2], or Purkinje fibers. The atrial type of pacemakers are used to sense the activity in the atrium and pace when needed [79]. Another kind of single chamber pacemaker uses the lead, which is implanted in the RV, and treats issues with the AV node, bundle of His, or Purkinje fibers [17]. In the case of atrial fibrillation (AF), the PM paces the ventricle to keep it as normal pacing as possible without tracking the atrium during rapid heart rate [18]. This kind of single chamber pacemaker is

used to sense the activity in the RV and to pace the RV when needed [16]. The most common modes used in single chamber pacemaker are VVI, VVT, and AAI [5].

2.1.2 Dual Chamber Pacemaker

This type of pacemaker has two leads, one is implanted in the RV and the other is implanted in the RA, this type is used for patients with SSS and AV block. It monitors the activity in both RA and RV and pace when necessary, either in both chambers or one of them [80].

2.1.3 Triple chamber (Biventricular) pacemakers

This type of pacemaker has an additional third lead that is implanted in the coronary sinus to pace the left ventricle (LV) and is used for patients with heart failure (HF) with ejection fraction (EF) less than 35% who have Left Bundle Branch Block (LBBB) to provide cardiac resynchronization. It also is known as CRT-P [20].

Figure 1 A) Sigle chamber pacemaker, B) Dual chamber pacemaker, C) Triple chamber pacemaker (CRT-P)

2.2 IMPLANTABLE CARDIOVERTER-DEFIBRILLATOR (ICD)

Implantable defibrillators represent the most significant advance in our ability to prevent sudden cardiac death due to ventricular arrhythmias [21]. ICD is a CIED that has the same

function as that of a pacemaker; in addition, it is capable of aborting Ventricular Tachycardia (VT) or Ventricular Fibrillation (VF) in high-risk patients by delivering shocks or Anti-Tachycardia Pacing (ATP) [1]. Three types of ICDs are in use single chamber, dual chamber, and triple chamber.

2.2.1 Single chamber ICD

This type of ICD has one lead which is implanted in the RV. This lead is different from pacemakers' lead, as it has proximal and coils in addition to provide sensing and pacing function. It can provide ATP or deliver high-voltage therapy (shock delivery-up to 41 joules) to abort VT or VF [22, 80]. The lead has two coils, these coils are used to deliver shocks in case the patient needs it. One coil is present in the right ventricle called RV distal coil, and the other coil is located in the area of the superior vena cava or SVC coil [22, 80]. A totally new concept of ICD was represented by Boston Scientific, Subcutaneous ICD (S-ICD). S-ICD is now available, where the defibrillator lead is tunneled underneath the skin completely avoiding venous access or direct contact with the heart [85].

2.2.2 Dual chamber ICD

This type of ICD has two leads implanted. One in RA for pacing and sensing, and another in RV which is capable of delivering of defibrillation and ATP [22].

2.2.3 Triple chamber ICD

In addition to the leads discussed in section 2.2.3. This triple chamber ICD has a defibrillation lead in RV instead of pace/sense lead. Indications for implantation are similar to those for section 2.1.3. [23].

Figure 2 A) Single chamber ICD B) Dual chamber ICD C) Triple chamber ICD (CRT-D)

2.3 CARDIAC DEVICE COMPONENTS

2.3.1 Battery

Battery system is one of the most important components of CIED and has been under development to increase device longevity and decrease PG size. The early battery used Li as an anode with I, MnO_2, CFx, $Ag_2O_4V_{11}$, and hybrid as the cathode. The batteries are either single use like in the pacemaker or multiple uses like in rechargeable batteries. Some devices need a special battery in order to provide a better service. Some precautions should be taken into consideration for special types of battery applications like power density, longevity, and how the battery depletes. Proper chemistry and how to apply these batteries were very helpful in the biomedical applications and in treatment [24].

The primary power source for permanent pacemakers was Mercury zinc [25]. These types of batteries were used in early pacemakers. The pacemakers could not be hermetically sealed as these batteries produced gasses over time that required venting. This could lead to fluid accumulation inside the PM and could cause damage to the circuit and the PM would not deliver therapy appropriately. Mercury zinc batteries have a short use of life and have sharp voltage drop. This makes predicting failure of these batteries difficult. No devices of this type are currently in use [21].

A. Lithium/iodine batteries

Cardiac devices need a power source to deliver therapy with small values of current (mAh). Li/I2–PVP system was the first battery composition that was patented and used in 1972 and some devices are still run on this system. Li/I2–PVP cells were the first choice for the biomedical application due to their high energy density in a small volume, safety, and accuracy. The reaction can be summarized in [26]

$$Anode: 2Li^{-} \xrightarrow{yields} 2Li^{+} + 2e^{-}$$

$$Cathode: MI_2 + 2e^{-} \xrightarrow{yields} M + 2I^{-}$$

$$Total\ reaction: 2Li + MI_2^{-} \xrightarrow{yields} M + 2LiI$$

M represents poly-2-vinyl pyridine.

B. Lithium/manganese dioxide batteries

Many medical devices- due to their high performance- require batteries that can deliver therapy to patients with a minimum consumption of power. Ikeda promoted the lithium/manganese dioxide early type in the 1970s and it is a good fit for these medium rate applications [27,28]. Manganese dioxide is also used in zinc carbon cells, but this material showed a significant heat treatment which made them a good composition for the lithium battery [27][28][29]. The lithium/Manganese dioxide system is used in a high number of medical devices due to its high potential, high energy density, and high capacity [29].

$$Anode: Li^{-} \xrightarrow{yields} Li^{+} + e^{-}$$

$$Cathode: Mn^{IV}O_2 + Li^{+} + e^{-} \xrightarrow{yields} LixMn^{III}O_2$$

$$Total\ reaction: Mn^{IV}O_2 + Li \xrightarrow{yields} LixMn^{III}O_2$$

C. Lithium/carbon monofluoride batteries

Another choice for implantable medical devices that need a small output power (0.5V to 8 V). This choice is the (Li/CFx) system. Carbon monofluoride was early promoted as a cathode material in batteries in the 1970s [30][31]. The low discharge values, high potential and high density of the LiCFx system have made it helpful for devices that need higher

values than expected [32]. Due to its insulation property, CFx is mixed during preparation to make the cathode with more storage capacity [33]. During the construction process of the cathode and lithium anode, they use an insulator between them. The insulator is lithium tetrafluoroborate ($LiBF_4$) that can be dissolved in butyrolactone [32] The reaction is [25]:

$$Anode: xLi^{-} \xrightarrow{yields} xLi^{+} + xe^{-}$$

$$Cathode: CF_x + xe^{-} \xrightarrow{yields} xLiF^{-} + xC$$

$$Total\ reaction: CF_x + xLi^{-} \xrightarrow{yields} C + xLiF$$

Where *C* represents carbon and *x* represents variable depending on how fluorine react with lithium [25].

D. Li/CFx–SVO hybrid batteries

Due to its high energy density which gives them a longer life than expected, these types of batteries are used in a wide range of various types of biomedical devices. In order to provide a high power, these batteries combine CFx with $Ag_2V_4O_{11}$. [34][35]. This type is mainly used with ICD and CRT-D (high voltage devices). In addition to all the benefit of the hybrid battery, they offer an enhanced end of life detection and alert the patient once it reaches the Elective Replacement Interval (ERI). A comparison between CFx and silver vanadium oxide is shown in Fig. 3d [35]. Fig.3 below shows different chemical

compositions of batteries, and how these compositions deliver energy to different biomedical implantable devices. Fig.3a shows how lithium iodine battery depletes under several loads. The loads applied from 4kΩ to 100kΩ [36]. Fig.3b shows Lithium/manganese dioxide battery discharge curve [37]. Fig.3c shows the depth of discharge of Lithium/carbon monofluoride batteries under several loads [38]. Fig.3d shows a comparison between carbon monofluoride and silver vanadium oxide, in addition to how these batteries are depleted under same workload [39]. It can be seen that carbon monofluoride has a parabolic curve then depleted sharply till the end of service. On the other hand, silver vanadium oxide has a sharp decline at the beginning of its service. And after 45% of cathode utilization, it starts to be consistent till the end of service.

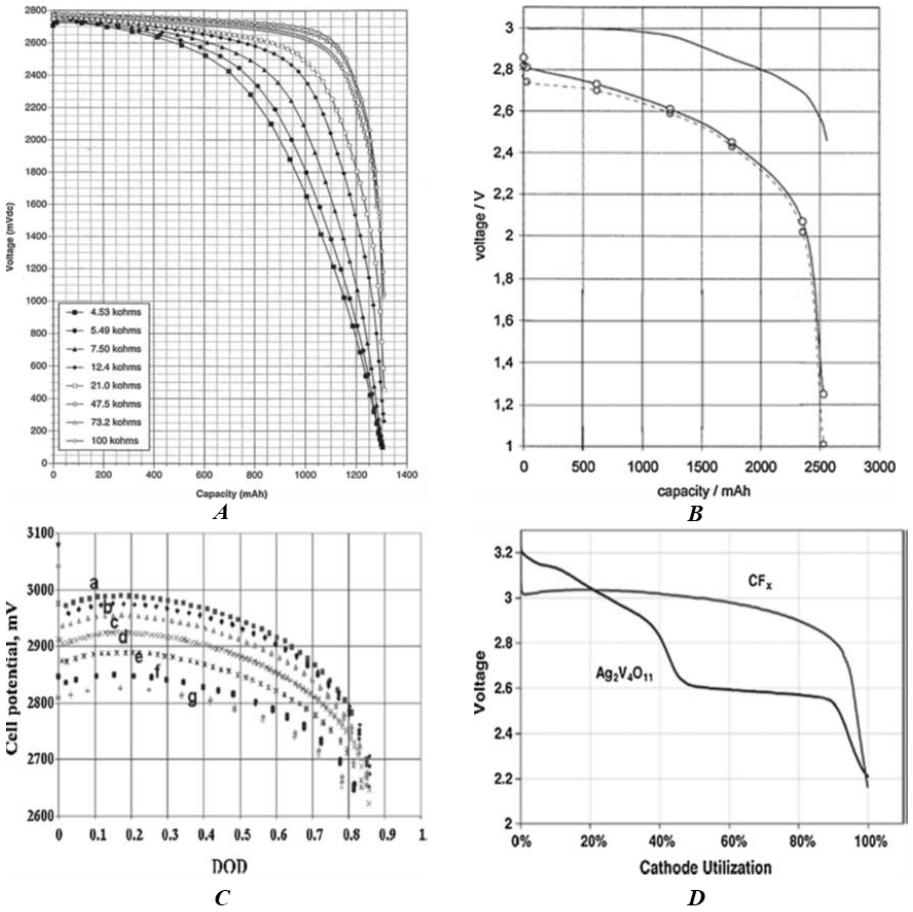

Figure 3 A) Li/I2–PVP discharge under several loads [36] B) $LiMnO_2$ discharge curve [37] C) Discharge LiCFx under several loads [38] DOD = depth of discharge D) Comparison between CFx and silver vanadium oxide [39].

2.3.2 Circuitry

The first invented medical devices were containing small resistance, transistor, and capacitors built together or placed on circuit board as shown in Fig.4 [2]. New devices are now more complex and more integrated CPU systems. They contain RAM and ROM. This led in a decrease in size, weight, and power consumption. There has also been a tremendous increase in features, reliability, flexibility, and longevity. The newer devices have large

data storage capabilities to track the function of the device as well as many different patient parameters. The latter includes a total number of cardiac events, the rate of these events, whether these were paced or intrinsic, and high rate episodes. The newest devices have the ability to store intracardiac electrograms and function as event monitors with the ability to playback the paced or sensed events. Fig.5 illustrates the block diagram of modern cardiac device circuit [2]. It shows how the device sense/pace the heart through electrodes embedded on leads that can filter the obtained waveforms from the heart. These waveforms transferred to a programmable logic to analyze it and decide what therapy should be delivered via therapy algorithm. Afterwards, these events stored in a memory which then can be reviewed by physician. Current generation implantable defibrillators as well as "high end" pacemakers are capable of recording actual cardiogram strips during a symptomatic episode. These recordings are extremely valuable in diagnosing the cause of patient symptoms as related to heart rhythms [21].

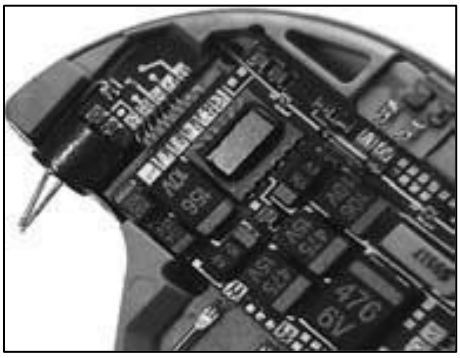

Figure 4 Modern Cardiac Device circuitry [2]

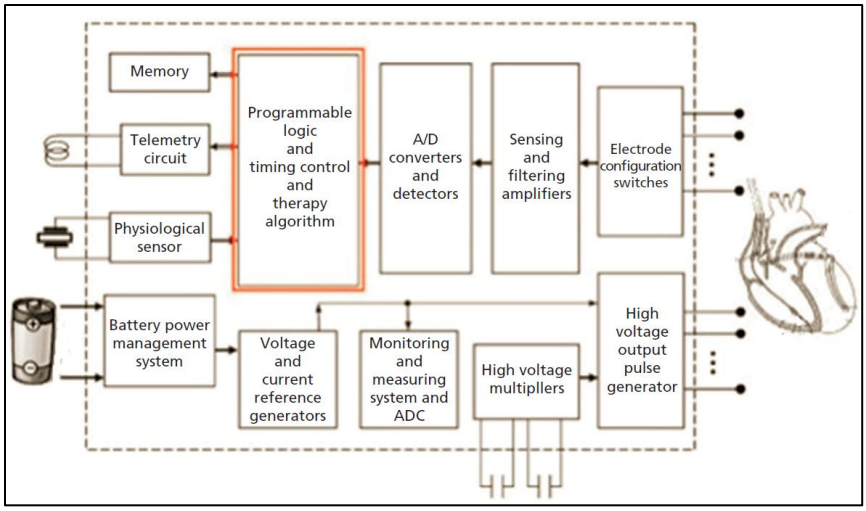

Figure 5 Block diagram of modern Cardiac device's circuit [2]

2.3.3 Connector Block

The connector block (also referred to as the "header") is the means by which the pacemaker/ICD wire is connected to the device circuitry. As shown in Fig. 6, there are many different sizes and styles of connector blocks. All have in common a method for securing the wire to the pacemaker and a method for making a secure electrical connection. If the wrong type of connector block is used the wire may not fit into it properly, the wire may be loose, and the electrical connection may be intermittent or lost. Any of these can result in malfunctioning/nonfunctioning pacing system. Most pacemakers use setscrews to both attach the lead to the pacemaker and make the electrical connection at the same time. If a bipolar connection (negative and positive on the same lead) is to be made there may be one set screw for the anode and another for the cathode (Fig. 6a). As many as eight setscrews may be present in a dual chamber biventricular ICD system. Another type of

connector uses a setscrew for the distal pin and a spring connector for the ring on the lead (Fig. 6b). Finally, some connectors do not use any setscrews (Fig. 6c). These have spring connectors for all of the electrical connections and a mechanism for gripping the lead body to hold it in place. The advantage of this last system is that it makes the electrical connection "automatic" and does not rely on the physician to make a secure connection with a screw [21].

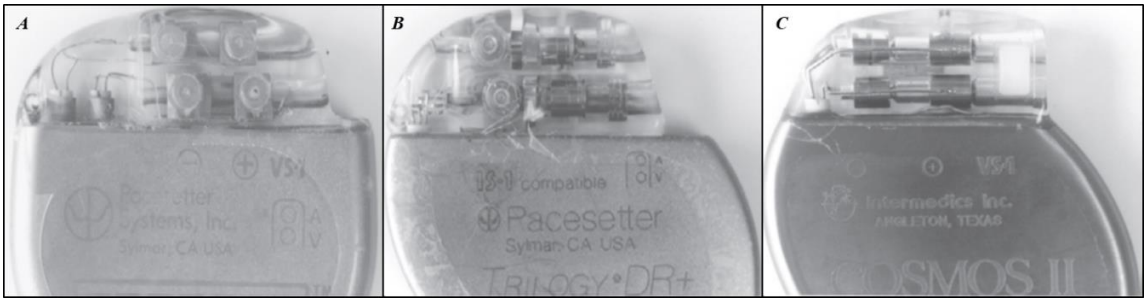

Figure 6 A) Connector block types. Two set screws for each lead (total of 4 in this bipolar dual chamber device), one for the anode and cathode. Each screw must be tightened to hold the lead and provide a secure electrical connection. B) One set screw for each lead to hold the distal pin (cathode). The anode is connected electrically by a spring-loaded band. A unipolar pacemaker would have only a single screw for each lead without the need for an anodal screw or spring anode connection. C) Non- screw design uses spring loaded bands to contact both the cathode and the anode. A plastic component is pressed in by hand that then grips the lead connector to prevent it from coming out of the connector block [21]

2.3.4 Lead

Leads are wires that connect the cardiac device to patient's heart. Leads are responsible for delivering therapy (low or high voltage therapy) to patient [2]. Several designs of leads are available in the market. Lead design can be classified as unipolar, bipolar, and multipolar. Unipolar is the earliest lead design and has simple design. It was the only option available at that time. It was then replaced by bipolar lead. It has only one coil that connects the pulse

generator (PG) to the cardiac muscle and covered by an insulator. The tip of the electrode represents the cathode while the PG is the anode. Cathode and anode represent pacing and sensing circuit, and it is called unipolar because only one electrode is in touch with the cardiac muscle. Because of their design, they show a significant resistance and they last longer than expected, some of them still active and some physicians prefer it due to its simple design [40]. Unipolar mode is inherently subject to electromagnetic interference leading to device malfunction [40].

While bipolar leads exclude the pacemaker from the circuit, the circuit contains the tip (cathode) and the ring (anode), both are in touch with the cardiac muscle. Bipolar leads have many advantages. There are two designs, the co-axial and co-radial. The co-axial, the inner conductor has a coil that runs to the cathode and is hollow from the inside to allow the guide wire or stylet to pass through it. While the outer conductor runs to the anode (ring) directly and both coils are separated by insulation (ETFE), as shown in Fig. 7. The lead is in touch with the cardiac muscle by one of the two fixation methods. The active fixation uses a kind of helix to attach for the cardiac muscle that can explanted easily compared to the passive fixation. The industry uses a four-layer coaxial design of different diameters and designs [40].

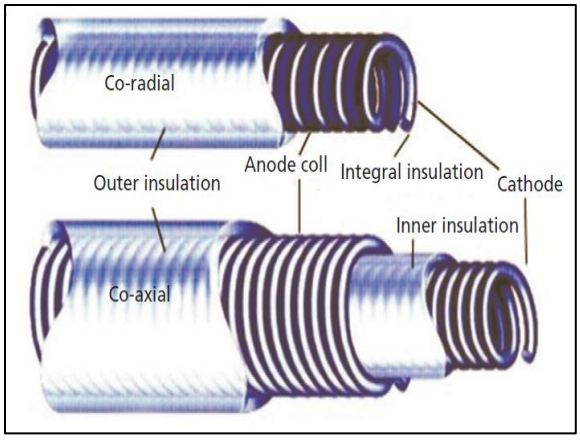

Figure 7 Pacemaker Lead Design [40]

ICD leads use a different type of configuration with multiple lumens to cover the sensing and defibrillation coils, but it has a larger diameter compared to pacemaker leads, as shown in Fig. 8.

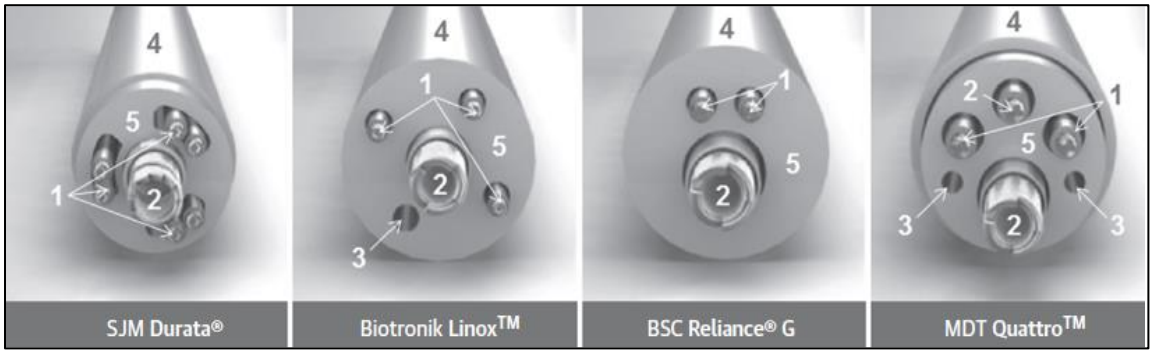

Figure 8 ICD Lead Design [42]

CRT leads are designed to pace LV from coronary sinus to provide mechanical synchrony. Early in its development, unipolar leads were designed to pace between lead tip to PG. Due to inherent problems with Electromagnetic Interference (EMI) these leads

were replaced by bipolar and quadripolar leads [40] as shown in Fig.9. Factors limiting successful pacing are higher pacing threshold, stimulating of phrenic nerve usually in diaphragmatic pacing, and pacing at an undesirable sites. These were mitigated by quadripolar leads which provide as many as twenty alternate vectors [40].

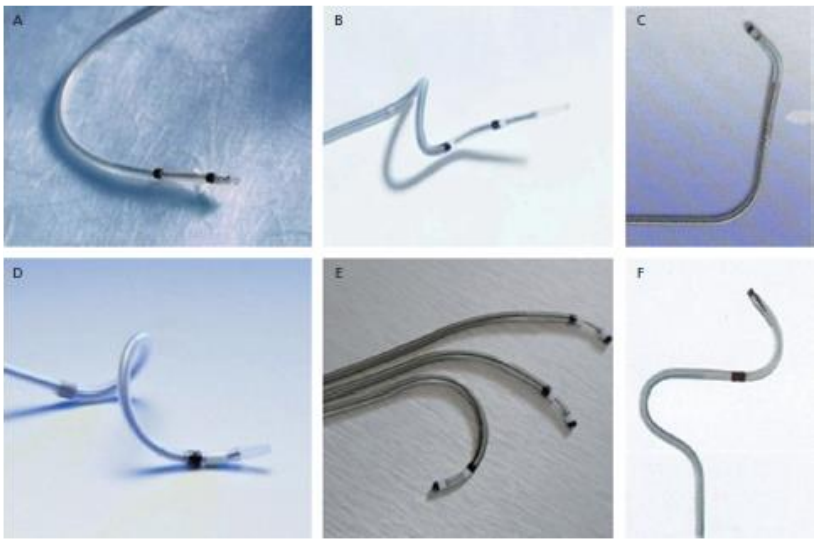

Figure 9 Examples of LV leads. (A) Bipolar (Boston Scientific); (B) helical bipolar (Boston Scientific); (C) bipolar (Medtronic); (D) helical unipolar (Boston Scientific); (E) bipolar (Boston Scientific); (F) S-biased bipolar pacing lead (Abbott-St. Jude Medical) [40]

2.3.5 Fixation mechanisms

Fixation is very important due to the therapy delivery depend on it and the lead should be fixed firm with the cardiac tissue. There are two types of fixation, different in the shape and mechanism of fixation. Passive Fixation (PF) and Active Fixation (AF) as shown in Fig.10. The early fixation method was the passive fixation in which electrodes inserted on endocardial surface [42]. Passive fixation is not widely used especially in the right

ventricle; however, the passive fixation can be held tightly because of the fibrous tissue that makes it hard to removing the lead especially after more than a year of implantation [42]. The PF tines make the outer diameter of the lead body larger. The pores in the PF tines are bigger than the active fixation helix and used for sensing and pacing (cathode). The active fixation is different from the PF, it uses helix that embedded into the right ventricle and the right atrium as shown in Fig.10 [42]. CS leads in CRT-D are exclusively passive as it is in CS lumen and cannot use active fixation at its distal end due to risks of perforation.

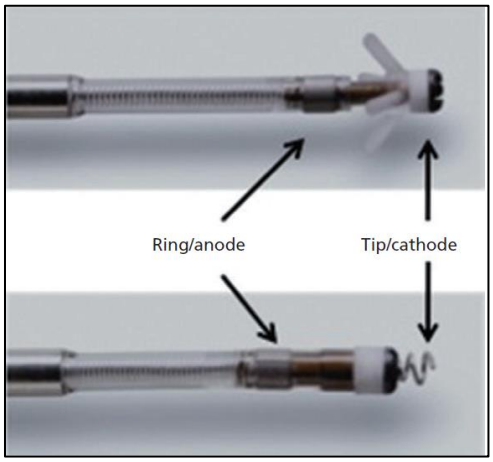

Figure 10 passive fixation (top) and active fixation (bottom) [42]

There are markers that can be found at the distal end of the lead. The use of these markers as an indicator for lead positioning are made under fluoroscope, and also can be used as an indicator for the helix which refers that it is completely inside the cardiac muscle. The LV lead fixation is different from the fixation in the RV and the RA. This lead

is used to pace the LV for the HF patients. They use different shapes for fixation like spiral curves, (J shape) and other curves in order to anchor into the coronary vein and prevent the movement of the lead in future for better performance, as shown in Fig.9. During the procedure of implantation of the LV lead, the lead is straight but once it is implanted in the proper position that provides the best threshold and impedance, the physician will pull the stylet or the guide wire to let the lead takes its position [42].

2.4 CARDIAC DEVICE MODES

Pacemaker modes are classified according to the North American Society of Pacing and Electrophysiology (NASPE) and British Pacing and Electrophysiology Group (BPEG) The PM has some abbreviation of three to five letters. Each letter represents specific chamber and specific function [5]. First letter represents which chamber the PM will pace, second letter represents which chamber the PM will sense, third one represents the reaction of the PM to the sensed episode, fourth and fifth letters represent some features for pacing (rate response) and defibrillation (Anti-Tachycardia Pacing). The below table summarizes each letter and the use of it [5].

Table 1 Pacemaker Modes [5]

Letter I	Letter II	Letter III	Letter IV	Letter V
Paced chamber(s)	Sensed chamber(s)	Response to sensing	PM feature	ICD feature
O=none	O=none	O=none	O=none	O=none
A=atrium	A=atrium	I=inhibited	R=rate modulation	P=pace
V=ventricle	V=ventricle		T=triggered	S=shock
D=dual	D=dual		D=dual (inhibited and triggered)	D=dual (pace and shock)

In some cases, special modes are used to maximize the benefit of the device. For instance, in Atrial Fibrillation (AF) DDI mode is used to prevent unnecessary RV pacing. In this mode PM automatically shuts off sensing in the RV when it detects Atrial Fibrillation avoiding unnecessary fast ventricular rates, but continues to provide backup pacing in RV. When sinus rhythm resumes, the PM switches back to normal functioning providing AV sequential pacing giving the maximum length of AV synchrony [43]. Table 2 below shows PM modes and what condition these modes are used for.

Table 2 Practical Pacemaker Codes [5]

Code	What does it mean	Which disease
AOO	Only pacing the atrium	SSS with no need to sense in the atrium
AAI	Atrial pace, atrial sense, inhibited by atrial signals	SSS
VOO	Ventricular pace, no sense, no inhibit	3rd degree AV block with AF or temporarily during MRI/cautery usage
VVI	Ventricular pace, ventricular sense, ventricular inhibit	3rd degree heart block with atrial fibrillation.
DOO	Dual pace, no sense, no inhibitions	3rd degree AV block or temporarily during MRI/cautery usage
DVI	Dual pace, ventricular sense, ventricular inhibit	3rd degree heart block with supraventricular tachycardias
DDD	Dual pace, dual sense, dual inhibit	3rd degree heart block.

2.5 LITERATURE REVIEW

Pulse generators and leads are vulnerable to failure. This failure can be either mechanical or clinical. Clinical failure related to lead insertion approach taken by physician to implant the lead. Mechanical failure related to lead insulation, in-vivo environment, and how often the device operates. In this section, a summary of previous researches will be introduced.

Mechanical failure of leads due to abrasion are the most common problem affecting ICD leads [44]. Abrasion arises when the lead comes in contact with the pulse generator at the area of the pocket, this type called can abrasion [45]. Furthermore, abrasion happens when the lead gets in contact with other lead, called lead-to-lead abrasion [45]. Since abrasion could lead to lead failure techniques to prevent such failures are coating the lead insulation [44]. One material is silicone-polyurethane copolymer, which is also known as Optim (trademark of Abbott). Optim has shown more abrasion resistance than silicone in more than 278,000 implanted lead with 99.9% survival after 5 years [46]. Hauser et al [44], have studied 15 Riata ST Optim (trademark of Abbott) and 37 Durata leads (trademark of Abbott). These 15 leads were exposed to in-vivo environment for 29.1±11.7 months. Eight of the 15 leads had can abrasion, and three had lead-to-lead abrasion. One death was reported due to this issue [44]. On the other hand, Durata leads were exposed to in-vivo environment for 22.2±10.6 months. Twelve out of 37 leads had shown can abrasion, and only six had shown lead-to-lead abrasion. No death was reported on this lead.

Another study was conducted to overcome the lead insulation failure. Ellenbogen et al [47] investigated the incidence of failure and the survival probability of Medtronic 6936 Sprint Fidelis ICD lead. This lead characterized as coaxial with bipolar active fixation. Medtronic 6936 ICD lead use two insulations, polyurethane 55D covers the inner coil, polyurethane 80A covers the middle coil and as outer insulation [48]. This study was performed on 76 ICD leads for more than two and half years of clinical follow up. It showed 37% survival probability at 68.6 months due to noise after shock delivery. This noise was caused by the polyurethane insulation after the device delivered a shock to the patient. The main reason for this issue is the metal ion oxidation that could cause polyurethane breakdown [49][50].

Estimation of Riata lead failure due to insulation breakdown was performed by Parvathaneni et al [51]. This study was performed at Vanderbilt University Medical Center, Nashville, TN, and the Tennessee Valley Health Systems/VA-Nashville. This study included 87 leads, which went under fluoroscopy and checked for any results of abnormality after extraction. Results showed that lead failure due to coil damage was seen in 29 out of 87 leads, and electrical failure was seen in 19 out of 64 leads. The reason for these issues was the insulation, as it can be seen in Fig. 11. Insulation breakdown of Riata leads was the main issue.

Figure 11 Showing insulation break due to fluoroscopy, and how the coil is damaged [51]

Lead failure can be a crucial issue when it comes in contact with other living tissues inside the human body. A study had been conducted to overcome the failure and complications of the lead at the level of the tricuspid valve. Erkapic et al [52], studied the risk of lead failure at this level. The study was performed on 357 patients who received a Riata family ICD leads. 6 leads out of 357 had insulation defect at the level of the tricuspid valve and only one lead had insulation defect at the level of SVC, as shown in Fig. 12. Device interrogation cannot detect insulation defect due to normal impedance found during the follow up. Therefore, physicians must perform routine fluoroscopic evaluation to avoid this issue.

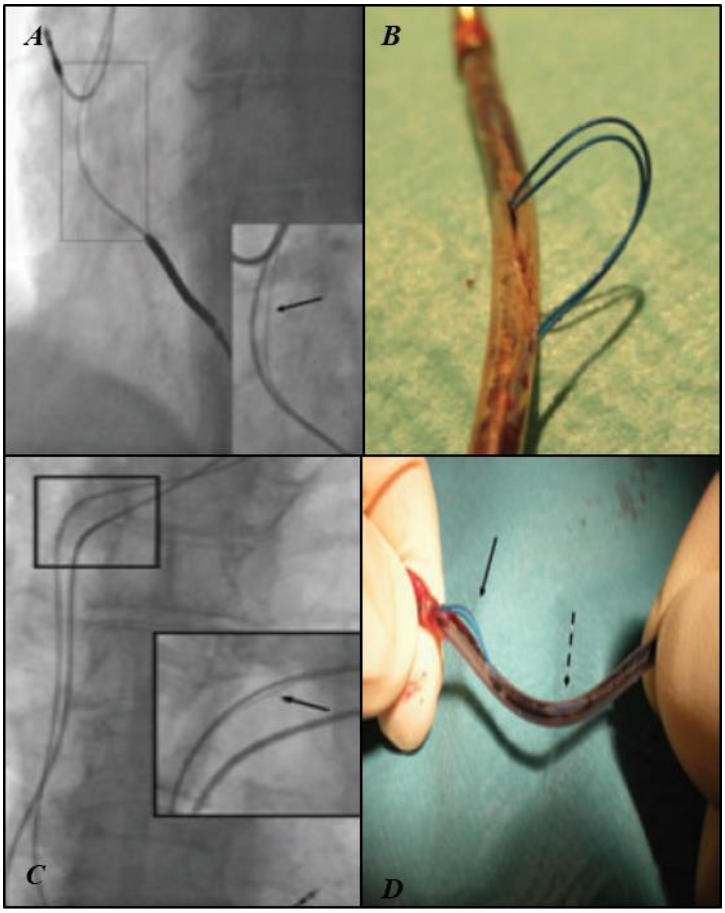

Figure 12 A) fluoroscopic image shows insulation defect at the tricuspid valve B) the same lead after extraction C) fluoroscopic image shows insulation defect at the superior vena cava D) the same lead after extraction [52]

A case study in which a 32 year old male found unconscious in a train [52] had Abbott Durata ICD lead. When he proceeded to ER, a discoloration was noted on the pulse generator (Fig. 13). Discoloration was caused by inappropriate shock delivered to the patient due to can abrasion. Despite the availability of the Optim coating on Durata lead, the lead failed due to abrasion at 11 cm away from the pulse generator.

Figure 13 A) Pulse generator discoloration B) ETFE abrasion C) External abrasion [52]

Antonelli et al. [53], discussed a new approach of lead failure. They compared lead insulation failure depending on the way the lead was inserted and insulation type. Two hundred ninety leads were followed for 57±30 months. 116 out of 290 used silicone as an insulator, and 174 out of 290 used polyurethane (151 80A and 23 55D). 170 out of 290 performed by subclavian approach, and 120 performed by cephalic approach. The results showed lead insulation failure were found in 13 leads using polyurethane insulation (twelve 80A and one 55D). 10% with subclavian approach, and 3% when cephalic approach was used. The results also showed significant difference in survival (*P-value =0.02*) between polyurethane and silicone. Polyurethane was exposed to more failure than silicone. Furthermore, subclavian approach showed 83.2% cumulative survival, and 95.1% survival with cephalic approach (*P-value =0.03*). They concluded [53] silicone leads did not experience insulation failure. On the other hand, polyurethane showed insulation failure due to abrasion and oxidation degradation.

The effects of electrocautery devices on lead insulation examined by Lim et al. [55]. Radiofrequency energy was delivered on different levels 10, 20, and 30 watts for 3 and 6 seconds. Silicone, polyurethane, and silicone-polyurethane copolymer were used in this study. Eleven leads and three manufacturers were investigated in this study. New method of determining level of insulation damage was presented. They used 0-3 scale (0= no damage, 1= slight damage, 2= significant damage, and 3= full insulation damage). Visual and microscopic inspection were performed. Significant insulation damage was seen on all the leads. Full insulation damage was accompanied with energy of 30 watts. Polyurethane has the same thermal damage as in copolymer; on the other hand, silicone did not suffer any thermal damage. While mechanical damage was observed on silicone insulation.

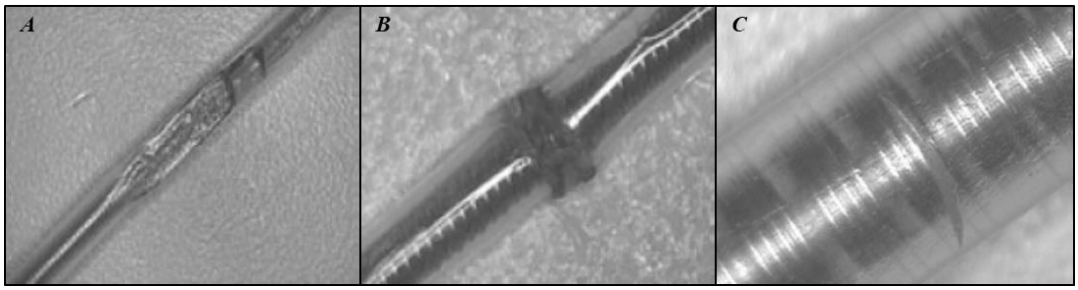

Figure 14 A) thermal damage on PU55D B) thermal damage on PU55D C) mechanical damage on silicone [55]

A study by Kron et al. [56] was conducted to determine the survival probability of leads and pulse generator depending on some criteria. For instance, lead survival probability was determined depending on three types of failure, dislodgment, infection, and lead fracture. On the other hand, pulse generator survival probability was determined

depending on the location of implantation, pectoral versus abdominal. 539 patients were enrolled in this study. The results showed that abdominal pocket had 13% failure, while pectoral pocket had 6% failure ($p<0.02$), as shown in Fig. 15a. Additionally, lead fracture was seen more than lead dislodgment, as shown in Fig. 15b.

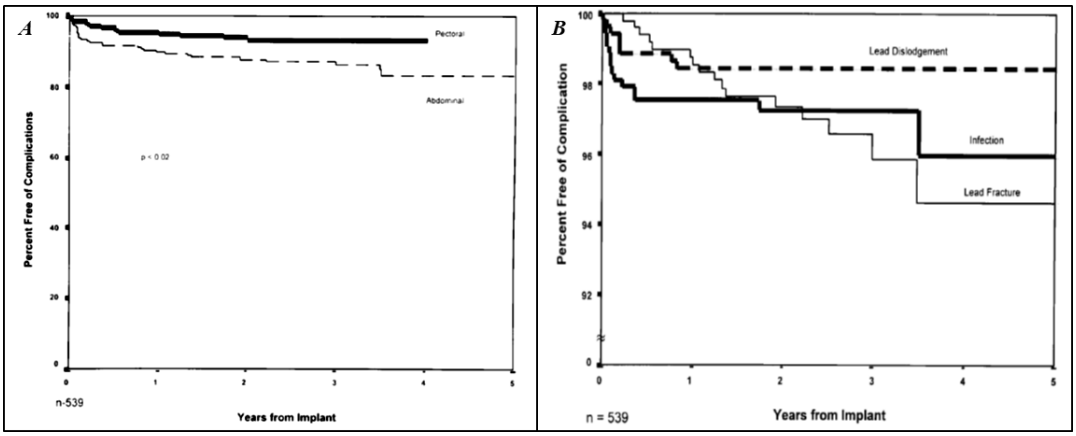

Figure 15 A) survival probability by location of pulse generator B) survival probability by lead failure type [56]

A case study was presented discussing the early abrasion of silicone insulation by Ząbek et al. [57]. Biotronik Setrox S53 lead was implanted and after 13 months of in-vivo environment, this lead failed. This lead failed due to "subclavian crush syndrome", where the lead is in contact with first rib and the clavicle [58].

Kołodzińska et al. [59], introduced how macrophages can affect the level of biodegradation. and it can be concluded that the biodegradation was initiated by the tearing around the surface of the lead.

Residual properties of leads were the most challenging studies. Few studies presented how residual properties deteriorating with in-vivo environment. For instance, Wilkoff et al. [60] studied three different insulations- Optim, P55D, and silicone elastomer. These leads categorized into three different in-vivo years (zero year, 2-3 year, and 4-5 year). Afterward, tensile test was performed to obtain the maximum load and extension. Results showed that Optim molecular weight decreased 20% after 2-3 years, then remained unchanged for 4-5 years. On the other hand, tensile strength decreased 25% after 2-3 years then stabilized for 4-5 years. Furthermore, elongation did not change at all. Molecular weight of polyurethane was not exposed to any changes during that period. Silicone showed significant biostability compared to polyurethane and Optim.

Chan et al. [10] studied Boston Scientific's FINELINE II STEROX 4456, Medtronic's CAPSURE SENSE 4074, and Abbott's ISOFLEX OPTIM 1948 leads. These leads exposed to in-vitro environment. They immersed the leads in 0.9 normal saline solution at room temperature for 10 days. Afterward, tensile test was performed. Boston Scientific's lead and Medtronic's lead showed same tensile strength; however, Abbott's lead showed lower tensile strength than BSX and MDT leads ($p<0.001$). This is an in-vitro study accelerated with time, and the in-vivo studies are totally different.

Starck et al. [11] categorized the leads in groups according to testing method used. First group was performed without central supporting stylet, second group was performed with central supporting stylet, while third group was performed with supporting stylet and

compression coil. Stylet and compression coils are used as a support to the lead. Stylet and compression coils are inserted inside the lead. Results showed tensile strength for group one was 28.3±0.3 N, for group two was 30.6±3.0 N, and for group three was 31.6±2.9 N. Modulus of elasticity for group one was 22.8±0.1 MPa, for group two was 2830.8±351.1 MPa, and for group three was 2447±510.5 MPa. This study introduced the supporting stylet that can enhance mechanical behavior of leads insulation.

CHAPTER 3 INVESTIGATION OF RETRIEVED CARDIAC DEVICES

3.1 INTRODUCTION

Cardiovascular diseases (CVD) are among the leading causes of mortality globally, especially in the developed countries [61]. While 17.3 million mortalities occurred from CVDs in 2008, it is projected to increase to 23 million by 2030 [62]. In the United States alone, about 92.1 million adults have cardiovascular disease with an estimated health-care cost of over $316 billion [62]. There are more than 1 million people around the world with implantable devices for cardiac conditions and quarter of these devices in the United States [63]. These numbers are projected to be increased many-folds with time and might reach 2 million in the US alone. A pacemaker delivers electrical impulses via electrodes causing the heart muscles to contract and regulate the heart beating. Therefore, there is a need to understand how these devices deteriorate after implantation so that corrective actions can be taken and *in vivo* performance enhanced.

Overall, the vast majority of the described cardiac devices consist of the pulse generator which is the body of the device and the leads [64]. The pulse generator contains the circuit board and the battery, it stores data such as a total number of cardiac events, the rate of these events, whether these were paced or intrinsic, and high rate episodes. Moreover, cardiac devices offer the ability to store intracardiac electrograms and function as event monitors with the ability to playback the paced or sensed events. These recordings

are extremely valuable in diagnosing the cause of symptoms as related to heart rhythms. On the other hand, the other major component that constitutes the cardiac devices is the leads. The leads are specially engineered wires that are designed to connect the pulse generator to the heart muscle. An electrical signal is transmitted through the leads allowing the pulse generator to sense and pace the heart whenever an abnormal behavior is detected. To prevent the electrical signal from travelling to other places, the leads are encased in an insulator which is made either from silicone or polyurethane [64]. In addition, the length of the pacemaker leads typically vary from 45 to 85 cm and the number of leads that are used depends on the type of the cardiac device implanted and of the heart failure symptoms to be monitored [64]. Generally, the malfunctions are defined as failure to pace or sense, or both, or failure to detect life threatening events and provide inappropriate shock which may be caused by problems with battery, the leads, the outer metal case, or the electronic components of the main circuit.

3.2 METHODOLOGY

The as received-devices were cleaned and sanitized for visual inspection. Serial numbers of the devices were tabulated. The inspection of the pulse generator carried out on the anterior and the posterior surfaces, Fig.16. The pulse generators were checked for scratches, surface deformation, pitting, discoloration, abrasion, and burnishing. Additionally, the leads were divided into three areas of inspection, the proximal part where the lead is connected to the connector block of the pulse generator, the middle part known as the conductor, and the distal part where the electrode is located and connects the lead to

the cardiac muscle, as shown in Fig. 17. Then these leads were checked for surface deformation, burnishing, pitting, scratching, delamination, insulation defect, coil damage, and abrasions.

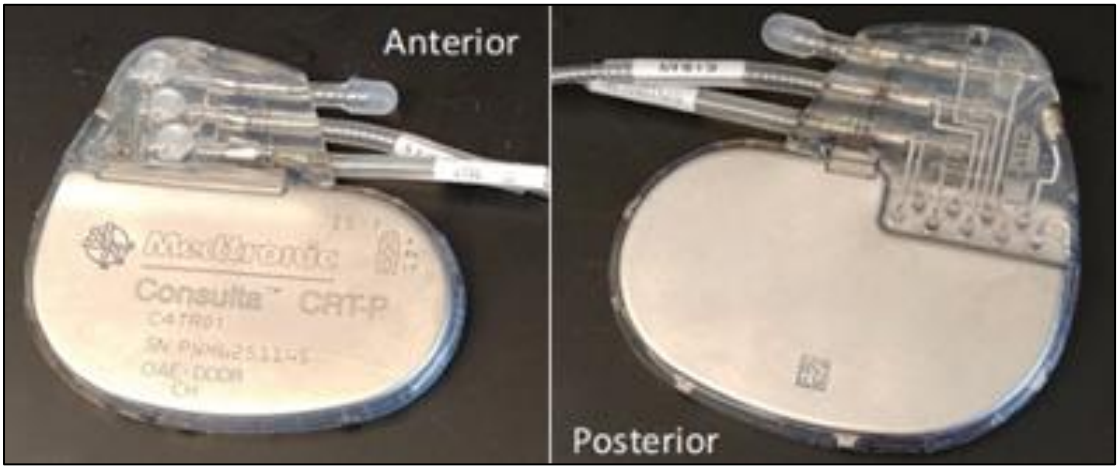

Figure 16 Anterior and Posterior side of the pulse generator

The damage modes identified as surface deformation was described by any minor or major warping that can be found on the surface of the device. Pitting described as a small hemispherical material loss that found on the surface of the device by corrosion. Scratches described as two-dimensional array lines as a result of rubbing. Abrasion described by shredding in the device materials. Discoloration was a change in the appearance (color) of the surface [65]. Insulation defect was described by a surface cracking on the surface of the lead or by complete insulation fracture. Coil damage described a cut in the coil protruding out of insulation or even damaged within the insulation [66].

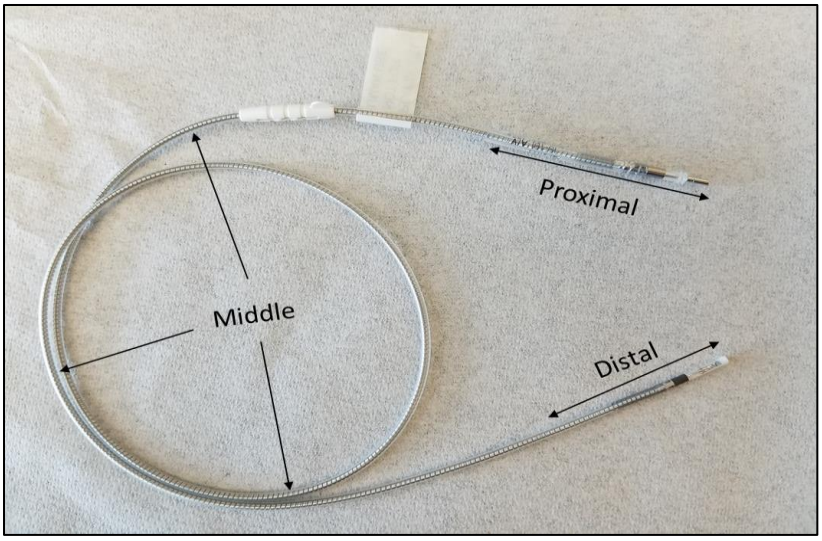

Figure 17 Lead as received from MDT, showing proximal, middle and distal parts

A damage scoring method was developed to represent damage in terms of individual damage fractions, added linearly to produce a total damage score for the pulse generators and leads. Three investigators performed the scoring method. These investigators received training of four hours to identify the damage modes to determine a composite score. The severity of different damage modes identified. Each damage mode was rated from 0 to 10 with regards to severity, and how deep the damage is, taking into consideration length and width of the damaged area. Where 0 meant no damage and 10 meant failure. For minor or superficial damages like shallow scratches, depending on the length, depth and the number of the scratches the rate was given from 1 to 5. On the other hand, the deep scratches that can be felt with the fingers were given a score of more than 5 based on the length, depth and the number of scratches. In cases where the device was

totally damaged and can affect the normal functionality of the device a total failure to pace or sense, the assigned values were from 7 to 10. Damage modes can interact and propagate to another type of damage. Depending on the severity of the damage, one damage could transform to another. For instance, in pulse generator, severe scratches could propagate to pitting and vice versa. In leads, abrasion could transform to insulation defect, and scratches could lead to pitting, which could turn to insulation defect as well.

The damage score equation for the pulse generator was developed to determine the damage percentage for each mode. The equation is as follow:

$$Pulse\ Generator\ Total\ Damage\ Score = \sum_{x=1}^{2}\sum_{y=1}^{n} Severity\ Score_{xy}$$

Where *x*= 1 through 2 and represents the anterior and posterior surfaces of the device, and y represents the damage mode where *y*=1 through 6.

y =1 Surface Deformation

y =2 Discoloration

y =3 Scratching/Indentation

y =4 Burnishing

y=5 Pitting

y=6 Abrasion

The results showed the average total damage score for the pulse generator was 0.502 ± 0.28. Then, the damage score equation for the lead was developed to determine the damage percentage for each mode. The equation is as follow:

$$Lead\ Total\ Damage\ Score = \sum_{x=1}^{2} \sum_{y=1}^{n} Severity\ Score_{xy}$$

Where *x*= 1 through 2 and represents the three parts of the lead (proximal, middle and distal) of the devices, and j represents the damage mode where *y*=1 through 9.

y =1 *Surface Deformation*

y =2 *Discoloration*

y =3 *Insulation Defect*

y =4 *Scratching/Indentation*

y =5 *Burnishing*

y =6 *Abrasion/Grooving*

y =7 *Coil Damage*

y=8 *Delamination*

y=9 *Pitting*

The results showed the average total damage score for the leads was 0.501 ± 0.29. These two equations characterize the accumulative damage made by each mode, and accounting for each part of the pulse generator and the lead. For the pulse generator, the number of the parts was two while the number of the damage modes varied according to different modes. For the lead, the number of the parts was three and the number of the damage features changed according to the equation above. All the devices were optically examined under the optical microscope. Most of the pulse generators had scratches; however, with the naked eye it was not possible to quantify how deep they were. With the use of the microscope, the coils were examined for cut, stretches and other damage modes.

Devices were interrogated at Miami Valley Cardiology Clinic and checked the internal components, parameters, remaining longevity, lead impedance, pacing, sensing threshold, time of implant, estimated time of retrieval and other information. The lead trend shows the impedances during the *in-vivo* life of the lead ranged 200-2000Ω for the pacing lead and 20-200Ω for the defibrillator lead. These impedances were measured to ensure the lead integrity to deliver therapy to the patient.

Each damage mode could cause specific failures to the leads and cause abnormal functionality. The failure of the lead is indicated by the one or more of the following failures: failure to capture, failure to sense, impedance out of range, conductor failure, extra-cardiac stimulation, cardiac perforation, lead dislodgement, and insulation defect [67, 68]. Failure to capture (loss of capture) is intermittent or complete failure of the lead to

stimulate the heart during a specific time programmed previously (mostly outside the refractory period). Failure to sense (loss of sensing) can be described as intermittent or complete failure of the lead to sense the intrinsic cardiac signal during the specific time programmed previously. Impedance out of range can be described as the impedance below 200Ω or above 2000Ω for the pacing lead and below 20Ω or above 200Ω for the defibrillator lead. Conductor failure can be seen either by the naked eye or electrically measured if mechanical break of the conductor occurred. Extra-cardiac stimulation occurs when the lead senses signal from other chambers and considers it as R-wave and may lead to inappropriate shock delivery. Cardiac perforation occurs when the lead tip penetrates through the myocardium and it can be observed visually and clinically. Lead dislodgement may be described as a spacing taken place between the lead tip and the cardiac muscle that could lead to inappropriate lead performance. Insulation defect can be described as an evidence of interruption or break in insulation [67, 68]. In order to check for extra-cardiac stimulation, cardiac perforation, and lead dislodgement, the distal part must be presented for examination. However, the other types of failures were observed in the proximal and the middle part of the lead.

3.3 RESULTS

3.3.1 Pulse Generator

The pulse generators of all the manufacturers are made of commercially pure titanium [69]. However, titanium accrues damage by scratching and discoloration as most devices

sustained scratching, Fig. 18a. 68% of the anterior surface of MDT devices, 66% SJM and 53% of BSC were scratched. The posterior surface of SJM showed no scratching on the surface, while 44% of MDT and 33% of BSC devices exhibited scratching. Surface deformation, as shown in Fig. 18b was also found on both surfaces. The anterior surface sustained higher deformation than the posterior surface. Discoloration was only found on BSC and MDT anterior and posterior surfaces, as shown in Fig. 18c. While burnishing was only found on the posterior surface of BSC devices. There were only three SJM devices and cannot be included in statistical analyses. All the damage modes are summarized in Fig. 19 illustrating the number of devices examined for each of the manufacturers, degree of surface deformation, scratching, burnishing, and discoloration on the anterior and posterior surfaces.

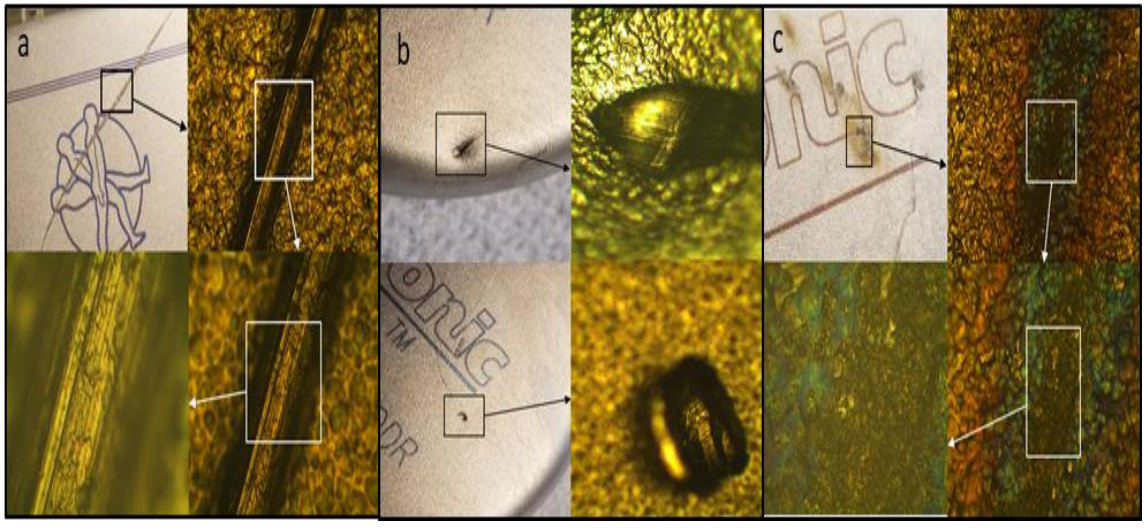

Figure 18 Pulse Generator Damage Modes, (a) Scratch, (b) Surface Deformation, (c) Discoloration

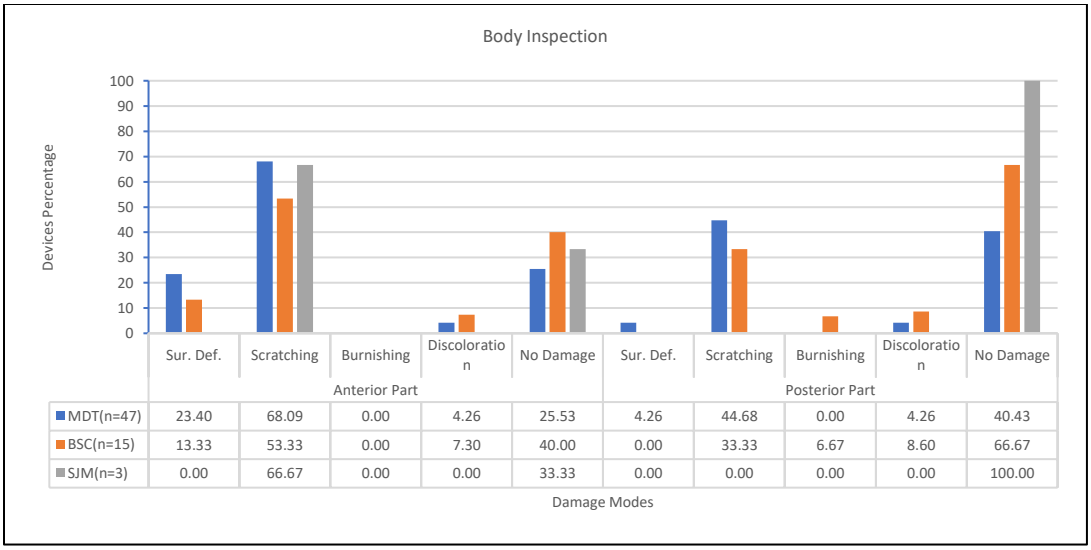

Figure 19 Pulse Generator Inspection, showing the percentage damage for each manufacturer

The damage modes of the pulse generator were compared to each other by using Fisher's LSD student test using JMP software. The scratching mode showed a significant difference when compared to the other damage modes. This test also showed no significant difference between surface deformation, pitting, discoloration, burnishing, and abrasion. The anterior and the posterior surfaces had compared to each other by using Fisher's LSD student test. The results showed a statistically significant difference between the anterior and the posterior surface (*P-value =0.0011*). Finally, the manufacturers were compared to each other by using Fisher's LSD student test, the results showed a significant difference for MDT when compared to BSC and SJM (*P-value =0.0399*). The damage modes of the pulse generator compared to each other by using Fisher's LSD student test. It showed a significant difference between scratching on the anterior and the posterior part. Also, the results showed a significant difference between scratching and other damage modes. The

pulse generator damage scoring distribution showed that the damage was between 10% and 70%. Higher number of devices with 10% damage, however, as percentage damage increased to 70%, number of devices decreased. Fig.20 illustrates cumulative distribution and total damage score.

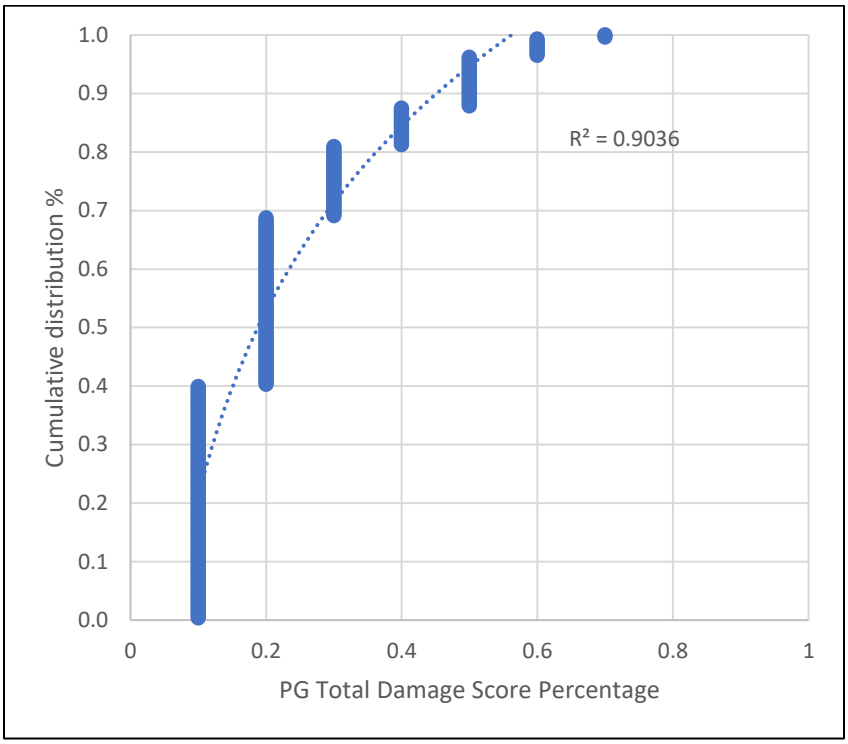

Figure 20 PG Damage Score Distribution

The battery life was checked using the corresponding program of each cardiac device, and the reports were obtained. Their longevity and the voltage were measured. A comparison was made between the battery depletion rate from the product reports. Using Ohm meter and the multi-meter, we observed that most batteries were depleted due to in

vivo usage of our as received devices. Fig.21 shows a sample report, and how the device longevity was estimated.

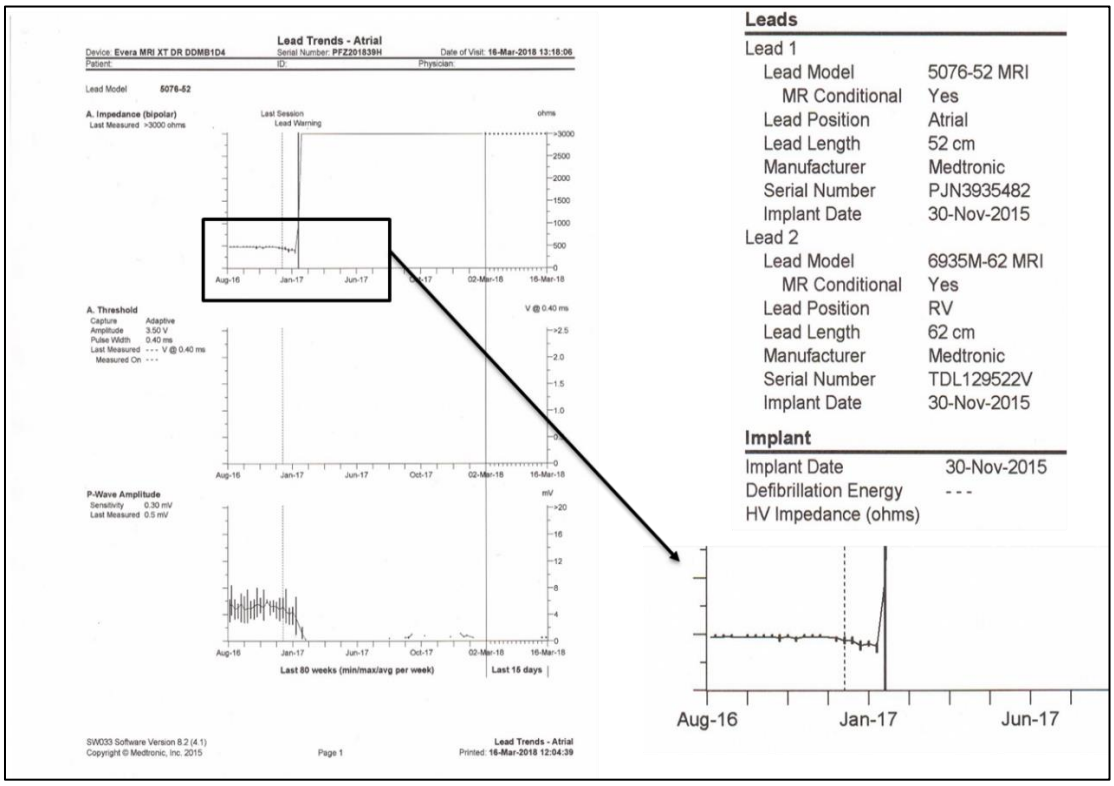

Figure 21 Sample report of device interrogation, and how device longevity was estimated

3.3.2 Lead

The leads showed visible cuts and stretches. The coaxial wires were stretched along with cuts. Optical microscope was able to resolve cuts and stretches under the insulation. The inner coil was also frayed in some parts and had numerous breaks. The coax wire on most of the devices was detached out of the insulation and appeared brittle, and in some occasions, broken easily. The distal parts of the leads were not retrieved during extraction

and submitted to us for investigation. For the pacing leads, the damage modes observed on both proximal and middle parts were abrasion (Fig.22a), discoloration (Fig.22d), scratching, coil damages (Fig.22b) and insulation defect (Fig.22c). The proximal part showed fewer damage than the middle part. Abrasion and discoloration on MDT and BSC leads were significant compared to SJM, where no abrasion and discoloration found in the proximal part. On the other hand, for the middle part, discoloration, coil damage, and insulation defect were highly present on SJM leads compared to MDT and BSC. The ICD leads showed more abrasion, scratching and insulation defect in the proximal part than the middle part. BSC had the most abraded and scratched leads when compared to MDT and SJM. SJM, BSC and MDT leads had almost equal insulation defect. For the middle part of the lead, discoloration was only found on MDT leads, and insulation defect was found on both MDT and BSC. SJM had only one lead in our inventory and this lead had no damage on both the proximal and the middle parts. MDT leads showed no damage, 71.43%, on the proximal part and 85.71% on the middle part, and BSC leads showed no damage 83.33% on the middle part. Even though the availability of the CRT devices in the lab is from both MDT and BSC, but all the leads used were only from MDT of three different types. On the proximal part, discoloration, scratching and insulation defect shared the same percentage with 6.67%. While this percentage increased significantly in the middle part, in addition to coil damage. The percentage of the undamaged parts in the proximal part was higher than the percentage in the middle part of the lead. The damage modes are summarized in Fig.23.

The damage modes of the lead were compared to each other by using Fisher's LSD student test using JMP software. The insulation defect showed a significant difference when compared to the other damage modes, and it showed a significant difference between discoloration, abrasion and coil damage. Then the proximal and the middle parts were compared to each other by using Fisher's LSD student test where the results showed a statistically significant difference between the proximal and the middle parts (*p-value<0.0004*). Also, the results showed no significant difference between discoloration in the middle part, coil damage in the middle part, insulation defect in the proximal part and abrasion in the proximal part. Finally, damage modes compared for the leads and it shows a significant difference between SJM insulation defect and other damage modes for both MDT and BSC. It also showed no significant difference between BSC insulation defect, MDT insulation defect, SJM discoloration, BSC abrasion, and SJM coil damage.

Figure 22 Samples of Lead Damage Modes, (a) Abrasion, (b) Coil Damage, (c) Insulation Defect, (d) Discoloration

The lead damage scoring distribution illustrates that the damage was between 0.1 and 1. The average damage on leads ranged between 0.1-0.3 damage score. With the increment of the damage score the number of damaged leads decreased, where 17.6% (24 out of 136) of leads with total damage. Fig.24 shows cumulative distribution of the leads and total damage score.

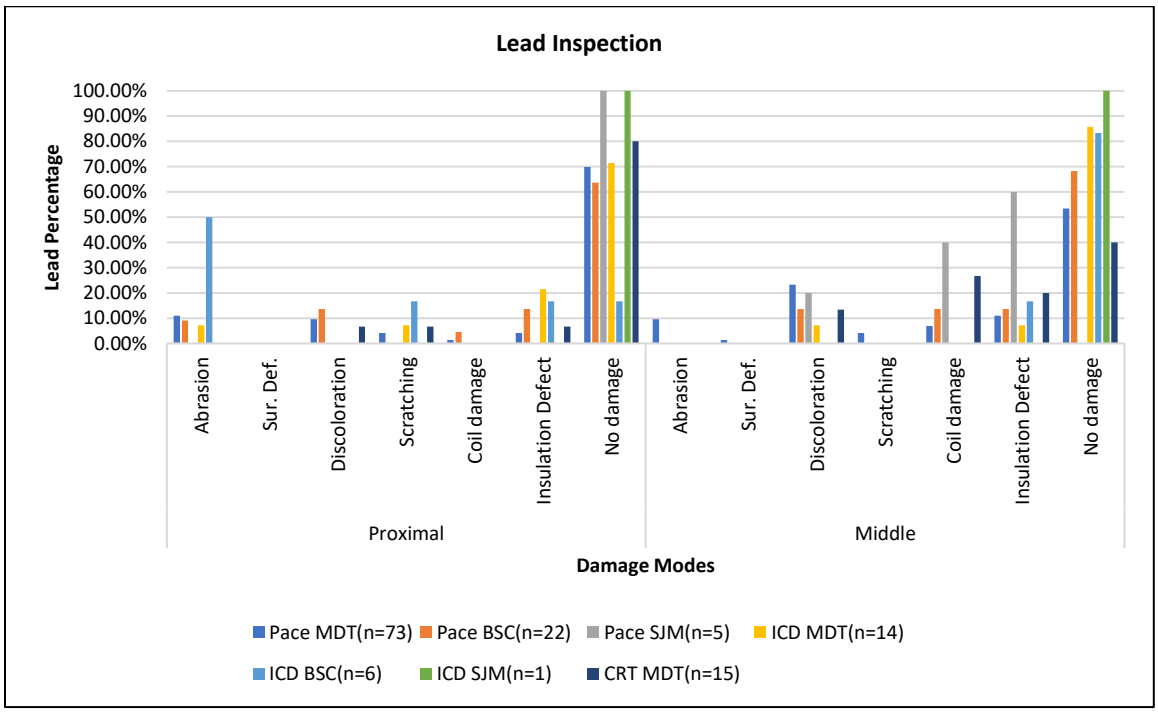

Figure 23 Lead Inspection, showing the damage modes versus different leads for different manufacturers

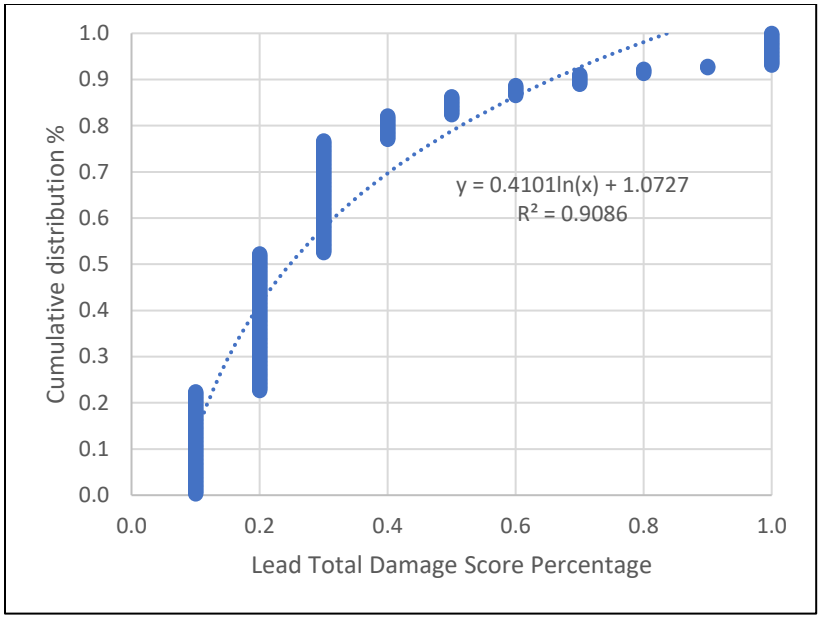

Figure 24 Lead Damage Score Distribution

All the above-mentioned damage modes could lead to several types of lead failure. These failures could affect the function of the device and may not deliver therapy appropriately. These types of failure can be failure to sense, failure to capture, impedance out of range and conductor fracture. Failure to sense can be defined as the device is unable to detect the intrinsic cardiac signal [68]. Failure to capture can be described as the device fails to stimulate the cardiac tissue [68]. Impedance out of range can be described as >30% fluctuation in the impedance measured (pacing leads impedance 200Ω-2000Ω, ICD lead impedance 20Ω-200Ω). Conductor fracture can be defined as a mechanical damage within the lead coils or/and electrodes [68].

Failure to capture can be a result of insulation defect, coil damage, and/or scratching. One or more damages can lead to this type of failure. Statistical analysis using JMP software was performed to validate the mathematical expression of failure to capture. Fig.25 shows the experimental results versus the predicted results (calculated using equation below). The analysis of experimental versus predicted results showed statistically no significant difference. Therefore, our proposed equation can be used to predict leads failure to capture. A failure to capture equation is developed and as follow:

$$Failure\ to\ Capture = \sum_{x=1}^{3} Damage\ Mode$$

x =1 *Insulation Defect*

x =2 *Coil Damage*

x =3 *Scratching/Indentation*

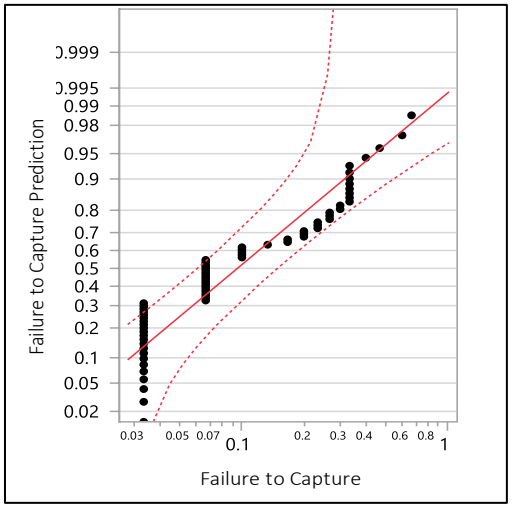

Figure 25 Failure to Capture Experimental vs Predicted score

Impedance out of range can be a result of insulation defect, abrasion, coil damage, and/or scratching. One or more damages can lead to this type of failure. Statistical analysis using JMP software was performed to validate the mathematical expression of impedance out of range. Fig.26 shows the experimental results versus the predicted results (calculated using equation below). The analysis of experimental versus predicted results showed statistically no significant difference. Therefore, our proposed equation can be used to predict leads impedance out of range. Impedance out of range equation is developed and as follow:

$$Impedance\ out\ of\ range = \sum_{x=1}^{4} Damage\ Mode$$

$x = 1$ *Insulation Defect*

$x = 2$ *Abrasion/Grooving*

$x = 3$ *Coil Damage*

$x = 4$ *Scratching/Indentation*

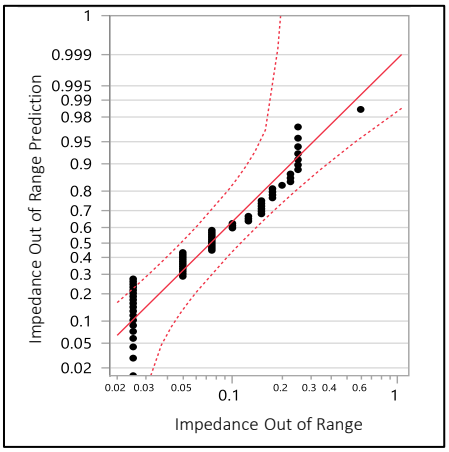

Figure 26 Impedance out of range Experimental vs Predicted score

Conductor fracture can be a result of insulation defect, abrasion, coil damage, and/or discoloration. One or more damages can lead to this type of failure. Statistical analysis using JMP software was performed to validate the mathematical expression of conductor fracture. Fig.27 shows the experimental results versus the predicted results (calculated using equation below). The analysis of experimental versus predicted results showed statistically no significant difference. Therefore, our proposed equation can be used to predict leads conductor fracture. Conductor fracture equation is developed and as follow:

$$Conductor\ fracture\ = \sum_{x=1}^{4} Damage\ Mode$$

x =1 *Insulation Defect*

x =2 *Abrasion/Grooving*

x =3 *Coil Damage*

x=4 *Discoloration*

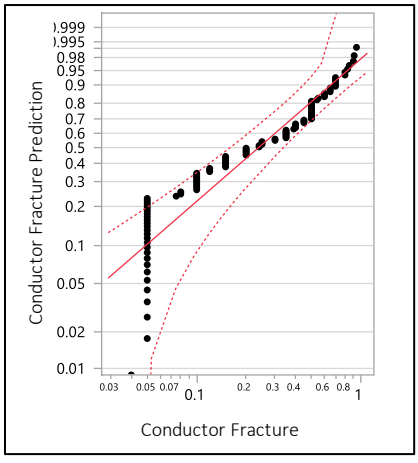

Figure 27 Conductor Fracture Experimental vs Predicted score

Failure to sense can be a result of insulation defect, coil damage, and/or scratching. One or more damages can lead to this type of failure. Statistical analysis using JMP software was performed to validate the mathematical expression of failure to sense. Fig.28 shows the experimental results versus the predicted results (calculated using equation below). The analysis of experimental versus predicted results showed statistically no significant difference. Therefore, our proposed equation can be used to predict leads failure to sense. A failure to sense equation is developed and as follow:

$$Failure\ to\ Sense = \sum_{x=1}^{3} Damage\ Mode$$

$x = 1$ *Insulation Defect*

$x = 2$ *Coil Damage*

$x = 3$ *Scratching/Indentation*

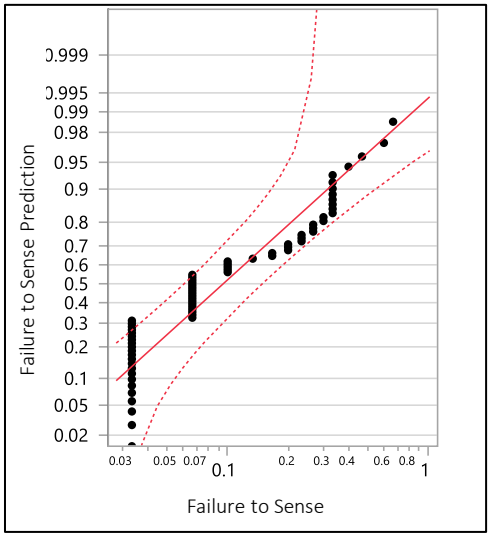

Figure 28 Failure to Sense Experimental vs Predicted score

According to the characterization of operational parameters, SJM showed higher failure types than MDT and BSC with 50% of its devices. The three manufacturers shared the same conductor fracture rate. Fig.29 shows the types of failure and the distribution of each type for each manufacturer, neglecting lead types. The number of leads that were investigated was 136, of which 102 were manufactured by MDT, while the rest were form BSC (28 leads), and SJM (6 leads). The results show that BSC leads had higher failure than MDT by 10% with respect to failure to sense, failure to capture and impedance out of range. The two most widely used pacing leads were taken and examined thoroughly to identify the types of failure modes. These leads were MDT 5076 CapSureFix Novus and BSC 4470 FINELINE II. The results showed the percentage of leads fail to sense, capture and impedance out of range were higher in BSC 4470 (25.00%) than MDT 5076 (15.69%). The conductor fracture in MDT 5076 was 6.67% compared to 8.7% in BSC 4470. Insulators for MDT was Silicone (MED-4719) [67], while BSC 55D polyurethane [70]. The two most widely used ICD leads were taken and inspected carefully to categorize the failure types, the leads are MDT 6947 Sprint Quattro Secure and BSC 0157 ENDOTAK RELIANCE. The percentage failure of MDT 6947 was lower than the percentage failure of BSC 0157 with 33.33% for MDT 6947 and 42.86% for BSC 0157, while no lead exposed to conductor fracture. MDT used polyurethane as the outer insulator and silicone rubber as inner insulator [40], while BSC silicone rubber as the lead insulator [40]. Therefore, three MDT CRT leads were examined to identify the types of failure. The three inspected leads were 4196 Attain Ability, 4194 Attain OTW and 4193 Attain OTW. The results showed that the

4196 Attain Ability lead had a lower failure rate than the other leads as well as no conductor fracture. All 4194 Attain OTW leads failed due to the damage modes discussed previously. While 50% of the 4196 and 4193 leads exhibited no damages. Fig.30 summarizes the failure types and the percentage that occurred to the pacing, ICD and CRT leads.

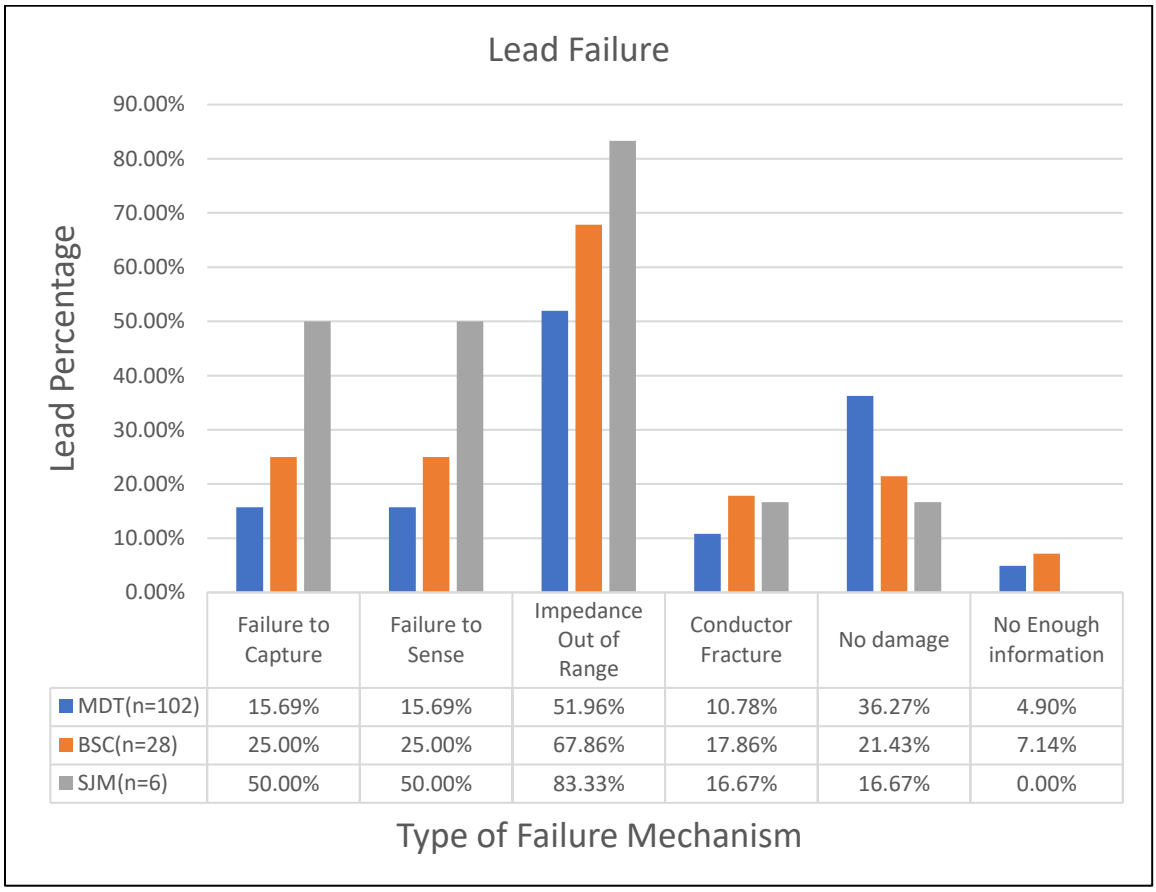

Figure 29 Types of Failure Mechanisms in Leads, showing the percentage of each failure type for each manufacture

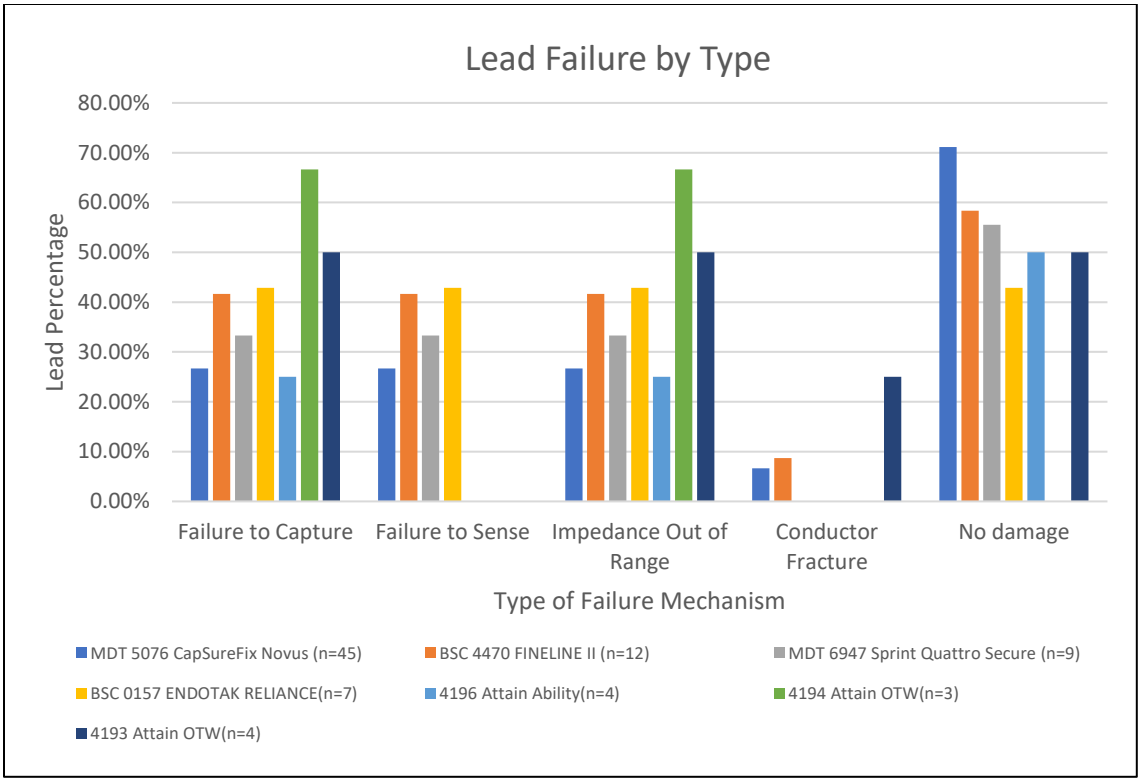

Figure 30 Types of Failure Mechanisms in leads, showing the comparison between the pacing and the ICD leads of MDT and BSC, and three MDT CRT leads.

40 out of 65 devices were still functioning and have a range of longevity from 3 months to 132 months. These devices are listed in Appendix I. Two of the active devices were connected to an oscilloscope to examine the functionality of these devices. The output waveform from the leads was measured. Fig.31 represents the obtained waveforms that verify the functionality of the device.

A worse case analysis of pulse generator survival for both MDT (n=37) and BSC (n=11) is shown by Kaplan-Meier curves in Fig. 32. The cumulative survival is 71% at one

year for both MDT devices and BSC devices, and 10% at six years for BSC devices and 10% at seven and half years for MDT devices. Pacemaker showed 88% and 91% survival rate after one year of implantation for BSC and MDT respectively. After four years, however, the survival reduced to 42% for MDT and 38% for BSC from the as received devices. No survival for BSC after six years of implantation, while 20% survival for MDT pacemakers. The survival probability of the as received damaged leads for both MDT (n=53) and BSC (n=9) is shown in Fig. 33. After 60 months, the survival is 60% for MDT and 68% for BSC. The survival is 6% for MDT and 25% for BSC after 160 months of implantation, and no survival for BSC after 176 months of implantation, while MDT is 6% survival after 180 months after implantation. 33% of BSC devices use MDT leads for different purposes.

Figure 31 Pulse width and the Voltage, obtained by connecting the devices to an oscilloscope

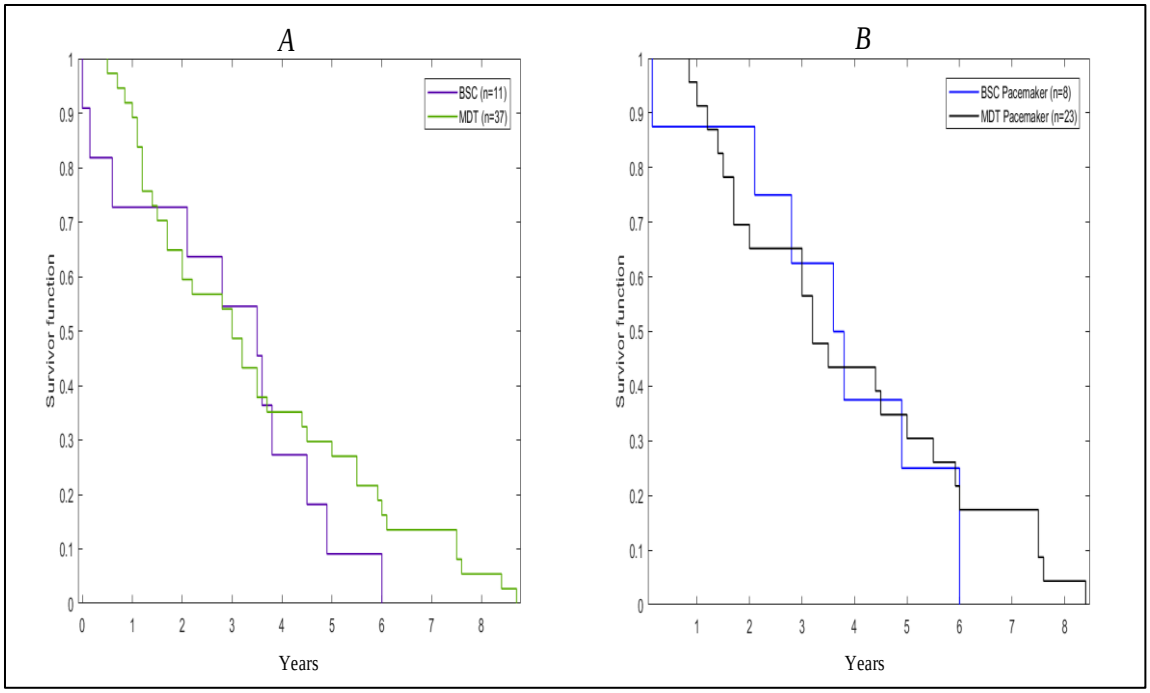

Figure 32 Kaplan-Meier analysis of survival of (A) Medtronic Devices (n=24) and Boston Scientific Devices (n=11), (B) Medtronic Pacemakers (n=13) and Boston Scientific Pacemakers (n=8).

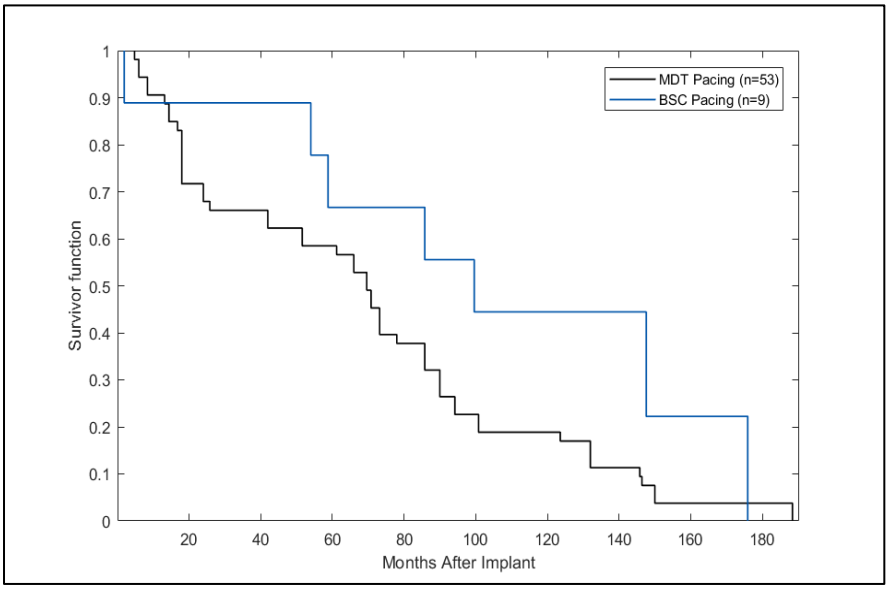

Figure 33 Kaplan-Meier analysis of survival of (A) Medtronic Pacing Leads (n=34) and Boston Scientific Pacing Leads (n=9)

Sensitivity can be defined by the capability of the device to sense the intrinsic heartbeat. It represents the minimum cardiac signal that can be sensed by the pacemaker to initiate or terminate the therapy. The sensitivity is measured in millivolts, the higher sensitivity the lower voltage programmed. When programming the sensitivity to a low value, in turn allows the device to sense additional signals than expected and could cause what is known as over-sensing. When programming the sensitivity to a higher value, prevents the device from detecting the intrinsic cardiac signal and could cause what is known as under-sensing.

Fig.34 illustrates the sensitivity distribution for all the investigated devices. The mean sensitivity is 1.188 mV and ranges from 0.25-4 mV. Additionally, the mean sensitivity value of the ventricular leads was 1.465 mV and ranged from 0.3-2.8 mV. Furthermore, the mean sensitivity value of the atrial leads was 1.188 mV and ranged from 0.25-4 mV. Fig.35 shows the difference between the sensitivity setting of the ventricular and atrial leads, and it shows the ventricular sensitivity setting was higher compared to the atrial sensitivity setting.

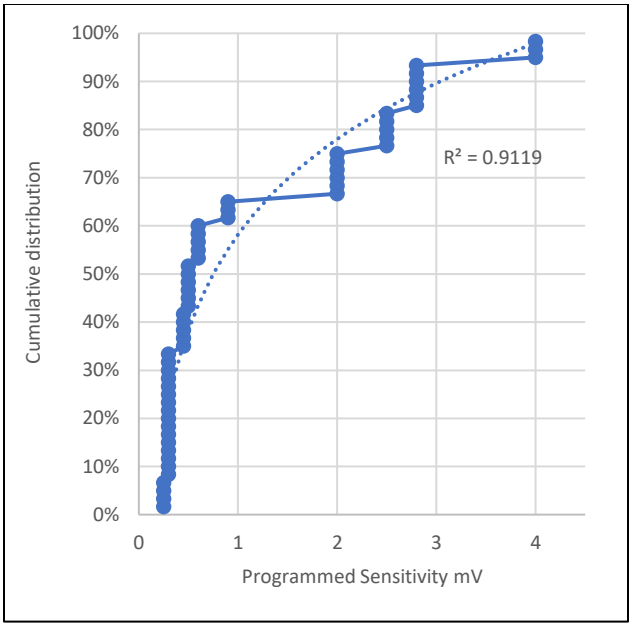

Figure 34 Sensitivity Distribution for all the leads

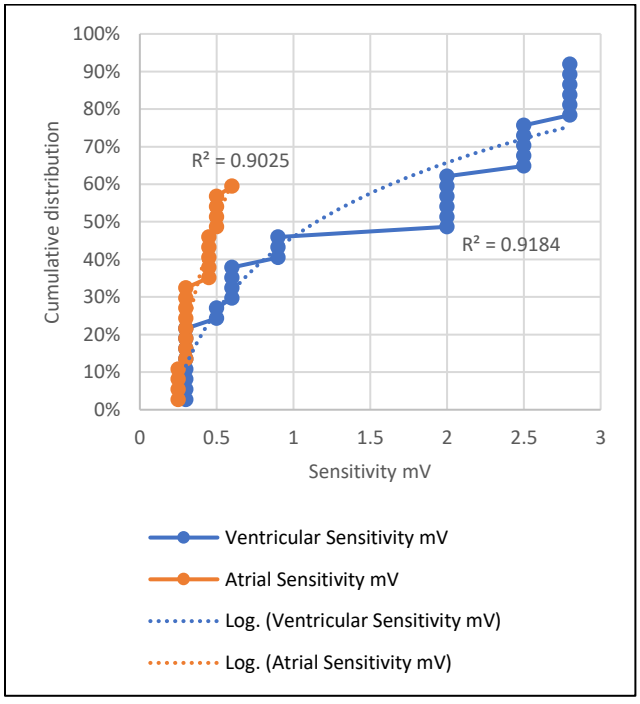

Figure 35 Sensitivity Distribution for both ventricular and atrial leads

3.4 MONTE CARLO SIMULATION

It is important to understand the effect, or the risk associated with the lead from the devices that we have in our lab. Our devices were received posthumously from diseased patients. So, it's important to perform the risk analysis for the leads, and Monte Carlo simulation is one of the tools that is used to understand the risk associated for the reliability purposes. In order to apply MCS, it's important to understand the data that we have for the leads in our lab, that we want to plot on a run chart and fit some statistical distribution to those data, and the best fits were found normal, lognormal, Weibull and gamma. In order to predict the probability of failure for large number of devices, Monte Carlo simulation was used. First, a domain was defined from the scoring method for the damage modes to determine the input of the simulation. These inputs were determined randomly relying on the probability distribution for the chosen domain. Second, Monte Carlo simulation was performed to predict the percentage failure of the devices and leads. Monte Carlo simulation used to produce 200, 500, 1000, 2000, 5000, and 10000 random variables data normally distributed within the mean and the standard deviation. Finally, generating a code using Matlab to compute the failure probability of pulse generators and leads were performed. Fig. 36 shows the predication data of 10,000 random values. The most conservative probability of failure distribution was taken predicate the failure rate for 10,000 devices. It shows ICD leads have significant failure to sense/capture compared to pacing and CRT leads (*P-value=0.0052*). This figure shows that the ICD leads failed to capture/sense with minor failures or damages. Then, it was consistent at 75% of failure

probability with 80% of damage. Another monte carlo simulation was performed for 10,000 random variables to predict the impedance out of range as shown in Fig.37. It shows CRT leads have significant impedance out of range compared to ICD and pacing leads (*P-value=0.031*). It shows that ICD and pacing leads probability of failure are high with minimum damage. On the other hands, it shows that CRT leads probability of failure is low compared to the same damage/failure of the ICD and pacing leads. Finally, monte carlo simulation was performed to predict conductor fracture for 10,000 random variables as shown in Fig38. It shows pacing leads have significant conductor fracture compared to ICD and CRT leads (*P-value=0.0249*). It shows the probability of failure of pacing leads are higher than the probability of failure of ICD and CRT leads for the same percentage of damage/failure.

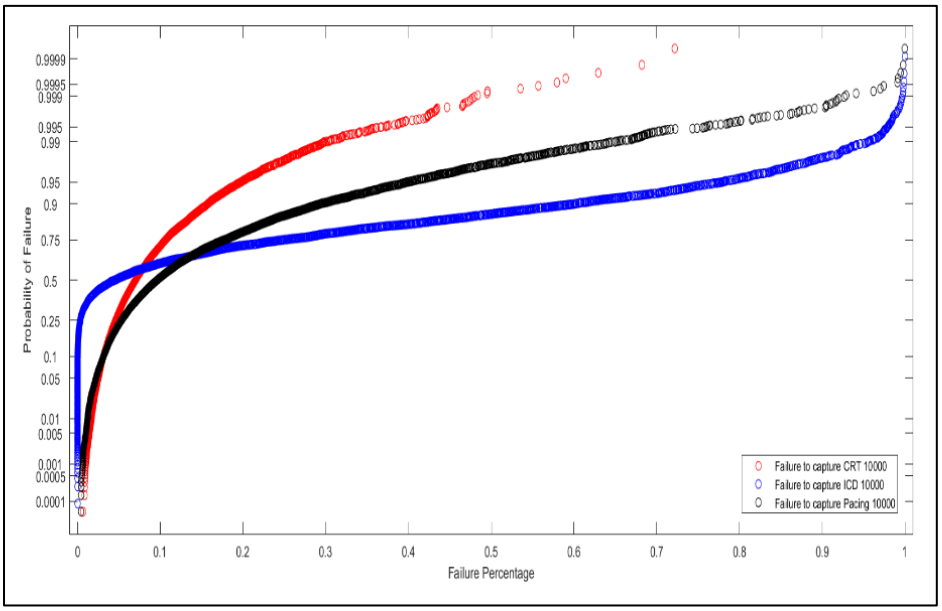

Figure 36 Monte Carlo Simulation for 10,000 random data For Failure to capture/sense

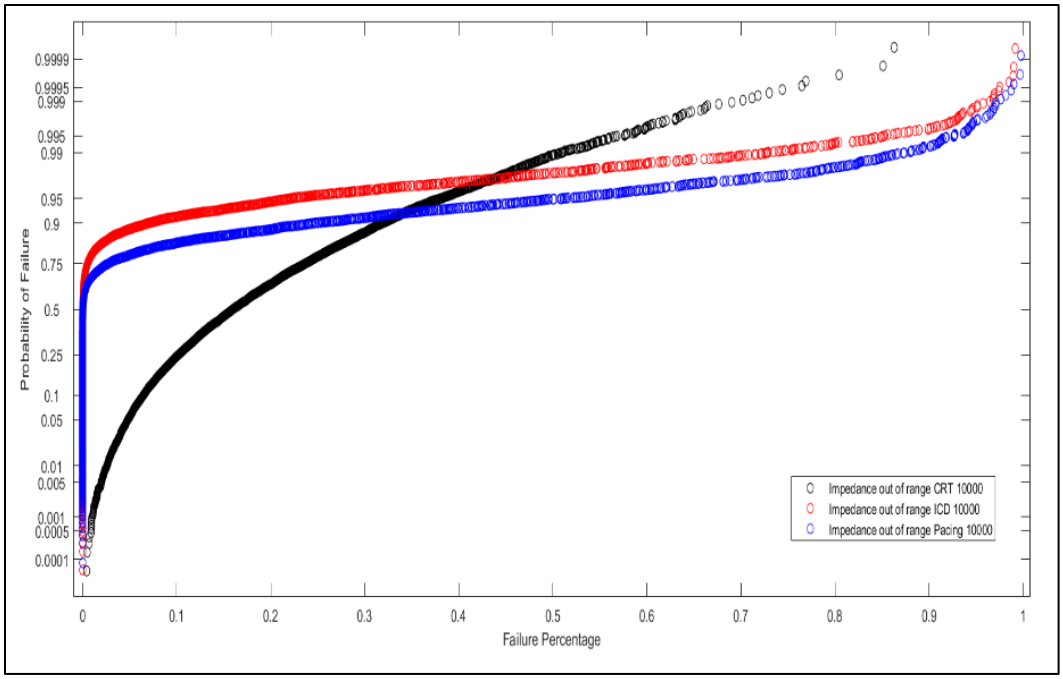

Figure 37 Monte Carlo Simulation for 10,000 random data For Impedance out of range

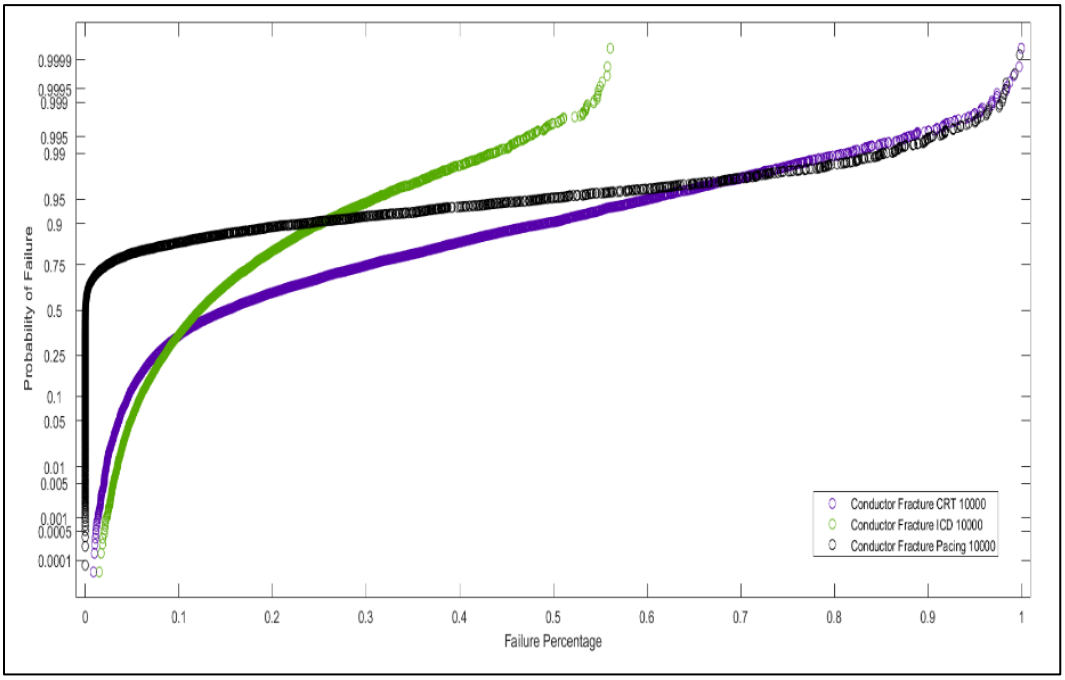

Figure 38 Monte Carlo Simulation for 10,000 random data For Conductor Fracture

Additionally, Monte Carlo simulation was performed to investigate the probability of failure of pacing, ICD, CRT leads with respect to different failure types. Student's T-test was performed to check for significance difference. The results showed that for pacing leads, conductor fracture has statistically significant difference than other failure types (*P-value<0.0001*). For ICD leads, results showed no significant difference between the four types of lead failure (*P-value =0.1101*). For CRT leads, there was significant difference between failure to capture/sense and other failure types (*P-value =0.0015*). Fig.39, Fig.40, and Fig.41 illustrate monte carlo simulation for 10,000 random data.

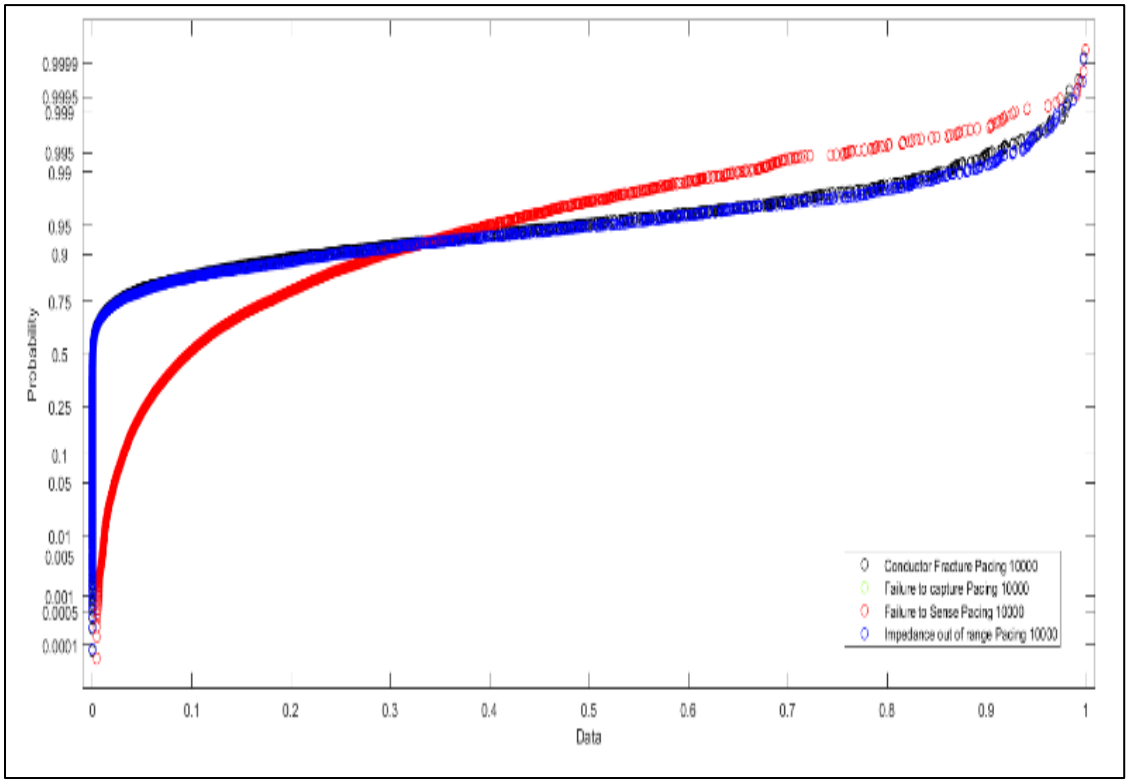

Figure 39 Monte Carlo Simulation for 10,000 random data for Pacing leads with respect to type of failure

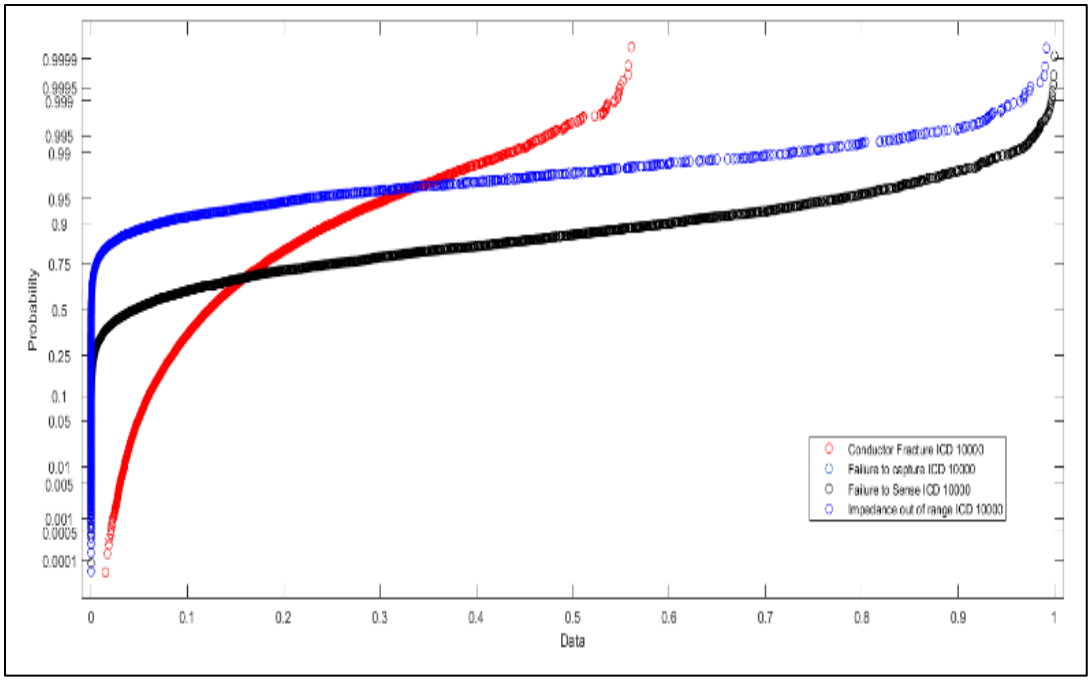

Figure 40 Monte Carlo Simulation for 10,000 random data for ICD leads with respect to type of failure

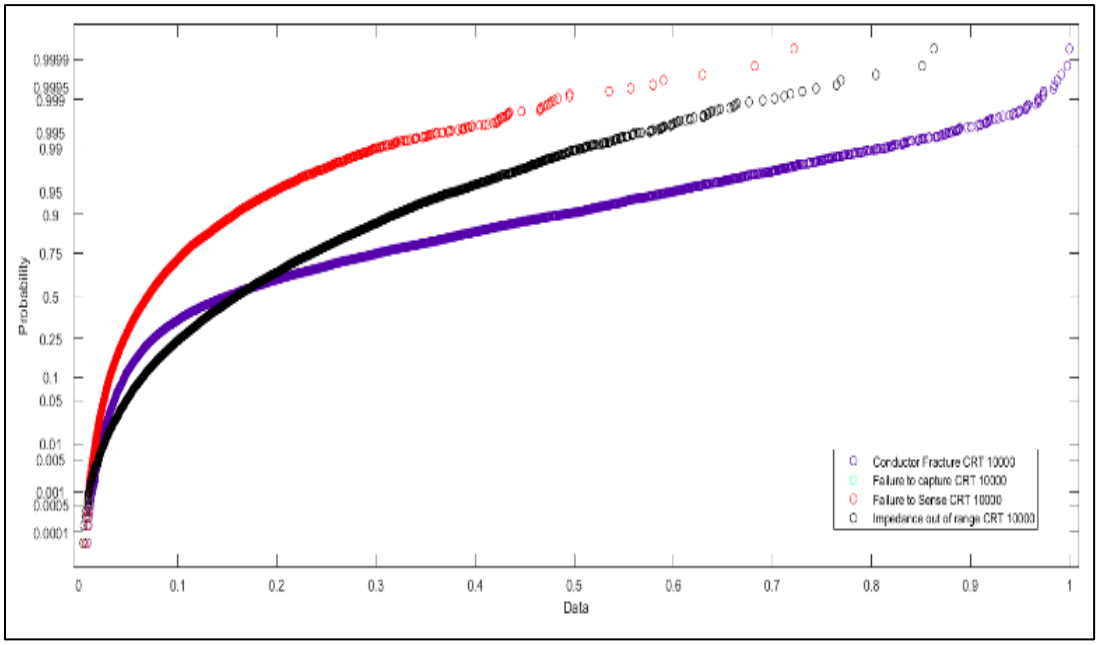

Figure 41 Monte Carlo Simulation for 10,000 random data for CRT leads with respect to type of failure

3.4 DISCUSSION

In literature the pulse generator of the cardiac device has rarely been investigated for damage. Most of the investigations were done on the leads. Discoloration was due to titanium oxide resulting in the white color and could have led to further biodegradation. The discoloration on the cases do not affect the functionality of the devices. However, it is likely that corrosion mechanisms and ions may dissolve in body fluids and their pathophysiology is outside the scope of this research. The percentage damage mode present on the pulse generator is shown in table 3. The damage percentage on the anterior part is 61.93% and on the posterior part is 38.07%.

Table 3 Pulse Generator Damage Mode Percentage, average damage and standard deviation

		Damage Mode	**Damage percentage**	**Average**	**SD**
Pulse Generator	Anterior	Surface Deformation	13.02%	0.47	1.03
		Pitting	0.00%	0	0
		Scratching	46.41%	1.63	1.63
		Burnishing	0.00%	0	0
		Abrasion	0.00%	0	0
		Discoloration	2.50%	0.1	0.46
	Posterior	Surface Deformation	2.17%	0.08	0.38
		Pitting	0.00%	0	0
		Scratching	33.56%	1.16	1.63
		Burnishing	0.67%	0.02	0.21
		Abrasion	0.00%	0	0
		Discoloration	1.67%	0.06	0.32

The leads showed visible cuts and stretches. The coax wires were stretched along with cuts. Optical microscopy shows several areas the insulation had been degraded scratched or even cut and may affect the functionality of the devices. The lead damage modes and the percentage of each mode is summarized in table 4.

Table 4 Lead Damage Mode Percentage, average damage and standard deviation

		Damage Mode	**Damage percentage**	**Average**	**SD**
Lead	Proximal	Surface Deformation	0.00%	0	0
		Pitting	0.00%	0	0
		Insulation Defect	12.82%	4.13	3.31
		Scratching	2.29%	1.39	0.69
		Burnishing	0.17%	0.67	0
		Abrasion	10.10%	2.44	1.44
		Coil Damage	0.34%	0.61	0.41
		Delamination	0.00%	0	0
		Discoloration	9.34%	2.33	1.68
	Middle	Surface Deformation	0.93%	2.68	0.12
		Pitting	0.00%	0	0
		Insulation Defect	28.52%	5.12	3.67
		Scratching	0.93%	1.09	0.57
		Burnishing	0.00%	0	0
		Abrasion	5.09%	2.37	1.42
		Coil Damage	12.05%	2.62	1.59
		Delamination	0.00%	0	0
		Discoloration	17.40%	2.49	1.54

Previous efforts from literature showed that electrical tests, optical microscopy and SEM [71] were performed on the lead. The work was presented to investigate for coil damage in 49 leads from one manufacturer. Additionally, Wiggins et al. [8] used optical microscopy, SEM and FTIR to determine the chemical degradation on the inner and outer insulation. This is a key feature of learning the residual properties of the leads and its insulation. They did their investigation about the biodegradation of the PU insulation of 7 leads. In addition, Hauser et al. investigated the lead failure in one lead type [66]. Additionally, Mehta et al. [82] performed clinical evaluation of 132 randomized patients for four years to identify the complication of leads. This study [82] showed the same results as current work that the ICD leads are more vulnerable than pacing leads in insulation breakdown. 39 out of 132 ICD leads experienced inappropriate shock due to insulation breakdown [82]. On the other hand, our research showed 4 out of 21 ICD leads experiences insulation breakdown. Furthermore, Kron et al. used data from 539 patients for 4 years, and it showed that 2.8% of the leads fractured. Fortescue et al [72] collected data from one pediatric center during 1980-2002. A total of 1007 leads were implanted in 497 patients. Lead failure occurred in 155 leads 15%, and the patients who experienced multiple failures were 28%. They found the insulation defect percentage was 32.2% of the failed leads. In general, the investigation in this paper was significant due to the variation of the devices involved. It involved 65 cardiac devices and 136 leads from different manufacturers. Visual inspection, optical microscope inspection and electrical tests were performed to determine the damage modes for these devices.

Sensitivity metric equation was created from the data that were generated during this investigation from the devices. The goal was to mathematically model the sensitivity for any given time. A principal component analysis was performed for the acquired data to isolate those parameters that are the most important to create the sensitivity metric expression (*S*). It was noticed that as the voltage increased the pulse width decreased and vice-versa. Therefore, sensitivity function parameters (F) were defined in terms of voltage, (F_1) and pulse width (F_2) as reciprocal, ($1/F_2$). It is important to note that if the voltage doubled, then the energy usage can be higher. Lastly, the time was a crucial component and by far the most important.

$$S = F_1 \frac{F_3 + F_4}{F_2}$$

F_1 is the voltage in millivolts, F_2 is the pulse width in milliseconds, F_3 is the in ohms, and lastly is F_4 the current in milli-amperes. The interrogation of the devices leads to numerous discoveries, and the relation between sensitivity setting, pulse width and impedance can be revealed through the obtained reports. Sensitivity plot generated using MATLAB R2017a, that contained impedance, pulse width, and sensitivity setting as shown in Fig.42. This plot shows that with low impedance and high pulse width, the sensitivity is low. However, the impedance increases the sensitivity and pulse width, this scenario depletes the battery earlier than estimated. Sensitivity plot help physicians to choose appropriate parameters that can help in patient therapy. From Fig.42 one can set the

sensitivity voltage according to either the sensing test or depending on the figure generated and can compare the normal impedance to the corresponding voltage and pulse width.

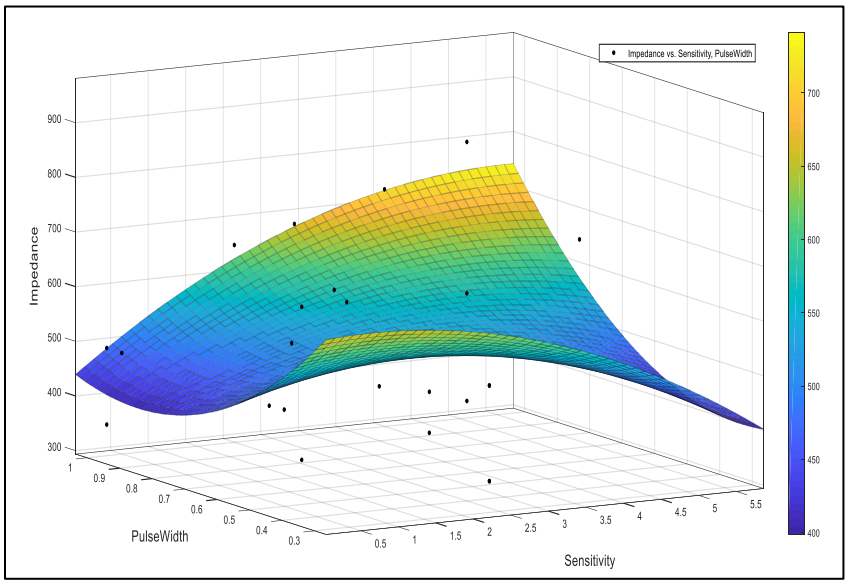

Figure 42 Sensitivity Plot

3.5 CONCLUSION

The devices used in this investigation were received from The Wright State Anatomical Gift Program. These devices were extracted posthumously and ranged from 3 months to 192 months of in-vivo exposure. It can be inferred that the pulse generator cases had mainly scratches that were shallow, narrow and could not have affected the functionality of the devices. The discoloration on the cases was caused by the growth of organic material from the body or due to the exposition to fluids (alcohol, bleach, dimethyl formaldehyde etc.) used in the sterilization process of the devices after their retrieval. However, the discoloration could not have affected the functionality of the devices. In addition, the

investigation showed that the anterior side was more exposed to damage than the posterior side. The leads, which consist of the inner coil, outer coil and the insulation around the coils, had visible insulation defect, stretches, and coil damages that caused different types of failures and could have affected the functionality of the devices. However, these damages may have happened during the extraction/pulling of the devices or during the replacement of the leads not during the *in vivo* usage. In general, Medtronic leads showed significant resistance to different damage modes when compared to Boston Scientific and St. Jude medical, and the middle part was more exposed to damage than the proximal part. A damage equations were developed to determine the percentage damage for each mode. A Failure types quantitative assessment was developed for different failure types. Then, monte carlo simulation was performed to predict the failure probability of different types of leads failures. The output data for failure types were plotted in terms of actual values versus predicted values using JMP software. Finally, sensitivity plot was generated using Matlab to help physicians in understanding how the pulse width, impedance, and sensitivity setting are related.

CHAPTER 4 RESIDUAL PROPERTIES OF LEAD

4.1 INTRODUCTION

5076 CapSureFix Novus MRI SureScan Lead is multi-length, active fixation, bipolar, coaxial design lead. The insulation is achieved by silicone (MED-4719) as an outer insulator and as an insulator between the two coils (Medtronic, Minneapolis, MN, USA). This lead received FDA approval in 2000 [67].

Silicone rubber was used during the 1960's for the first time in the cardiac devices as an insulator for leads. It is biocompatible and biostable. However, it can tear easily at the same time possesses a high coefficient of friction. The silicon rubber also has tendency to creep, which leads to insulation necking at the area of sustained stresses [73]. Silicon was modified to overcome abrasion, tear and creep with higher tensile strength and abrasion resistance. These include high-performance (HP) silicone, extra-tear-resistant (ETR) silicone, and Novus (Med-4719, Nusil Technologies, Carpinteria, Calif), produced by hybridizing HP and MDX4 silicone [74]. 5076 CapSureFix Novus MRI SureScan Lead uses Novus (Med-4719) as an insulator [67].

Residual properties of leads are found in the literature sparingly. Few studies presented how residual properties deteriorating with in-vivo exposure [10, 11, 60, 75]. For instance, Helguera et al. [75], studied 992 silicon leads of 26 (2.6%) predicted to fail after a period of 5-10 years, while 10 (1.0%) leads were actually failed after that period. Other

feature reported by Chan et al. [10], Starck et al. [11], and Wilkoff et al. [60] is discussed in chapter two.

4.2 METHOD

Twenty 5076 CapSureFix Novus MRI SureScan pacing leads were used in the experiment. This lead is 52 cm active fixation, bipolar, coaxial design, with silicone (MED-4719) as an outer insulator and as an insulator between the two coils (Medtronic, Minneapolis, MN, USA). Two of the leads were provided by Medtronic. The rest of the leads were received from the Wright State University Anatomical Gift Program. *In vivo* implantation duration was different for each lead with an average of 62±55 months. Test Resources Q series system was used to perform the tensile test. Fig.43 demonstrates the test procedure including the samples' length before and after the test, the fixture, and the cross-section of the sample under the microscope showing the coils and two insulators. Complying to ASTM Standard D 1708-02a [76] (Standard Test Method for Tensile Properties of Plastic by Use of Microtensile Specimens) and ASTM Standard D 412-06a [77] (Standard Test Methods for Vulcanized Rubber and Thermoplastic Elastomers-Tension). The length of the samples were fixed to 38mm for all tested leads, 8mm in the grip and 22mm between the grips. The leads were tested with the coil inside the insulation. The lead was fixed in the grips by sand paper to avoid slippering. The tensile test was performed by applying specific loads on the samples, and the corresponding displacement measured. The tensile test was repeated at least five times and the average of the results was calculated. First, the diameter was measured for each specimen at three locations and the average diameter was

calculated. A gage of 22 mm length was used for all the specimens. Also, all leads were examined under the optical microscope to investigate the damage before and after the tests as shown in Fig.44. The tensile test was applied at a rate of 1 mm/sec, and the body of the lead was observed for extension. In addition, load to failure, elongation to failure, percentage elongation at 5N, ultimate tensile strength, and modulus of elasticity were calculated after the lead insulation separated. Finally, the equivalent data were compared with respect to the *in-vivo* exposure in years.

Table 5 List of the Leads used with their SN, implant date and estimated retrieval date

#	Lead Type	SN	Insulation	Implant Date	Estimated explant date	IN-VIVO Duration
1	5076	PJN3644744	Silicon	NA	NA	New Lead
2	5076	PJN2329144	Silicon	November/2010	January/2017	74 months
3	5076	PJN2815001	Silicon	September/2012	March/2018	66 Months
4	5076	PJN2814368	Silicon	September/2012	March/2018	66 Months
5	5076	PJN3973695	Silicon	January/2016	March/2018	26 Months
6	5076	PJN2621551	Silicon	October/2011	December/2017	73 Months
7	5076	PJN4619372	Silicon	June/2017	September/2017	3 MONTHS
8	5076	PJN2206204	Silicon	June/2010	September/2011	15 Months
9	5076	PJN2213707	Silicon	June/2010	September/2011	15 Months
10	5076	PJN3633312	Silicon	May/2015	December/2016	18 MONTHS
11	5076	PJN3722285	Silicon	May/2015	December/2016	18 MONTHS
12	5076	PJN4057165	Silicon	March/2016	August/2016	6 MONTHS

13	5076	PJN4070036	Silicon	March/2016	August/2016	6 MONTHS
14	5076	PJN4043721	Silicon	March/2016	November/2016	8 MONTHS
15	5076	PJN4060504	Silicon	March/2016	November/2016	8 MONTHS
16	5076	PJN3935482	Silicon	November/2015	January/2017	13 MONTHS
17	5076	PJN2412482	Silicon	December/2011	October/2017	71 MONTHS
18	5076	PJN625058V	Silicon	August/2004	May/2012	94 Months
19	5076	PJN641773V	Silicon	August/2004	May/2012	94 Months
20	5076	PJN1086898	Silicon	December/2006	December/2017	132 MONTHS

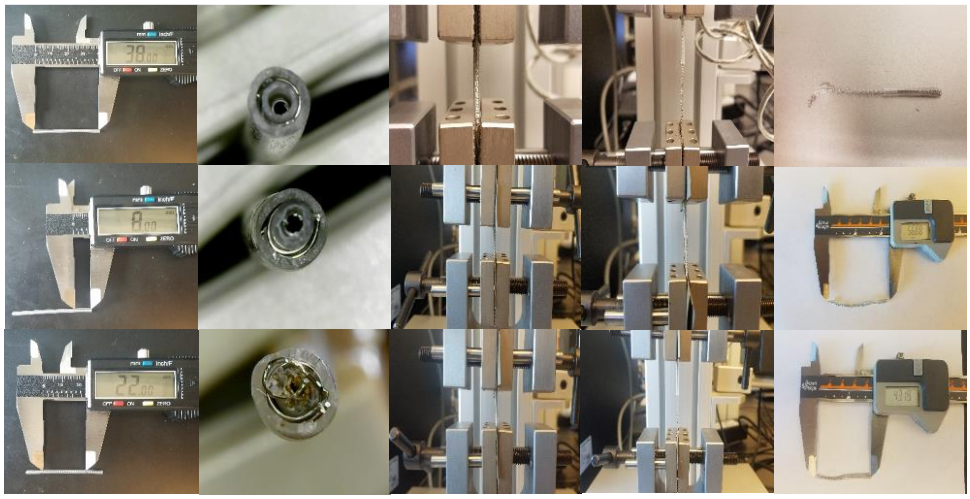

A *B* *C* *D* *E*

Figure 43 A) Specimen measurement, (B) Cross-section of the lead, (C) During the test, (D) At the break point, (E) After deformation

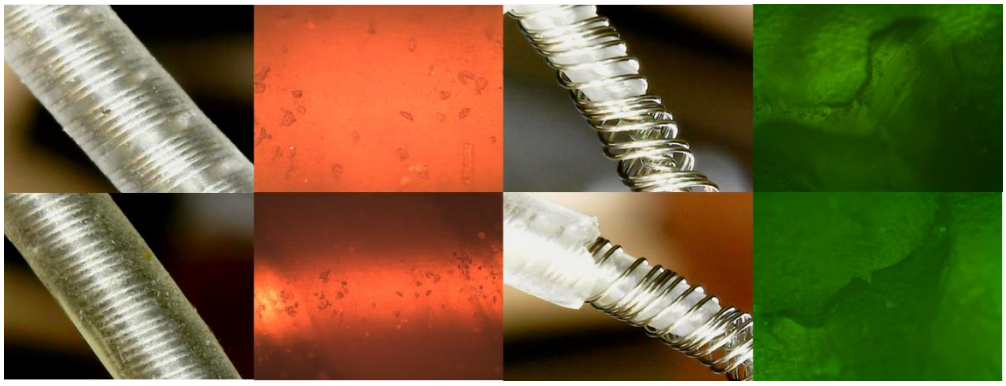

Figure 44 Microscopic inspection for the lead before and after tensile test

4.3 RESULTS

4.3.1 Load to Failure

The load to failure of the new lead was 26.477N ± 3.4 N. However, this value had deteriorated to 24.918N ± 0.55 N after 6 months of *in-vivo* implantation. The maximum load had decreased slightly after 9 months to reach 24.7543N±0.2N. Then the load to failure declined to 18.012N ± 5.33 N after 18 months of implantation (*P-value <0.0001*) and continued to decline to 13.3682N ±0.345N after 132 months of in-vivo exposure, as shown in Fig. 45.

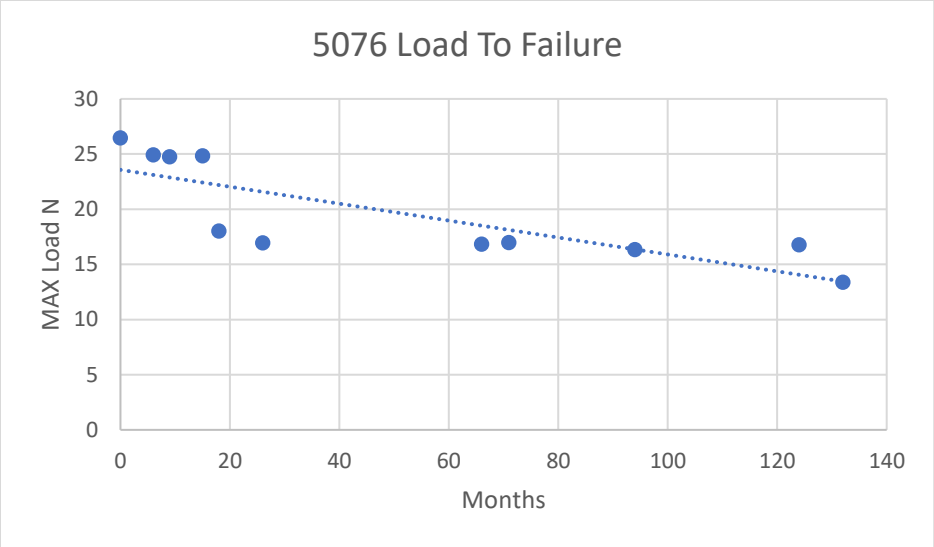

Figure 45 Representative Load to Failure vs in-vivo months plot of 5076 CapSureFix Novus MRI SureScan pacing leads

A mathematical model developed to predict the maximum load with respect to the number of in-vivo months:

$$Load\ to\ Failure = -0.0767x + 23.57$$

Where τ represents number of months.

Statistical analysis performed for the maximum load and found that there is a significant difference in maximum load after 18 months (*P-value <0.0001*), this difference can be represented by the drop of the load from 24.343N to 18.3566N. Student's T test used to compare between all the data in term of number of in-vivo months(α=0.01), and the connecting letters report was generated as shown in table 6.

Table 6 Connecting letter report for load to failure statistical analysis. Levels not connected by same letter are significantly different.

Connecting Letters Report			
Months			Mean
0	A		25.5091
6	A		24.9183
9	A		24.6585
15	A		24.3435
18		B	18.3566
26		B	16.9615
94		B	14.7436
124		B	14.3256
132		B	13.3192

4.3.2 Elongation to Failure

In addition, similar outcomes were found for the elongation to failure, as it declined from 173.2255 % ± 40.484% for the new lead to 140.761% ± 8.603% after 8 months of implantation. The percentage elongation dropped to 110.39% ± 2.25% after 15 months and continued to drop to 106.96% ± 5.4% after 94 months as shown in Fig.46. A mathematical model developed to predict the percentage elongation with respect to the number of in-vivo months:

$$Elongation\ to\ Failure = -0.3433x + 138.63$$

Where τ represents the number of months.

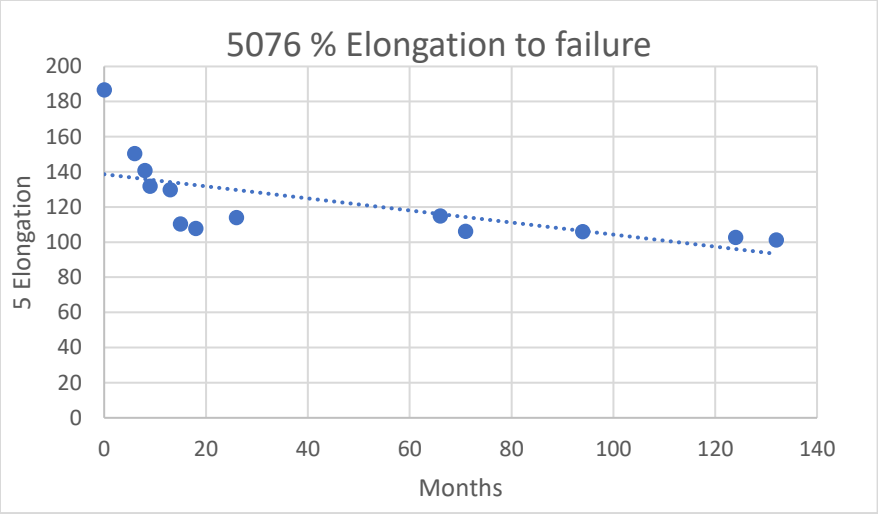

Figure 46 Representative Percentage Elongation vs in-vivo months plot of 5076 CapSureFix Novus MRI SureScan pacing leads

Statistical analysis performed for the elongation to failure. It was found there is a significant difference in elongation to failure after 94 months (*P-value<0.0001*), this difference can be represented by the drop of the elongation to failure from 132.2695 % to 111.507%. Then Student's T test used to compare between all the data in term of number of in-vivo months, and the connecting letters report generated as shown in table 7.

Table 7 Connecting letter report for percentage elongation statistical analysis. Levels not connected by same letter are significantly different

Connecting Letters Report				
Months				Mean
0	A			180.696
6		B		150.146
8		B		145.361
13		B	C	132.27
26		B	C	120.848

66		B	C	114.795
94			C	111.507
18			C	110.55
15			C	110.391
124			C	109.934
132			C	106.966
71			C	106.1

4.3.3 Percentage Elongation at 5N force

The percentage elongation was investigated in this study for 5 N force, as literature showed that the maximum load that can be applied to the lead in-vivo is within the range of 5 N [83]. Percentage elongation at 5N force was similar to percentage elongation during load to failure and resulting percentage elongation after tests. It showed there is a significant difference after 66 months of in-vivo exposure when compared to new lead (*P-value=0.0037*), as shown in table 8. A mathematical model developed to predict the 5N force percentage elongation with respect to the number of in-vivo months:

$$5N\ Force\ Percentage\ Elongation = -0.1205x + 21.905$$

Where τ represents the number of months.

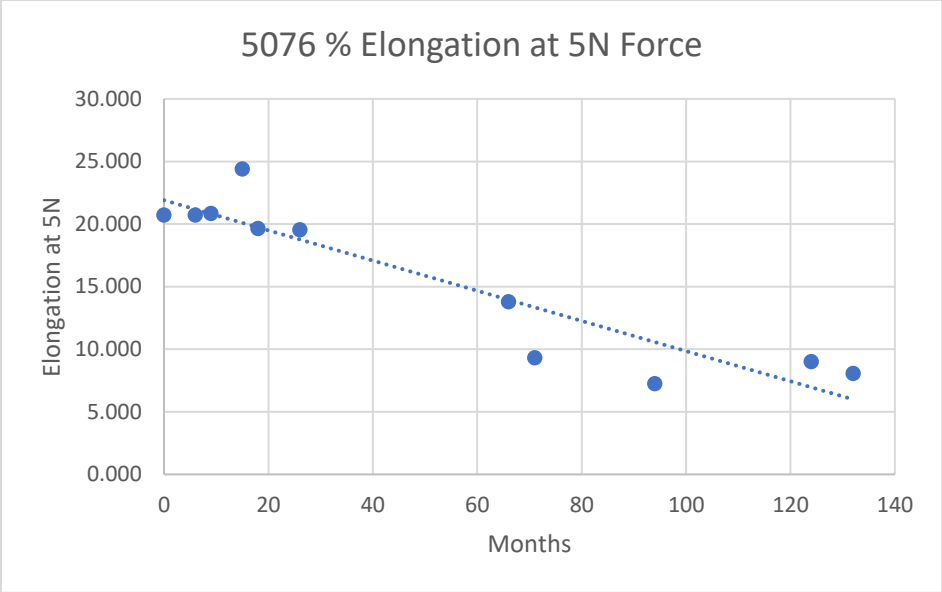

Figure 47 Representative Percentage Elongation at 5N vs in-vivo months plot of 5076 CapSureFix Novus MRI SureScan pacing leads

Table 8 Connecting letter report for 5N percentage elongation statistical analysis. Levels not connected by same letter are significantly different

Connecting Letters Report				
Months				Mean
0	A			20.73325
8	A			20.34955
15	A			19.1
66		B		13.79487
71		B	C	9.32
94			C	7.295
132			C	7.032

4.3.4 Ultimate Tensile Strength

Additionally, the ultimate tensile strength (UTS) was found to be 8.762 MPa ± 0.623 MPa for the new leads. The UTS has slightly decreased to 8.095 MPa ± 2.448 MPa after 6 months of implantation and continues decreasing until 73 months with significant decrement (*P-value =0.0339*) compared to the new lead. A mathematical model developed to predict ultimate tensile strength with respect to the number of in-vivo months:

$$UTS = -0.0331\tau + 8.4992$$

Where τ represents the number of months.

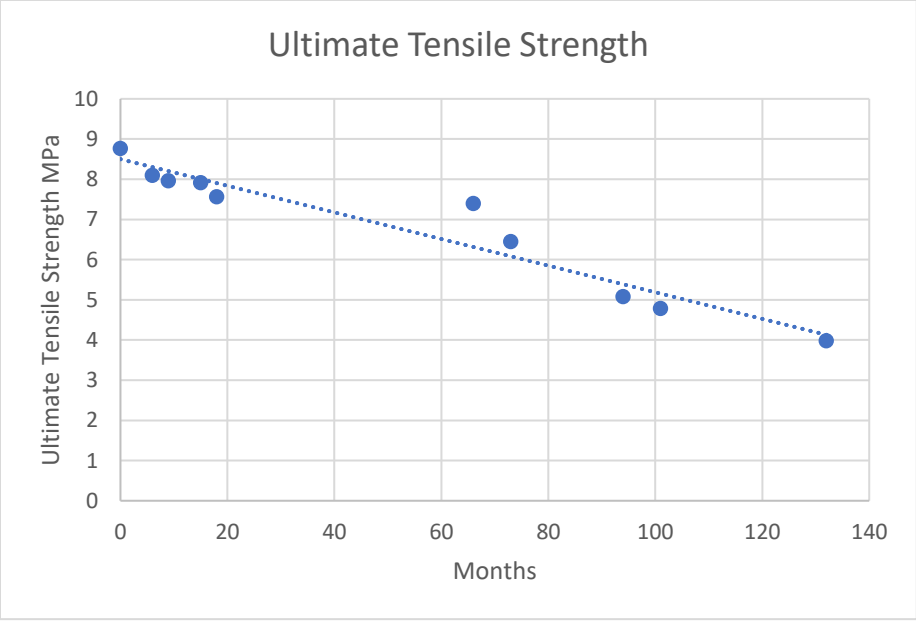

Figure 48 Representative Ultimate Tensile Strength vs in-vivo months plot of 5076 CapSureFix Novus MRI SureScan pacing leads

Table 9 Connecting letter report for Ultimate tensile strength statistical analysis. Levels not connected by same letter are significantly different

Connecting Letters Report						
Months						Mean
0	A					8.7615
6	A	B				8.09478
9	A	B				7.96449
15	A	B				7.91193
66	A	B				7.39405
18	A	B				7.03019
73		B	C			6.44735
74		B	C	D		6.18506
94			C	D	E	5.07465
124				D	E	4.86972
101			C	D	E	4.78037
132					E	3.9767

4.3.5 Modulus of Elasticity

Finally, the modulus of elasticity is calculated and statistically analyzed. Modulus of elasticity was directly proportional to the number of in-vivo exposure as shown in Fig.44. The statistical analysis showed a significant increase in modulus of elasticity after 73 months (*P-value =0.0051*). A mathematical model developed to predict the modulus of elasticity with respect to the number of in-vivo months:

$$E = 0.1077\tau + 9.4292$$

Where τ represents the number of months.

The residual properties of leads tested during this research are summarized in table 11. Duration of in-vivo environment, load to failure, elongation to failure, percentage elongation at 5N force, ultimate tensile strength, and modulus of elasticity presented along with where the insulation broke.

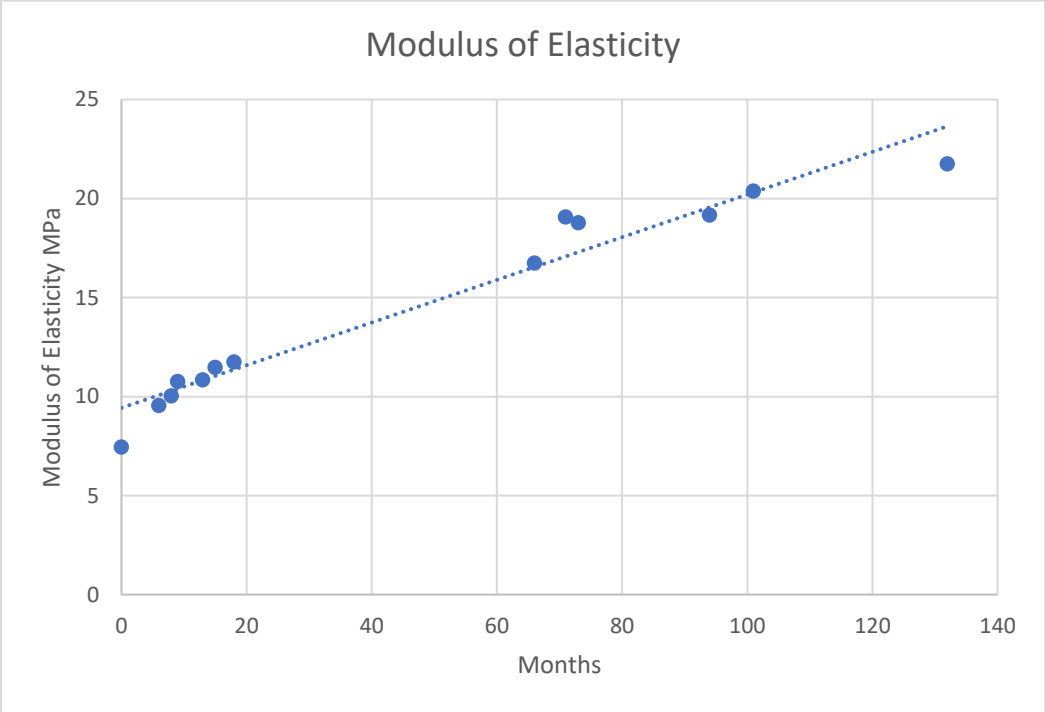

Figure 49 Representative Modulus of Elasticity vs in-vivo months plot of 5076 CapSureFix Novus MRI SureScan pacing lead

Table 10 Connecting letter report for Modulus of Elasticity statistical analysis. Levels not connected by same letter are significantly different

Connecting Letters Report							
Months							Mean
132	A						21.7643
101	A	B					20.3861
94	A	B	C				19.1738
71	A	B	C	D	E		19.0779
73	A	B	C	D			17.5802
66	A	B	C	D	E	F	16.751
18				D	E	F	11.7585
15			C	D	E	F	11.4847
13		B	C	D	E	F	10.8521
9			C	D	E	F	10.7684
8					E	F	10.0472
6				D	E	F	9.56144
0						F	7.45253

Table 11 Residual properties of the tested leads with corresponding area of insulation break

In-vivo Duration	**Load to failure (N)**	**Max. Elongation (%)**	**5N Elongation (%)**	**UTS (MPa)**	**Modulus of Elasticity (MPa)**	**No. of samples tested**	**Area of Insulation break**
New Lead	26.477	186.684	20.733	8.761	7.453	8	Middle
6 Months	24.918	150.365	20.711	8.095	9.561	7	Middle
9 Months	24.754	131.884	20.855	7.964	10.768	6	Middle

15 Months	24.843	110.391	24.394	7.912	11.485	7	Middle
18 Months	18.012	107.815	19.650	7.566	11.758	7	Middle
26 Months	16.962	114.045	19.550	5.653	9.419	6	Middle
66 Months	16.826	114.795	13.794	7.394	16.751	5	Lower
71 Months	16.976	106.100	9.320	6.447	19.078	8	Middle
94 Months	16.334	105.893	7.240	5.075	19.174	5	Middle
124 Months	15.291	102.673	9.023	4.780	20.386	5	Lower
132 Months	13.368	101.236	8.060	3.977	21.764	4	Middle

4.4 DISCUSSION

Understanding the deterioration of the residual properties and the performance of the leads after implantation is very important in order to improve lead materials and durability inside the human body. In this study, an investigation of the residual properties of the Medtronic 5076 CapSureFix Novus MRI SureScan lead was performed with respect to *in vivo* implantation duration. The results showed that the load to failure, UTS, and elongation dropped significantly after 18, 73 and 94 months of *in-vivo* exposure respectively. This is due to the effect of internal body environment on the insulator (silicone (MED-4719)). Longer exposure does not lower the mechanical properties at the same rate as it does during the first 18 months of exposure. Finally, a significant drop in the residual properties

occurred after 73 months of implantation, which is probably as a result of creep, abrasion, tear and environmental interaction [74].

On the other hand, modulus of elasticity showed an increase as the number of in-vivo months increased and reaches maximum elasticity at 132 months of in-vivo environment. This due to the reaction between blood and the lead, which may increase the temperature around the lead. Since silicone rubber has high coefficient of friction, its temperature increases easily due the chemical reaction that occurs around the surface of lead [75].

All in-vivo years are plotted individually, and a comparison was made between experimental results and predicted results, as shown in Fig. 50. All prediction equation are summarized in table 12.

The sensitivity plot (Fig.51) shows a relation between load to failure, elongation, and in-vivo exposure in years. And it can be inferred that both load to failure and elongation decrease with the increase of in-vivo exposure. Fig.52 shows a mathematical relationship of the measured parameters with each other. A sensitivity plot indicates with the increase in in-vivo exposure the modulus of elasticity increases, and the ultimate tensile strength decreases and vice versa.

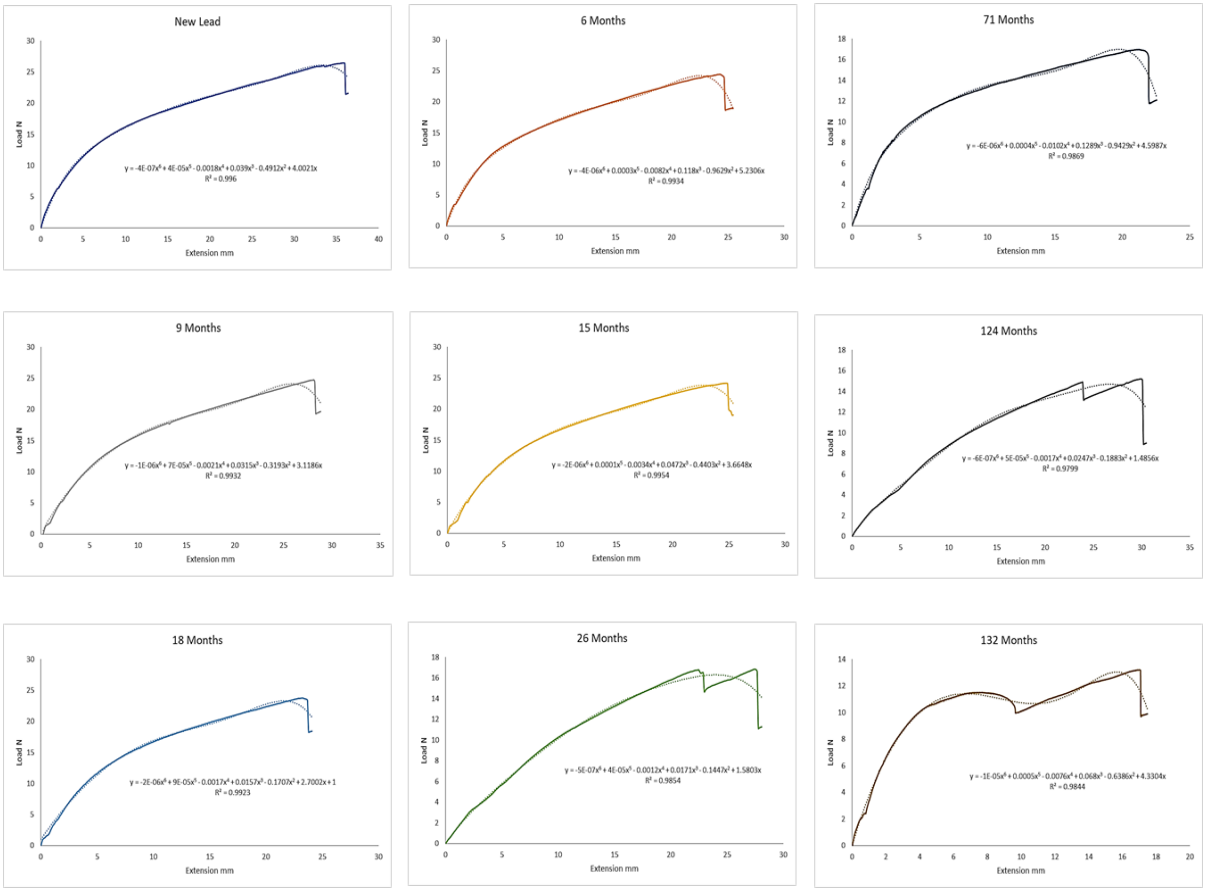

Figure 50 Representative Load vs extension plot for different In Vivo Implantation Durations

Table 12 Prediction Equations for each in-vivo duration, where x is the lead extension in mm

In-vivo Duration	**Prediction equation**	**R-squared**
New Lead	Pred.= -4E-07x^6 + 4E-05x^5 - 0.0018x^4 + 0.039x^3 - 0.4912x^2 + 4.0021x	0.996
6 months	Pred.= -4E-06x^6 + 0.0003x^5 - 0.0082x^4 + 0.118x^3 - 0.9629x^2 + 5.2306x	0.9934
9 months	Pred.= -1E-06x^6 + 7E-05x^5 - 0.0021x^4 + 0.0315x^3 - 0.3193x^2 + 3.1186x	0.9932
15 months	Pred.= -2E-06x^6 + 0.0001x^5 - 0.0034x^4 + 0.0472x^3 - 0.4403x^2 + 3.6648x	0.9954

18 months	Pred.= $-2E-06x^6 + 9E-05x^5 - 0.0017x^4 + 0.0157x^3 - 0.1707x^2 + 2.7002x + 1$	0.9923
26 months	Pred.= $-5E-07x^6 + 4E-05x^5 - 0.0012x^4 + 0.0171x^3 - 0.1447x^2 + 1.5803x$	0.9854
71 months	Pred.= $-6E-06x^6 + 0.0004x^5 - 0.0102x^4 + 0.1289x^3 - 0.9429x^2 + 4.5987x$	0.9869
124 months	Pred.= $-6E-07x^6 + 5E-05x^5 - 0.0017x^4 + 0.0247x^3 - 0.1883x^2 + 1.4856x$	0.9799
132 months	Pred.= $-1E-05x^6 + 0.0005x^5 - 0.0076x^4 + 0.068x^3 - 0.6386x^2 + 4.3304x$	0.9844

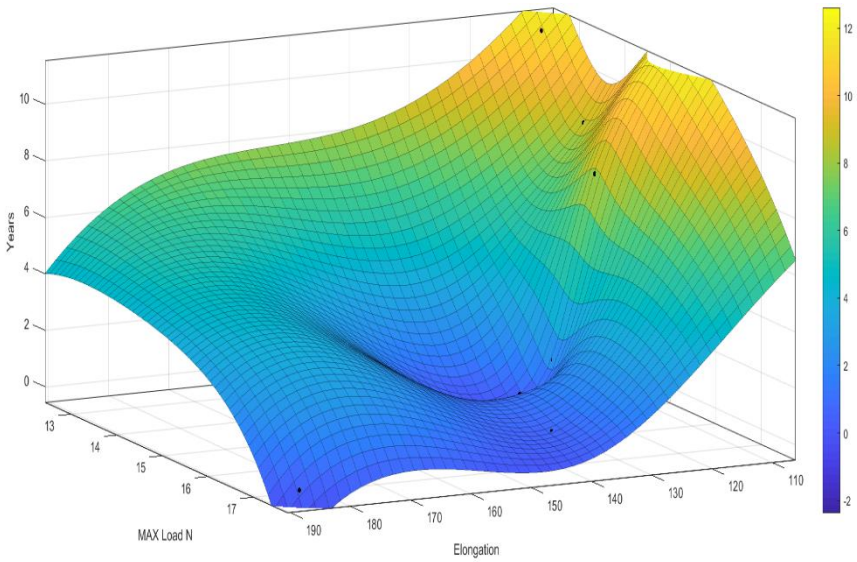

Figure 51 Sensitivity Plot representing Max. load vs Elongation vs in-vivo years

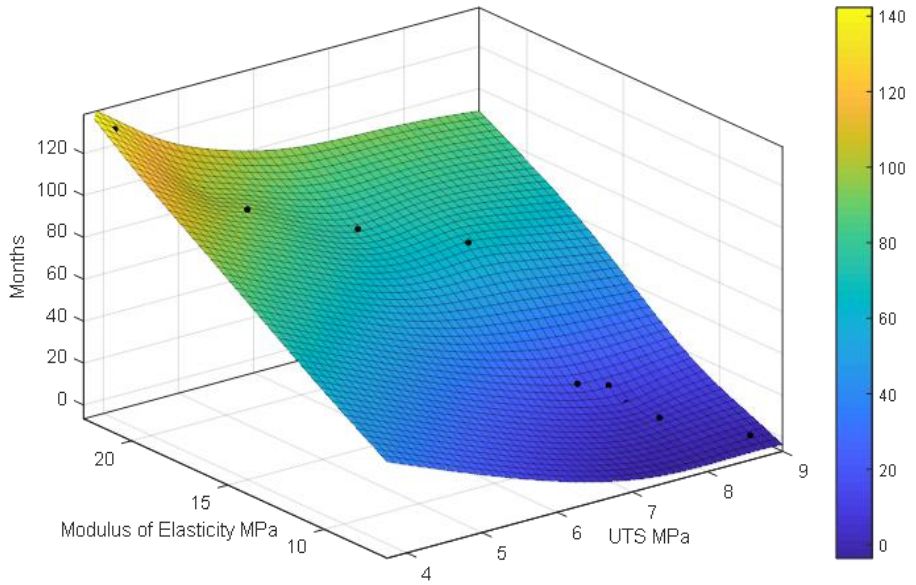

Figure 52 Sensitivity Plot representing Modulus of elasticity vs Ultimate tensile strength vs in-vivo months

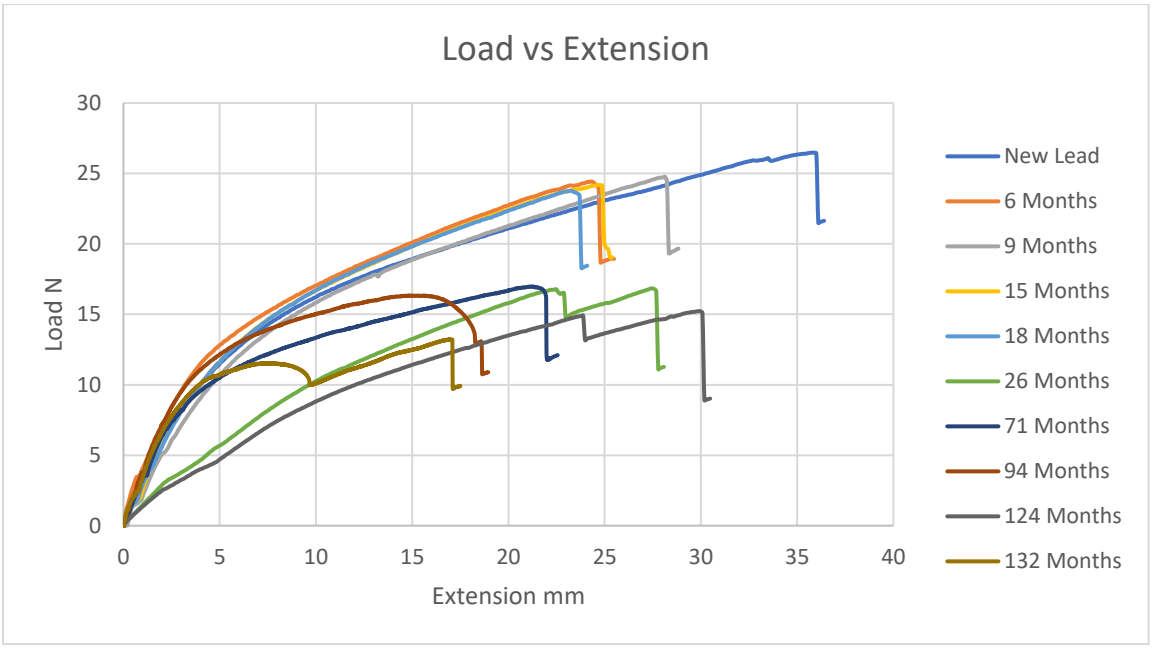

Figure 53 Representative Load vs extension plot of 5076 CapSureFix Novus MRI SureScan pacing leads

4.5 CONCLUSION

Medtronic 5076 CapSureFix Novus MRI SureScan Lead is still used as the main lead in their systems, and further investigations are required to fully understand it's in-vivo behavior. The materials used in the insulation are subjected to failure due to creep and wear. Load to failure showed a significant decrease after 18 months of in-vivo exposure (*P-value =0.0008)*. Percentage elongation showed a significant decrease after 94 months of in-vivo exposure (*P-value <0.0001*). Ultimate tensile strength showed significant decrease after 73 months of in-vivo exposure (*P-value =0.0339*) and percentage elongation at 5N force showed significant decrease after 66 months of in-vivo exposure (*P-value =0.0037*). On the other hand, modulus of elasticity was directly proportional with the in-vivo exposure time and showed significant increase (*P-value =0.0051*) after 73 months.

CHAPTER 5: CONCLUSION AND FUTURE RECOMMENTDATIONS

The devices used in this investigation were received from The Wright State Anatomical Gift Program. These devices were extracted posthumously and ranged from 3 months to 192 months of in-vivo exposure. It can be inferred that the pulse generator cases had mainly scratches that were shallow, narrow and could not have affected the functionality of the devices. The discoloration on the cases was caused by the growth of organic material from the body or due to the exposition to fluids (alcohol, bleach, dimethyl formaldehyde etc.) used in the sterilization process of the devices after their retrieval. However, the discoloration could not have affected the functionality of the devices. In addition, the investigation showed that the anterior side was more exposed to damage than the posterior side.

The leads, which consist of the inner coil, outer coil and the insulation around the coils, had visible insulation defect, stretches, and coil damages that caused different types of failures and could have affected the functionality of the devices. However, these damages may have happened during the extraction/pulling of the devices or during the replacement of the leads not during the *in vivo* usage. In general, Medtronic leads showed significant resistance to different damage modes when compared to Boston Scientific and St. Jude medical, and the middle part was more exposed to damage than the proximal part.

Damage summation equations were developed to determine the total damage for pulse generators and leads. A quantitative scoring assessment was performed for pulse generators and leads. Linear summation of damage modes described the total damage on both PG and leads. Using the survival probability of the devices from interrogation data and damage scores. Monte carlo simulation was performed to predict the failure probability associated risks. The output data for failure types were plotted in terms of actual values versus predicted values using JMP software.

Medtronic 5076 CapSureFix Novus MRI SureScan Lead is still used as the main lead in their systems, and further investigations are required to fully understand its in-vivo behavior. The materials used in the insulation are subjected to failure due to creep and wear. Load to failure showed a significant decrease after 18 months of in-vivo exposure (*P-value =0.0008*). Percentage elongation showed a significant decrease after 94 months of in-vivo exposure (*P-value<0.0001*). Ultimate tensile strength showed significant decrease after 73 months of in-vivo exposure (*P-value=0.0339*) and percentage elongation at 5N force showed significant decrease after 66 months of in-vivo exposure (*P-value =0.0037*). On the other hand, modulus of elasticity was directly proportional with the in-vivo exposure time and showed significant increase (*P-value =0.0051*) after 73 months. This thesis provides valuable data that could assist in the design of novel cardiac devices and enhance durability.

REFERENCES

[1] Fitzpatrick, D. (2015). *Implantable electronic medical devices* San Diego, CA : Elsevier/Academic Press, 2015].

[2] Kenny, T. (2005). *The nuts and bolts of cardiac pacing* Malden, Mass. : Blackwell Futura, 2005.

[3] Lin, G., Meverden, R. A., Hodge, D. O., Uslan, D. Z., Hayes, D. L., & Brady, P. A. (2008). Age and gender trends in implantable cardioverter defibrillator utilization: a population based study. *Journal of Interventional Cardiac Electrophysiology*, 22(1), 65-70.

[4] Bernard, M. L. (2016). Pacing without wires: leadless cardiac pacing. *Ochsner Journal*, *16*(3), 238-242.

[5] Vardas, P. E., Auricchio, A., Blanc, J. J., Daubert, J. C., Drexler, H., Ector, H., ... & Sutton, R. (2007). † Guidelines for cardiac pacing and cardiac resynchronization therapy: The Task Force for Cardiac Pacing and Cardiac Resynchronization Therapy of the European Society of Cardiology. Developed in Collaboration with the European Heart Rhythm Association. *European heart journal*, *28*(18), 2256-2295.

[6] Zhang, S., Kriza, C., Schaller, S., & Kolominsky-Rabas, P. L. (2015). Recalls of cardiac implants in the last decade: What lessons can we learn?. *PloS one*, *10*(5), e0125987.

[7] Jacobs, D. M., FINK, A. S., MILLER, R. P., ANDERSON, W. R., MCVENES, R. D., LESSAR, J. F., ... & BUBRICK, M. P. (1993). Anatomical and morphological evaluation of pacemaker lead compression. *Pacing and Clinical Electrophysiology*, *16*(3), 434-444.

[8] Wiggins, M. J., Wilkoff, B., Anderson, J. M., & Hiltner, A. (2001). Biodegradation of polyether polyurethane inner insulation in bipolar pacemaker leads. *Journal of Biomedical Materials Research Part A*, *58*(3), 302-307.

[9] Kron, J., Herre, J., Renfroe, E. G., Rizo-Patron, C., Raitt, M., Halperin, B., ... & Olarte, A. (2001). Lead-and device-related complications in the antiarrhythmics versus implantable defibrillators trial. *American heart journal*, *141*(1), 92-98.

[10] Chan, C. W., Chan, L. K., Lam, T., Tsang, K. K., & Chan, K. W. (2018). Comparative study about the tensile strength and yielding mechanism of pacing lead among major manufacturers. *Pacing and Clinical Electrophysiology*, *41*(7), 828-833.

[11] Starck, C. T., Stepuk, A., Holubec, T., Steffel, J., Stark, J. W., & Falk, V. (2014). Compression coil provides increased lead control in extraction procedures. *Ep Europace*, *17*(3), 499-503.

[12] Wilkoff, B. L., Rickard, J., Tkatchouk, E., Padsalgikar, A. D., Gallagher, G., & Runt, J. (2016). The biostability of cardiac lead insulation materials as assessed from long-term human implants. *Journal of Biomedical Materials Research Part B: Applied Biomaterials*, *104*(2), 411-421.

[13] Sardu, C., Paolisso, P., Sacra, C., Santamaria, M., de Lucia, C., Ruocco, A., ... & Marfella, R. (2018). Cardiac resynchronization therapy with a defibrillator (CRTd) in failing heart patients with type 2 diabetes mellitus and treated by glucagon-like peptide 1 receptor agonists (GLP-1 RA) therapy vs. conventional hypoglycemic drugs: arrhythmic burden, hospitalizations for heart failure, and CRTd responders rate. *Cardiovascular diabetology*, *17*(1), 137.

[14] Magnusson, P., & Liv, P. (2018). Living with a pacemaker: patient-reported outcome of a pacemaker system. *BMC cardiovascular disorders*, *18*(1), 110.

[15] Brignole, M., Auricchio, A., Baron-Esquivias, G., Bordachar, P., Boriani, G., ... & Elliott, P. M. (2013). 2013 ESC Guidelines on cardiac pacing and cardiac resynchronization therapy: the Task Force on cardiac pacing and resynchronization therapy of the European Society of Cardiology (ESC). Developed in collaboration with the European Heart Rhythm Association (EHRA). *European heart journal*, *34*(29), 2281-2329.

[16] Kenny, T. (2018). *The nuts and bolts of cardiac pacing*. John Wiley & Sons.

[17] Lamas, G. A., Lee, K. L., Sweeney, M. O., Silverman, R., Leon, A., Yee, R., ... & Hellkamp, A. S. (2002). Ventricular pacing or dual-chamber pacing for sinus-node dysfunction. *New England Journal of Medicine*, *346*(24), 1854-1862.

[18] Saksena, S., Prakash, A., Ziegler, P., Hummel, J. D., Friedman, P., Plumb, V. J., ... & DAPPAF Investigators. (2002). Improved suppression of recurrent atrial fibrillation

with dual-site right atrial pacing and antiarrhythmic drug therapy. *Journal of the American College of Cardiology*, *40*(6), 1140-1150.

[19] Waks, J. W., Passman, R. S., Matos, J., Reynolds, M., Thosani, A., Mela, T., ... & Zimetbaum, P. (2018). Intermittent anticoagulation guided by continuous atrial fibrillation burden monitoring using dual-chamber pacemakers and implantable cardioverter-defibrillators: Results from the Tailored Anticoagulation for Non-Continuous Atrial Fibrillation (TACTIC-AF) pilot study. *Heart rhythm*, *15*(11), 1601-1607.

[20] Tayal, B., Gorcsan, J., Bax, J. J., Risum, N., Olsen, N. T., Singh, J. P., ... & Krum, H. (2018). Cardiac resynchronization therapy in patients with heart failure and narrow QRS complexes. *Journal of the American College of Cardiology*, *71*(12), 1325-1333.

[21] Love, C. J., & Love, C. J. (2006). *Cardiac pacemakers and defibrillators* Georgetown, Tex. : Landes Bioscience, c2006; 2nd ed.

[22] Nordkamp, L. R. O., Postema, P. G., Knops, R. E., van Dijk, N., Limpens, J., Wilde, A. A., & de Groot, J. R. (2016). Implantable cardioverter-defibrillator harm in young patients with inherited arrhythmia syndromes: a systematic review and meta-analysis of inappropriate shocks and complications. *Heart Rhythm*, *13*(2), 443-454.

[23] Hayes, D. L., & Friedman, P. A. (2011). *Cardiac pacing, defibrillation and resynchronization: a clinical approach*. John Wiley & Sons.

[24] Bock, D. C., Marschilok, A. C., Takeuchi, K. J., & Takeuchi, E. S. (2012). Review article: Batteries used to power implantable biomedical devices. *Electrochimica Acta, 84*, 155-164. doi:10.1016/j.electacta.2012.03.057

[25] MOND, H. G., & FREITAG, G. (2014). The Cardiac Implantable Electronic Device Power Source: Evolution and Revolution. *Pacing & Clinical Electrophysiology*, *37*(12), 1728–1745. https://doi-org.ezproxy.libraries.wright.edu/10.1111/pace.12526

[26] Takeuchi, E. S., & Leising, R. A. (2002). Lithium batteries for biomedical applications. MRS bulletin, 27(8), 624-627.

[27] Ikeda, H. (1977). S: U6no, T. Saito, S. Nakaido, and H. Tamura. Denki Kagaku, 45, 391.

[28] Bock, D. C., Marschilok, A. C., Takeuchi, K. J., & Takeuchi, E. S. (2012). Batteries used to power implantable biomedical devices. *Electrochimica acta*, *84*, 155-164.

[29] Nishio, K. (2009). PRIMARY BATTERIES–NONAQUEOUS SYSTEMS| Lithium–Manganese Dioxide.

[30] Watanabe, N., & Fukuda, M. (1970). *U.S. Patent No. 3,536,532*. Washington, DC: U.S. Patent and Trademark Office.

[31] Watanabe, N., & Fukoda, M. (1972). U.S. Patent No. 3,700,502. Washington, DC: U.S. Patent and Trademark Office.

[32] Greatbatch, W., Holmes, C. F., Takeuchi, E. S., & Ebel, S. J. (1996). Lithium/carbon monofluoride (LI/CFx): a new pacemaker battery. Pacing and clinical electrophysiology, 19(11), 1836-1840.

[33] Brodd, R. J., Bullock, K. R., Leising, R. A., Middaugh, R. L., Miller, J. R., & Takeuchi, E. (2004). Batteries, 1977 to 2002. Journal of the Electrochemical Society, 151(3), K1-K11.

[34] Gan, H., Rubino, R. S., & Takeuchi, E. S. (2005). Dual-chemistry cathode system for high-rate pulse applications. *Journal of power sources*, *146*(1), 101-106.

[35] Chen, K., Merritt, D. R., Howard, W. G., Schmidt, C. L., & Skarstad, P. M. (2006). Hybrid cathode lithium batteries for implantable medical applications. Journal of power sources, 162(2), 837-840.

[36] Holmes, C. (2007). The lithium/iodine-polyvinylpyridine pacemaker battery-35 years of successful clinical use. ECS Transactions, 6(5), 1-7.

[37] Drews, J., Fehrmann, G., Staub, R., & Wolf, R. (2001). Primary batteries for implantable pacemakers and defibrillators. Journal of power sources, 97, 747-749.

[38] Davis, S., Takeuchi, E. S., Tiedemann, W., & Newman, J. (2007). Simulation of the Li–CF x System. Journal of the Electrochemical Society, 154(5), A477-A480.

[39] Chen, K., Merritt, D. R., Howard, W. G., Schmidt, C. L., & Skarstad, P. M. (2006). Hybrid cathode lithium batteries for implantable medical applications. Journal of power sources, 162(2), 837-840.

[40] Ellenbogen, K. A., & Kaszala, K. (2014). *Cardiac pacing and ICDs* Chichester, West Sussex : John Wiley & Sons, 2014; Sixth edition.

[41] Swerdlow, C. D., Kalahasty, G., & Ellenbogen, K. A. (2016). Implantable cardiac defibrillator lead failure and management. *Journal of the American College of Cardiology*, *67*(11), 1358-1368.

[42] Korpas, D. (2013). *Implantable cardiac devices technology*. Springer.

[43] Adapta, M. (2017). Versa™, Sensia™, Relia™ Pacemaker Reference Guide, M965319A001 C. Accessed June, 26, 55432-5604.

[44] Hauser, R. G., Abdelhadi, R. H., McGriff, D. M., & Kallinen Retel, L. (2012). Failure of a novel silicone–polyurethane copolymer (Optim™) to prevent implantable cardioverter-defibrillator lead insulation abrasions. *Europace*, *15*(2), 278-283.

[45] De Lurgio, D. B., Sathavorn, C., Mera, F., Leon, A., Walter, P. F., & Langberg, J. J. (1997). Incidence and implications of abrasion of implantable cardioverter-defibrillator leads. *The American journal of cardiology*, *79*(10), 1409-1411.

[46] Jenney, C., Tan, J., Karicherla, A., Burke, J., & Helland, J. (2005). A new insulation material for cardiac leads with potential for improved performance. *Heart Rhythm*, *2*(5), S318-S319.

[47] Ellenbogen, K. A., Wood, M. A., Shepard, R. K., Clemo, H. F., Vaughn, T., Holloman, K., ... & Verness, D. (2003). Detection and management of animplantable cardioverter defibrillator lead failure: Incidence and clinical implications. *Journal of the American College of Cardiology*, *41*(1), 73-80.

[48] Degeratu, F. T., Khalighi, K., Peters, R. W., Shorofsky, S. R., & Gold, M. R. (2000). Sensing lead failure in implantable defibrillators: a comparison of two commonly used leads. *Journal of cardiovascular electrophysiology*, *11*(1), 21-24.

[49] Hayes, D. L., Graham, K. J., Irwin, M., Vidaillet, H., Disler, G., Sweesy, M., ... & Seebandt, M. (1995). Multicenter experience with a bipolar tined polyurethane ventricular lead. *Pacing and Clinical Electrophysiology*, *18*(5), 999-1004.

[50] Antonelli, D., Rosenfeld, T., Freedberg, N. A., Palma, E., Gross, J. N., & Furman, S. (1998). Insulation lead failure: is it a matter of insulation coating, venous approach, or both?. *Pacing and clinical electrophysiology*, *21*(2), 418-421.

[51] Parvathaneni, S. V., Ellis, C. R., & Rottman, J. N. (2012). High prevalence of insulation failure with externalized cables in St. Jude Medical Riata family ICD leads: fluoroscopic grading scale and correlation to extracted leads. *Heart Rhythm*, *9*(8), 1218-1224.

[52] Erkapic, D., Duray, G. Z., Bauernfeind, T., De Rosa, S., & Hohnloser, S. H. (2011). Insulation defects of thin high-voltage ICD leads: an underestimated problem?. *Journal of cardiovascular electrophysiology*, *22*(9), 1018-1022.

[53] Shah, A. D., Hirsh, D. S., & Langberg, J. J. (2016). Sudden and fatal malfunction of a durata defibrillator lead due to external insulation failure. *Pacing and Clinical Electrophysiology*, *39*(1), 101-104.

[54] Antonelli, D., Rosenfeld, T., Freedberg, N. A., Palma, E., Gross, J. N., & Furman, S. (1998). Insulation lead failure: is it a matter of insulation coating, venous approach, or both?. *Pacing and clinical electrophysiology*, *21*(2), 418-421.

[55] LIM, K. K., Reddy, S., Desai, S., Smelley, M., Kim, S. S., Beshai, J. F., ... & Knight, B. P. (2009). Effects of electrocautery on transvenous lead insulation materials. *Journal of cardiovascular electrophysiology*, *20*(4), 429-435.

[56] Kron, J., Herre, J., Renfroe, E. G., Rizo-Patron, C., Raitt, M., Halperin, B., ... & Olarte, A. (2001). Lead-and device-related complications in the antiarrhythmics versus implantable defibrillators trial. *American heart journal*, *141*(1), 92-98.

[57] Ząbek, A., Małecka, B., Kołodzińska, A., Maziarz, A., Lelakowski, J., & Kutarski, A. (2012). Early abrasion of outer silicone insulation after intracardiac lead friction in a patient with cardiac device-related infective endocarditis. *Pacing and Clinical Electrophysiology*, *35*(6), e156-e158.

[58] Magney, J. E., FLYNN, D. M., PARSONS, J. A., STAPLIN, D. H., CHIN-PURCELL, M. V., MILSTEIN, S., & HUNTER, D. W. (1993). Anatomical mechanisms explaining damage to pacemaker leads, defibrillator leads, and failure of central venous catheters adjacent to the sternoclavicular joint. *Pacing and Clinical Electrophysiology*, *16*(3), 445-457.

[59] Kołodzińska, A., Kutarski, A., Kozłowska, M., Grabowski, M., Marchel, H., Drela, N., & Opolski, G. (2013). Biodegradation of the outer silicone insulation of endocardial leads. *Circulation: Arrhythmia and Electrophysiology*, *6*(2), 279-286.

[60] Wilkoff, B. L., Rickard, J., Tkatchouk, E., Padsalgikar, A. D., Gallagher, G., & Runt, J. (2016). The biostability of cardiac lead insulation materials as assessed from long-term human implants. *Journal of Biomedical Materials Research Part B: Applied Biomaterials*, *104*(2), 411-421.

[61] Gaziano, T. A., Bitton, A., Anand, S., Abrahams-Gessel, S., & Murphy, A. (2010). Growing epidemic of coronary heart disease in low-and middle-income countries. *Current problems in cardiology*, *35*(2), 72-115.

[62] Vilahur, G., Badimon, J. J., Bugiardini, R., & Badimon, L. (2014). Perspectives: The burden of cardiovascular risk factors and coronary heart disease in Europe and worldwide. *European Heart Journal Supplements*, *16*(suppl_A), A7-A11.

[63] Haddad, S. A. P., & Serdijn, W. A. (2009). *Ultra low-power biomedical signal processing: an analog wavelet filter approach for pacemakers*. Springer Science & Business Media.

[64] Hesselson, A. B. (2008). Simplified Interpretation of Pacemaker ECGs: An Introduction. John Wiley & Sons.

[65] Childs, K., Crosby, L., & Goswami, T. (2016). Quantitative Analysis of Retrieved Glenoid Liners. *Lubricants*, *4*(1), 3.

[66] Hauser, R. G., McGriff, D., & Retel, L. K. (2012). Riata implantable cardioverter-defibrillator lead failure: analysis of explanted leads with a unique insulation defect. *Heart Rhythm*, *9*(5), 742-749.

[67] Medtronic Inc. Medtronic CRM product performance report— Issue 78 MDT CRHF PPR 2018 1st Edition.

[68] (November 1, 2000). Guidance for the Submission of Research and Marketing Applications for Permanent Pacemaker Leads and for Pacemaker Lead Adaptor 510(k) Submissions. US Department of Health and Human Services, Food and Drug Administration, Center for Devices and Radiological Health and Interventional Cardiology Devices Branch, Division of Cardiovascular and Respiratory Devices, Office of Device Evaluation.

[69] Rack, H. J., & Qazi, J. I. (2006). Titanium alloys for biomedical applications. *Materials Science and Engineering: C*, *26*(8), 1269-1277.

[70] Fortescue, E. B., Berul, C. I., Cecchin, F., Walsh, E. P., Triedman, J. K., & Alexander, M. E. (2004). Patient, procedural, and hardware factors associated with pacemaker lead failures in pediatrics and congenital heart disease. *Heart Rhythm*, *1*(2), 150-159.

[71] Jacobs, D. M., FINK, A. S., MILLER, R. P., ANDERSON, W. R., MCVENES, R. D., LESSAR, J. F., ... & BUBRICK, M. P. (1993). Anatomical and morphological evaluation of pacemaker lead compression. *Pacing and Clinical Electrophysiology*, *16*(3), 434-444.

[72] Fortescue, E. B., Berul, C. I., Cecchin, F., Walsh, E. P., Triedman, J. K., & Alexander, M. E. (2004). Patient, procedural, and hardware factors associated with pacemaker lead failures in pediatrics and congenital heart disease. *Heart Rhythm*, *1*(2), 150-159.

[73] Kusumoto, F. M., & Goldschlager, N. F. (Eds.). (2007). *Cardiac pacing for the clinician*. Springer Science & Business Media.

[74] Haqqani, H. M., Epstein, L. M., & Cooper, J. M. (2011). Engineering and construction of pacemaker and ICD leads.

[75] Helguera, M. E., Maloney, J. D., Pinski, S. L., Woscoboinik, J. R., WILKOEE, B. L., & Castle, L. W. (1994). Long-term performance of endocardial pacing leads. *Pacing and Clinical Electrophysiology*, *17*(1), 56-64.

[76] ASTM, D. (2004). 1708-02a "Standard Test Method for Tensile Properties of Plastics By Use of Microtensile Specimens". *Annual Book of ASTM Standards*, 394-398.

[77] Standard, A. S. T. M. D412-06a (2013) Standard test methods for vulcanized rubber and thermoplastic elastomers—tension. *ASTM International, West Conshohocken, PA. doi*, *10*.

[78] Miller, M. A., Neuzil, P., Dukkipati, S. R., & Reddy, V. Y. (2015). Leadless cardiac pacemakers: back to the future. *Journal of the American College of Cardiology*, *66*(10), 1179-1189.

[79] Nazif, T. M., Dizon, J. M., Hahn, R. T., Xu, K., Babaliaros, V., Douglas, P. S., ... & Miller, D. C. (2015). Predictors and clinical outcomes of permanent pacemaker implantation after transcatheter aortic valve replacement: the PARTNER (Placement of AoRtic TraNscathetER Valves) trial and registry. JACC: Cardiovascular Interventions, 8(1 Part A), 60-69.

[80] Edwards, S. J., Karner, C., Trevor, N., Wakefield, V., & Salih, F. (2015). Dual-chamber pacemakers for treating symptomatic bradycardia due to sick sinus syndrome without atrioventricular block: a systematic review and economic evaluation.

[81] Wilkoff, B. L., Cook, J. R., Epstein, A. E., Greene, H. L., Hallstrom, A. P., Hsia, H., ... & Sharma, A. (2002). Dual-chamber pacing or ventricular backup pacing in patients with an implantable defibrillator: the Dual Chamber and VVI Implantable Defibrillator (DAVID) Trial. Jama, 288(24), 3115-3123.

[82] Mehta, D., Nayak, H. M., Singson, M., Chao, S., CAMUÑAS, J. L., & GOMES, J. A. (1998). Late complications in patients with pectoral defibrillator implants with transvenous defibrillator lead systems: high incidence of insulation breakdown. Pacing and clinical electrophysiology, 21(10), 1893-1900.

[83] Lennerz, C., Pavaci, H., Grebmer, C., von Olshausen, G., Semmler, V., Buiatti, A., ... & Kolb, C. (2014). Forces applied during transvenous implantable cardioverter defibrillator lead removal. BioMed research international, 2014.

[84] Greenspon, A. J., Patel, J. D., Lau, E., Ochoa, J. A., Frisch, D. R., Ho, R. T., ... & Kurtz, S. M. (2012). Trends in permanent pacemaker implantation in the United States from 1993 to 2009: increasing complexity of patients and procedures. *Journal of the American College of Cardiology*, *60*(16), 1540-1545.

[85] Lambiase, P. D., Barr, C., Theuns, D. A., Knops, R., Neuzil, P., Johansen, J. B., ... & Reeve, H. L. (2014). Worldwide experience with a totally subcutaneous implantable defibrillator: early results from the EFFORTLESS S-ICD Registry. European heart journal, 35(25), 1657-1665.

APPENDIX I LIST OF DEVICES

Table 13 Devices Serial numbers, model, type, manufacturer, and status

#	Model	Type	SN	Manufacturer	Status
1	EnPulse DDDR	Pacemaker DR	PNB453720H	MDT	Not Active
2	EnPulse DDDR	Pacemaker DR	PN8474286H	MDT	Active
3	EnPulse DDDR	Pacemaker DR	PNB462475H	MDT	Not Active
4	EnPulse DDDR	Pacemaker DR	PWU411542H	MDT	Not Active
5	REAVEAL XT	Loop Recorder	RAB508196H	MDT	Not Active
6	ADVISA DR MRI	Pacemaker DR	PAY287174H	MDT	Active
7	ADVISA DR MRI	Pacemaker DR	PAY354210H	MDT	Active
8	ADAPTA DDDR	Pacemaker DR	PWB261682H	MDT	Not Active
9	ADAPTA DDDR	Pacemaker DR	NWB540331H	MDT	Active
10	SENSIA SSIR	Pacemaker SR	NWR205596H	MDT	Not Active
11	SENSIA SSIR	Pacemaker SR	NWE205745H	MDT	Active
12	SENSIA DDDR	Pacemaker DR	NWL230140H	MDT	Active
13	SENSIA DDDR	Pacemaker DR	NWL230175H	MDT	Not Active
14	REVO MRI DDDR	Pacemaker DR	PTN264280H	MDT	Active
15	SECURA DR	ICD DR	PUG205844H	MDT	Not Active
16	CONCERTO II CRT-D	CRT-D	PZA204401H	MDT	Active
17	VIVA XT CRT-D	CRT-D	BLF234921H	MDT	Active
18	VIVA XT CRT-D	CRT-D	BLF221559H	MDT	Not Active
19	CONSULTA CRT-D	CRT-D	PUD220940H	MDT	Not Active
20	EVERA MRI XT DR	ICD DR	PFZ201839H	MDT	Active
21	ENRHYTHM DDDR	Pacemaker DR	PNP488829H	MDT	Active
22	ENRHYTHM DDDR	Pacemaker DR	PNP422130H	MDT	Active
23	ADAPTA DDDR	Pacemaker DR	NWB424054H	MDT	Active
24	ADAPTA DDDR	Pacemaker DR	NWB201749H	MDT	Not Active
25	ADAPTA DDDR	Pacemaker DR	PWB268153H	MDT	Not Active
26	ADAPTA DDDR	Pacemaker DR	NWB528525H	MDT	Not Active
27	KAPPA DDDR	Pacemaker DR	PGU402621H	MDT	Not Active
28	SIGMA S DR	Pacemaker DR	PJD194315H	MDT	Not Active
29	SYNCRA CRT-P	CRT-P	PZX603451S	MDT	Active
30	CONSULTA CRT-D	CRT-D	PUD227370H	MDT	Not Active
31	ENTRUST DR	ICD DR	PNR425289H	MDT	Not Active
32	CONSULTA CRT-D	CRT-D	PUD205493H	MDT	Not Active
33	MAXIMO II DR	ICD DR	PZM201316H	MDT	Not Active

34	Adapta DR	Pacemaker DR	NWB217705H	MDT	Active
35	Adapta DR	Pacemaker DR	NWB525560H	MDT	Active
36	Adapta DR	Pacemaker DR	NWB558100H	MDT	Active
37	Adapta DR	Pacemaker DR	BWB297611H	MDT	Not Active
38	Advisa DR MRI SureScan	Pacemaker DR	PAY338992H	MDT	Active
39	Claria MRI SureScan	CRT-D	RPT200404H	MDT	Active
40	Viva XT CRT-D	CRT-D	BLF225581H	MDT	Active
41	Viva XT CRT-P	CRT-P	PVZ602494S	MDT	Active
42	Consulta CRT-P	CRT-P	PVX625114S	MDT	Active
43	Consulta CRT-P	CRT-P	PVX621568S	MDT	Active
44	Evera XT VR	ICD-VR	BWI215647H	MDT	Not Active
45	Evera XT VR	ICD-VR	BWI214708H	MDT	Active
46	Protecta XT	ICD DR	PSA212334H	MDT	Active
47	Evera XT DR	ICD DR	BWB207000H	MDT	Active
48	INSIGNIA PLUS SSIR	Pacemaker SR	111673	BSC	Not Active
49	INSIGNIA 1 PLUS DDDR	Pacemaker DR	952466	BSC	Active
50	ESSENTIO DDDR	Pacemaker DR	733737	BSC	Active
51	COGNIS 100-D	CRT-D	202270	BSC	Active
52	ENERDEN ICD	ICD-DR	111850	BSC	Active
53	VITALITY DS	ICD-DR	124431	BSC	Active
54	VITALITY HE	ICD-DR	200093	BSC	Active
55	ALTRUA 60 DDDR	Pacemaker DR	952367	BSC	Active
56	ADVANTIO DDDR	Pacemaker DR	118816	BSC	Active
57	COGNIS 100-D	CRT-D	485497	BSC	Active
58	Teligen 100	ICD-DR	250119	BSC	Not Active
59	Advantio	Pacemaker DR	121699	BSC	Active
60	Altura 60 DR	Pacemaker DR	843287	BSC	Active
61	Accolade MRI	Pacemaker SR	739063	BSC	Active
62	Ingenio VR	Pacemaker SR	116716	BSC	Active
63	Fortify Assura	ICD DR	7230932	St. Jude	Active
64	ZEPHYR XL DR	Pacemaker DR	1294876	St. Jude	Not Active
65	PARAGON DDDC	Pacemaker DR	34400	St. Jude	Not Active

APPENDIX II TOTAL DAMAGE SCORE EQUATIONS

Pulse Generator Total Damage Score

$$Pulse\ Generator\ Total\ Damage\ Score = \sum_{x=1}^{2}\sum_{y=1}^{n} Severity\ Score_{xy}$$
$$= \sum_{x=1}^{2} Surface\ Deformation\ Severity\ Score_x + \sum_{x=1}^{2} Discoloration\ Severity\ Score_x + \sum_{x=1}^{2} Scratching\ Severity\ Score_x + \sum_{x=1}^{2} Burnishing\ Severity\ Score_x + \sum_{x=1}^{2} Pitting\ Severity\ Score_x + \sum_{x=1}^{2} Abrasion\ Severity\ Score_x$$

Where x=1 through 2 represents the anterior and posterior part of the pulse generator.

Lead Total Damage Score

$$Lead\ Total\ Damage\ Score = \sum_{x=1}^{2}\sum_{y=1}^{n} Severity\ Score_{xy}$$
$$\sum_{x=1}^{3} Surface\ Deformation\ Severity\ Score_x + \sum_{x=1}^{3} Discoloration\ Severity\ Score_x + \sum_{x=1}^{3} Scratching\ Severity\ Score_x + \sum_{x=1}^{3} Burnishing\ Severity\ Score_x + \sum_{x=1}^{3} Insulation\ Defect\ Severity\ Score_x$$

$$+\sum_{x=1}^{3} Abrasion\ Severity\ Score_x$$
$$+\sum_{x=1}^{3} Coil\ Damage\ Severity\ Score_x$$
$$+\sum_{x=1}^{3} Delamination\ \ Severity\ Score_x$$
$$+\sum_{x=1}^{3} Pitting\ Severity\ Score_x$$

Where x=1 through 2 represents each part of the lead.

APPENDIX III PULSE GENERATOR

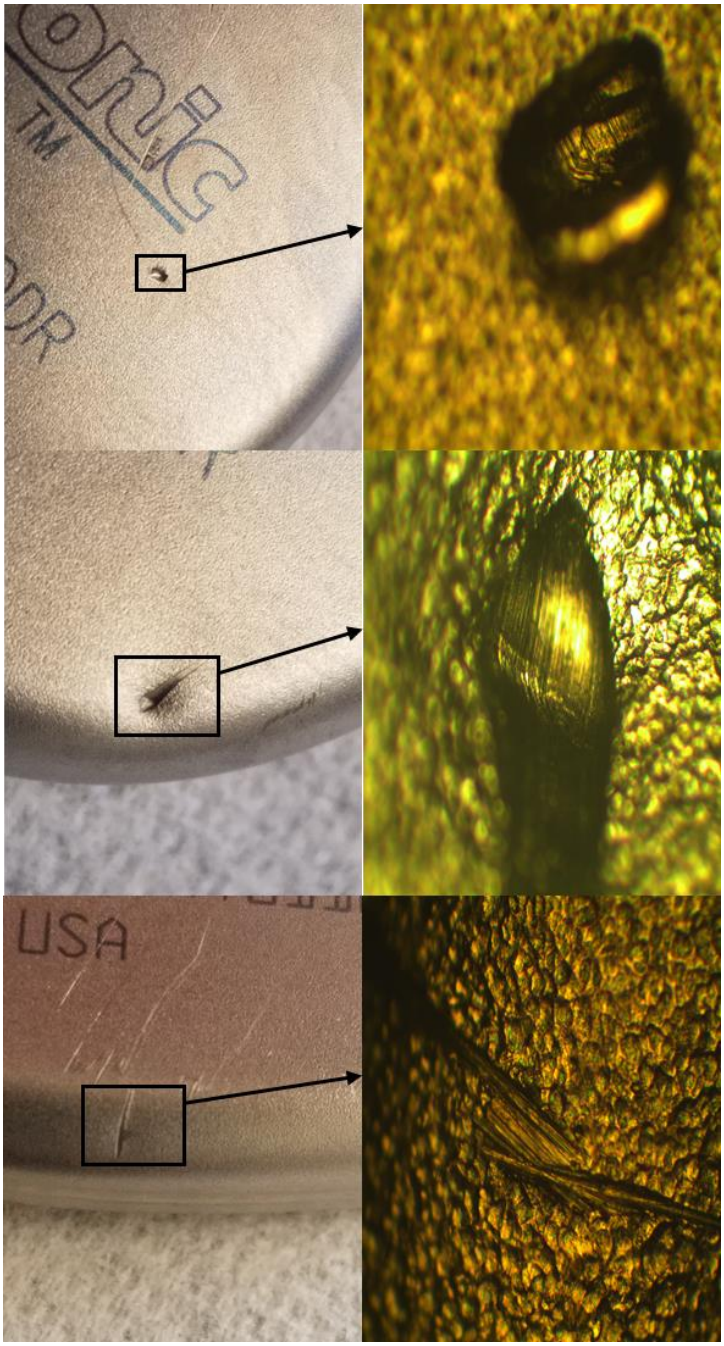

Figure 54 ADAPTA (PWB297611H

Figure 55 Adapta DR (NWB528525H)

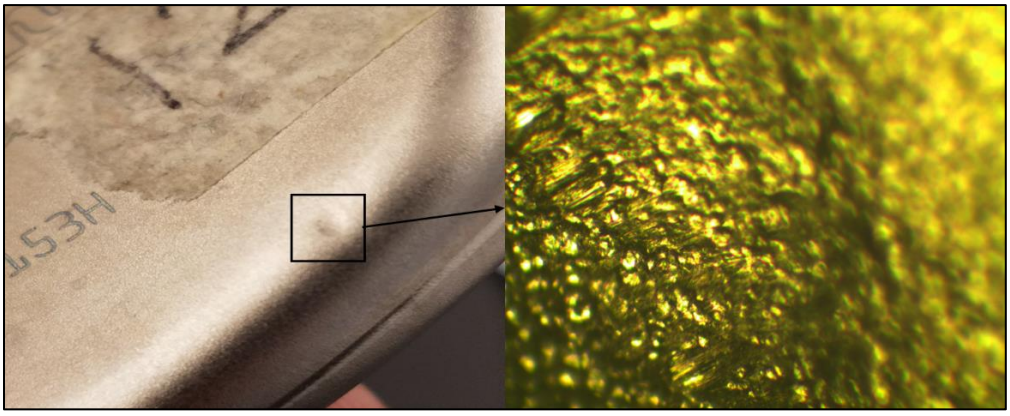

Figure 56 Adapta DR (PWB268153H)

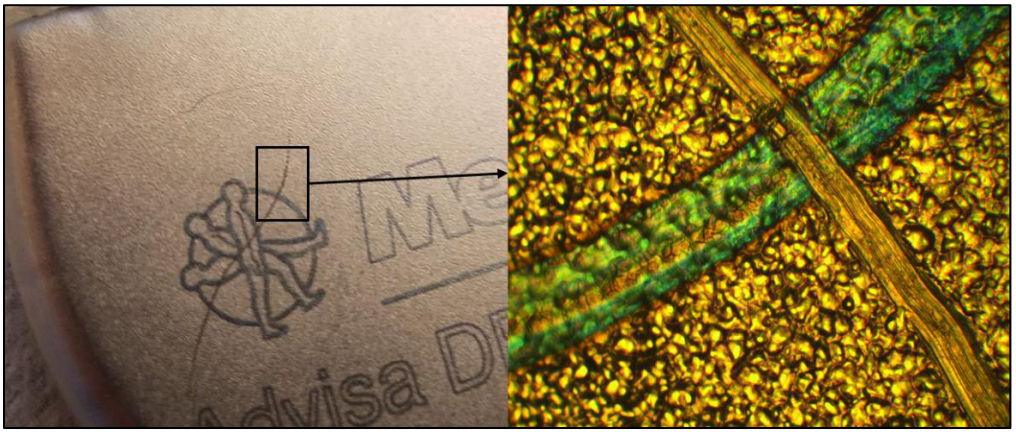

Figure 57 Advisa DR MRI (PAY287174H)

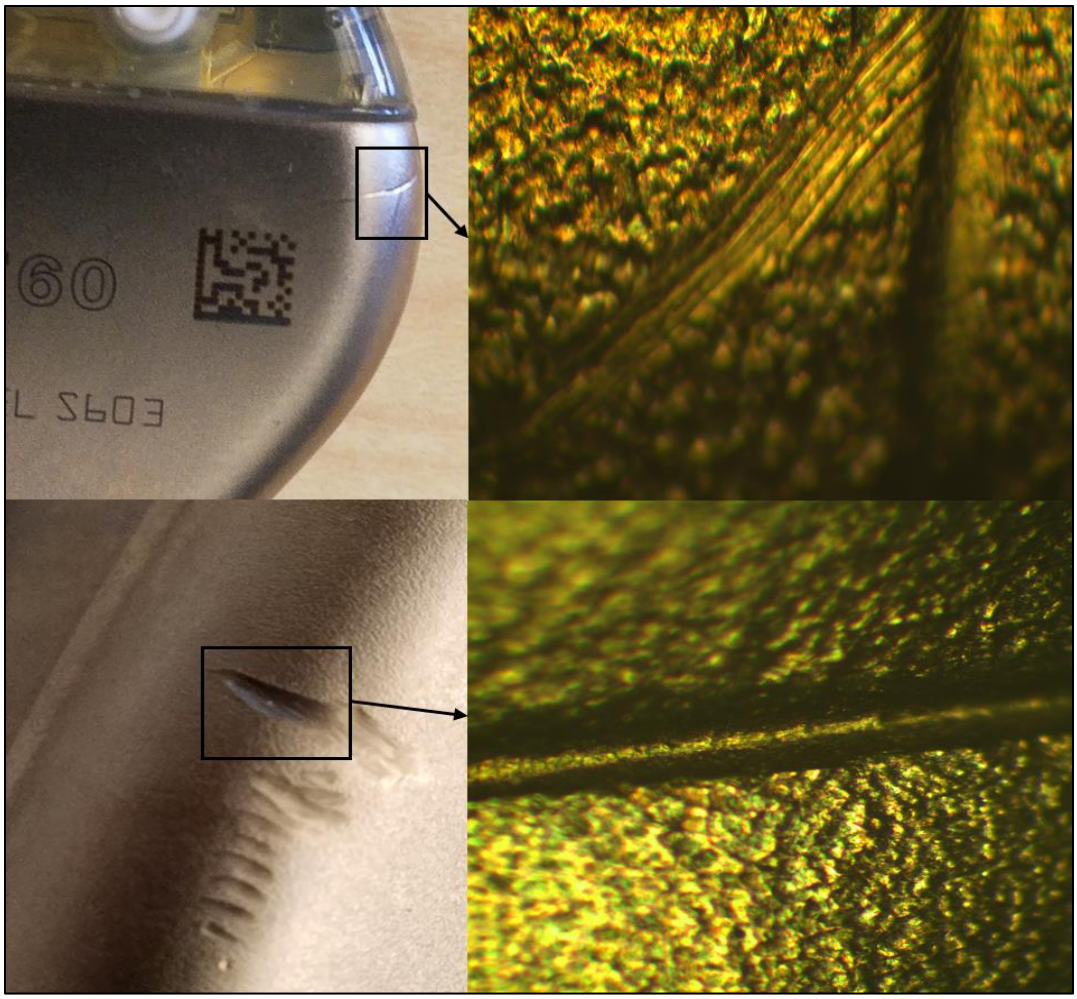

Figure 58 Altrua 60 (843287)

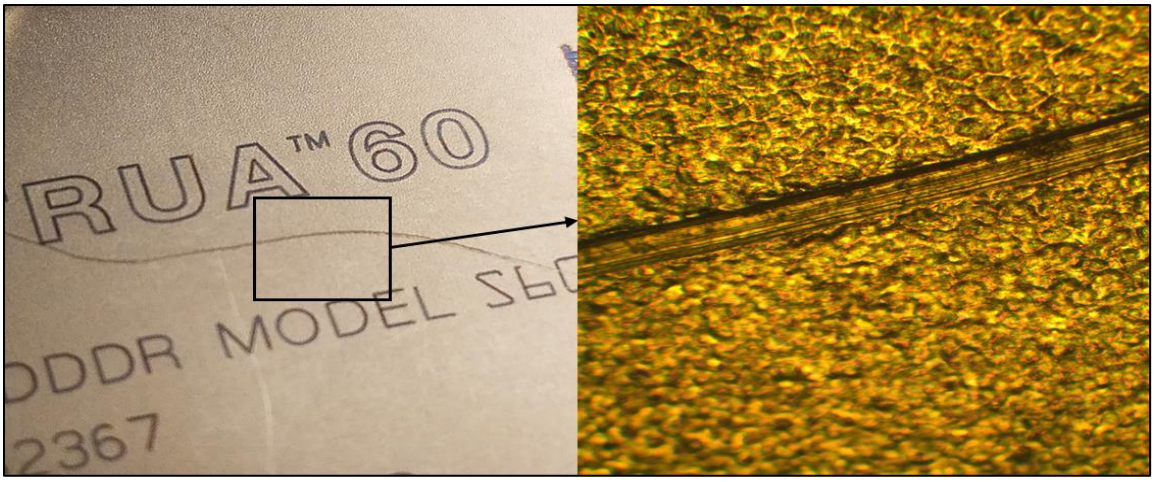

Figure 59 Altrua 60 DR (952367)

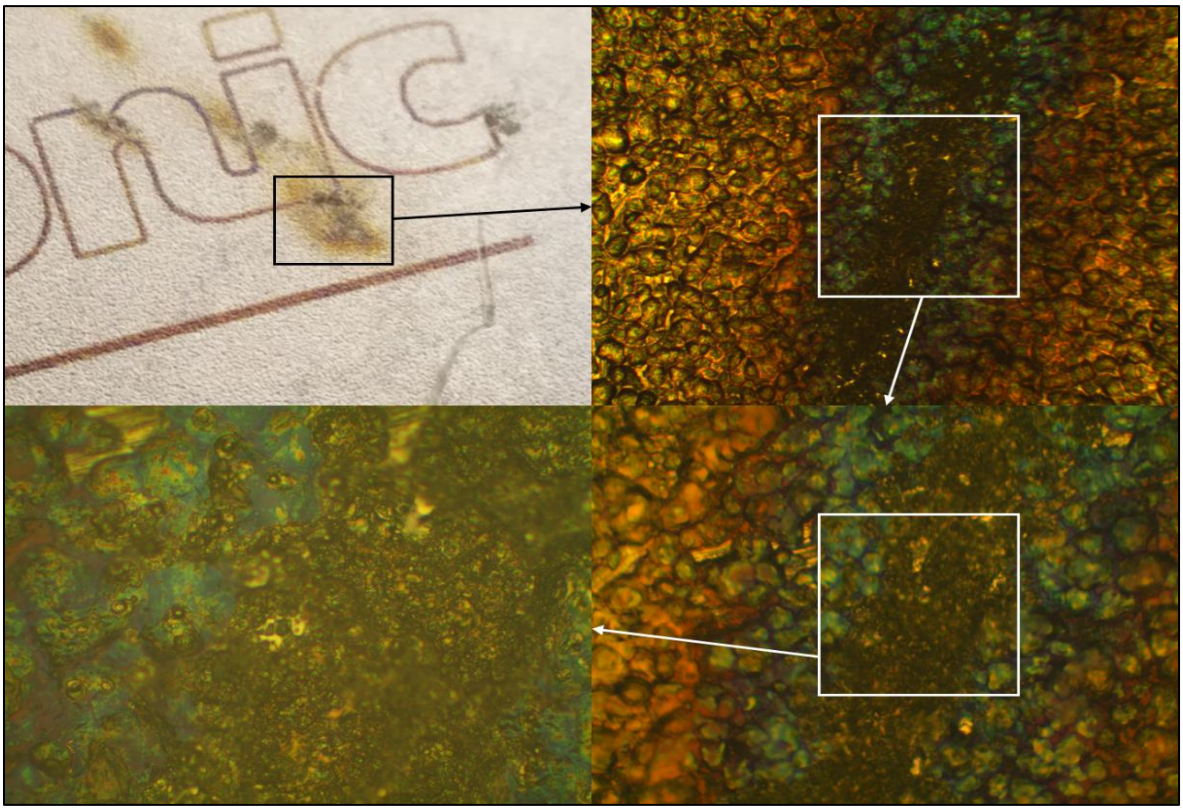

Figure 60 Entrust (PNR425289H)

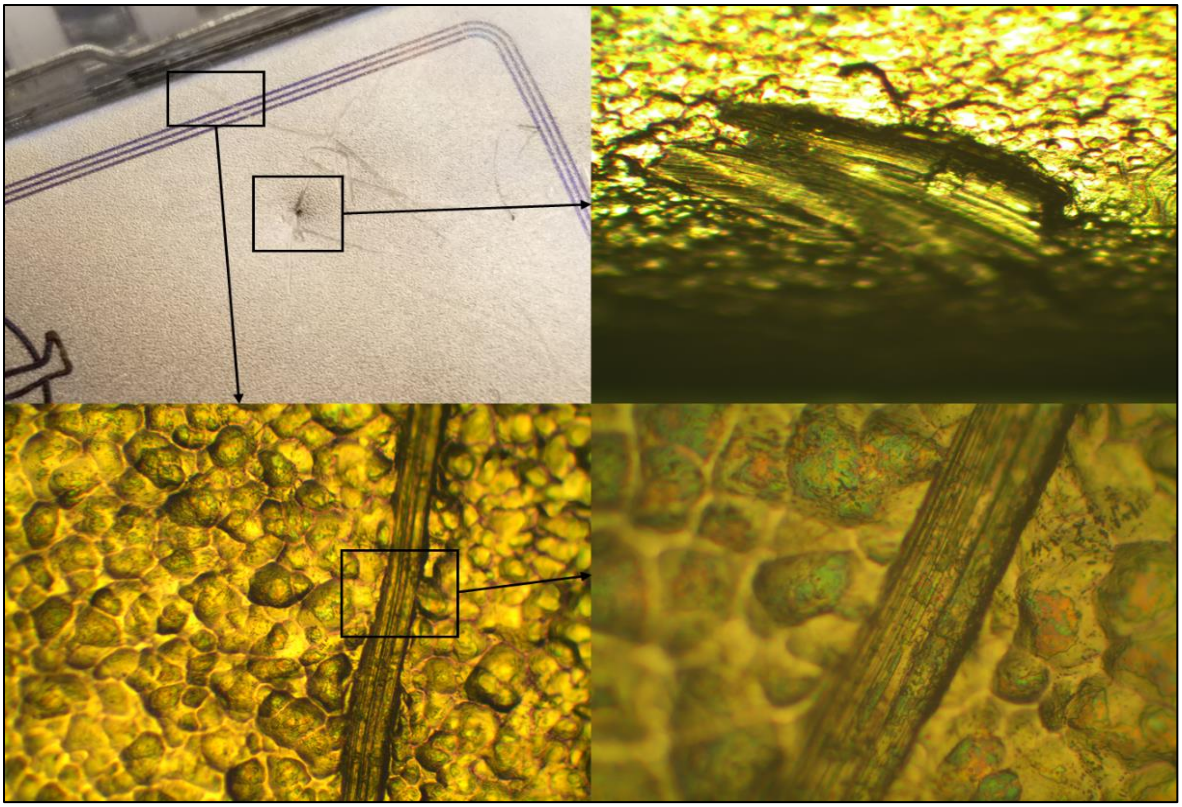

Figure 61 Evera XT VR (BWI214708H)

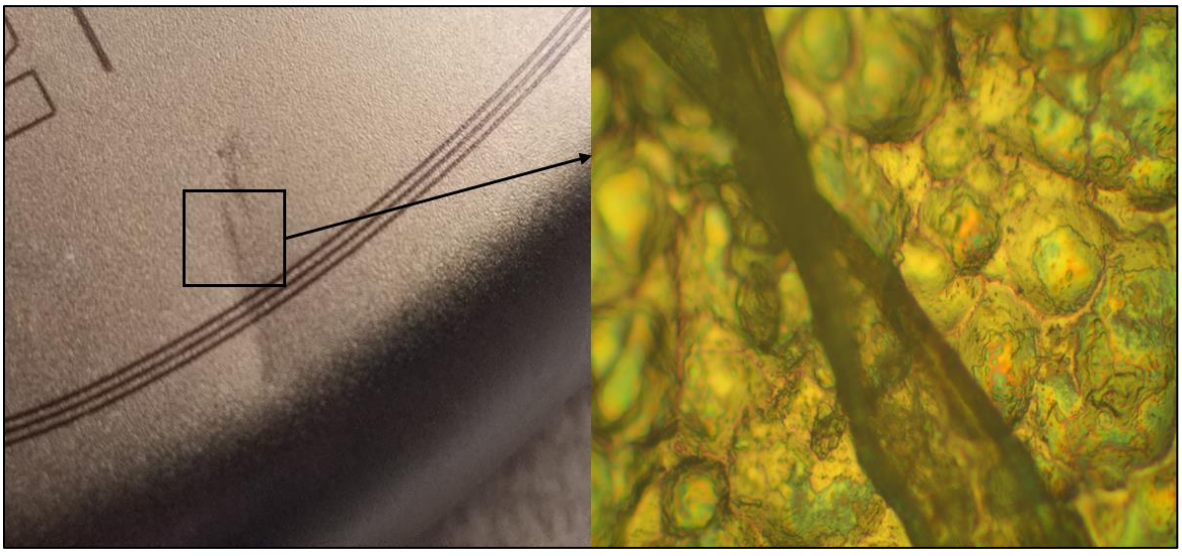

Figure 62 Evera XT VR (BWI215647H)

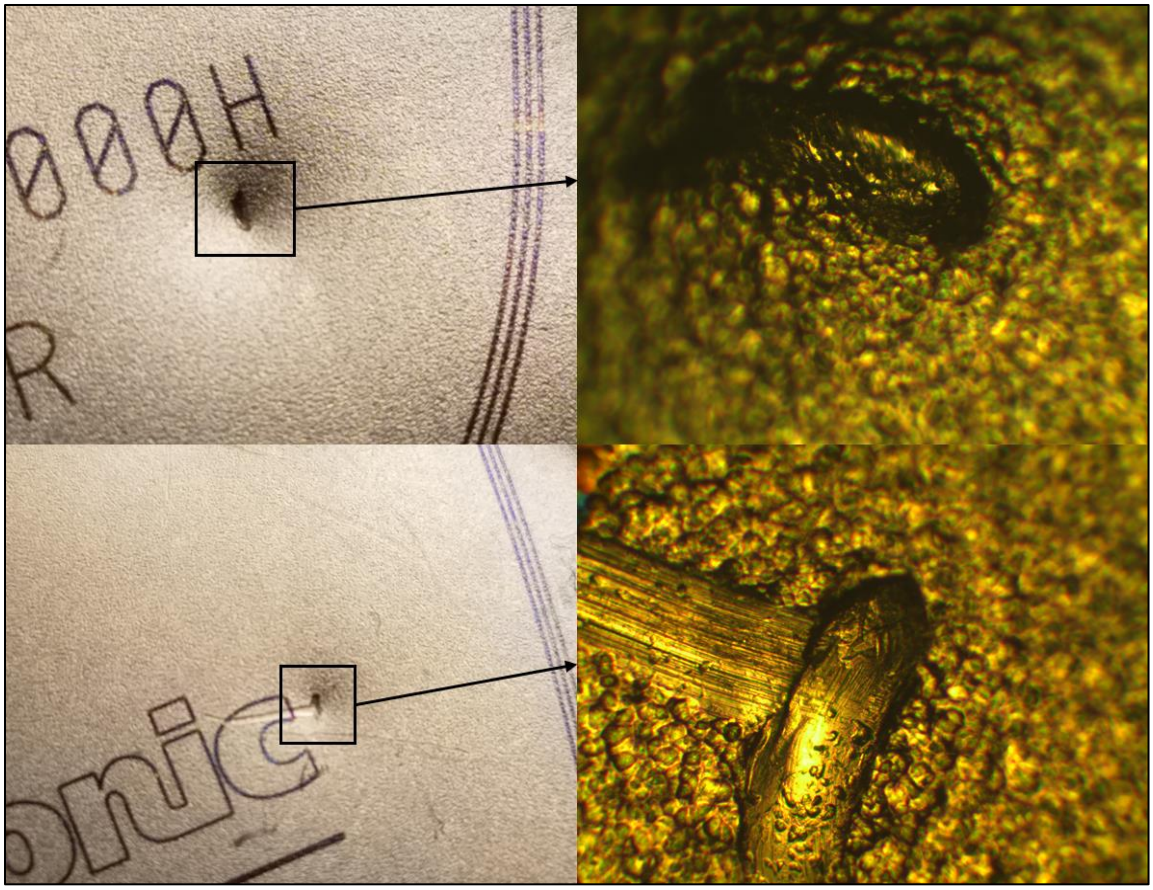

Figure 63 Evera XT DR (BWB207000H)

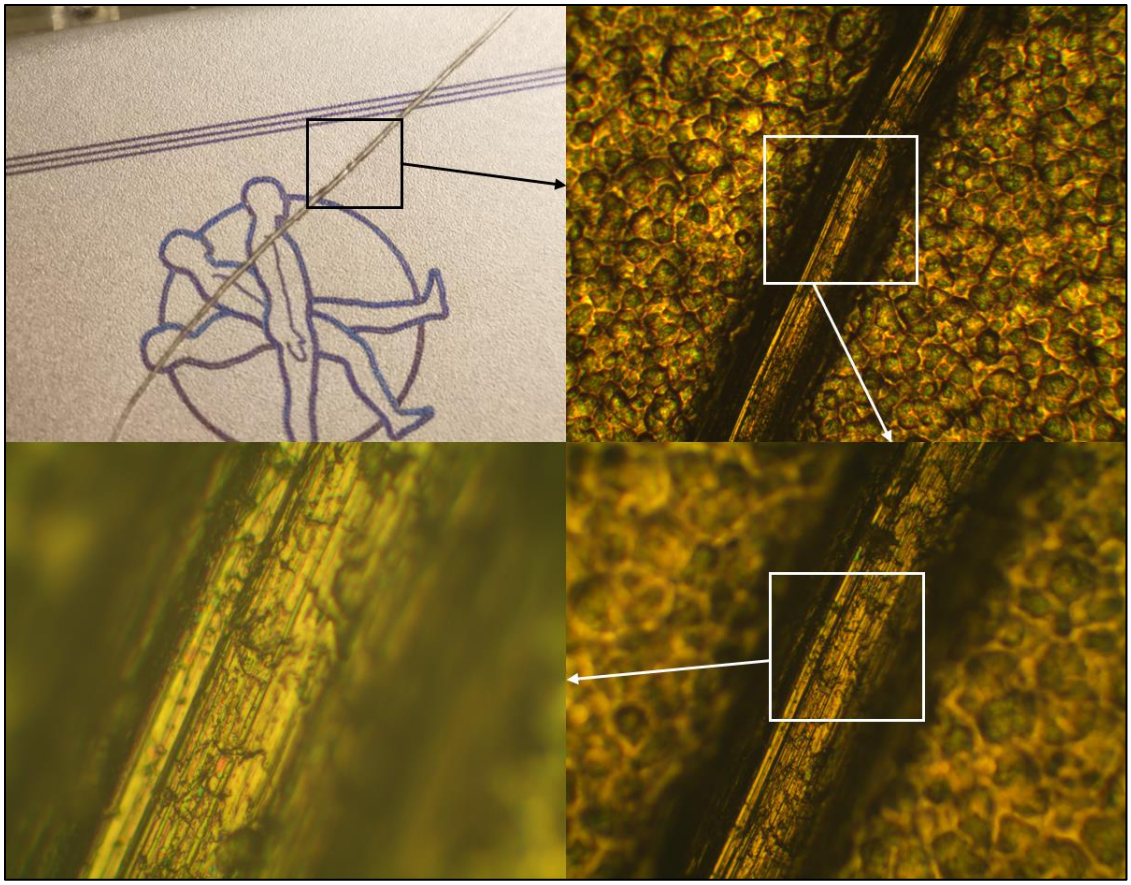

Figure 64 Maximo II (PZM201316H)

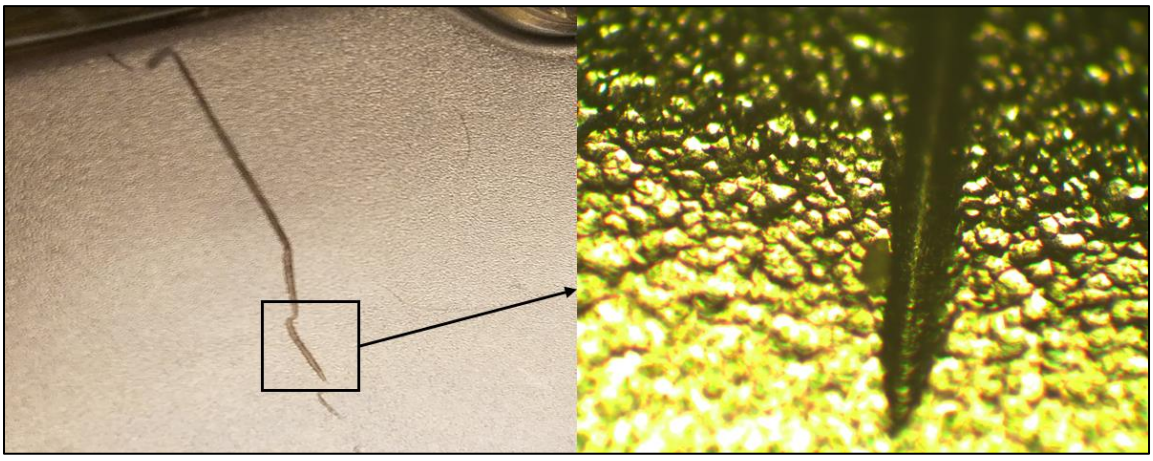

Figure 65 Protecta XT VR (PSA212334H)

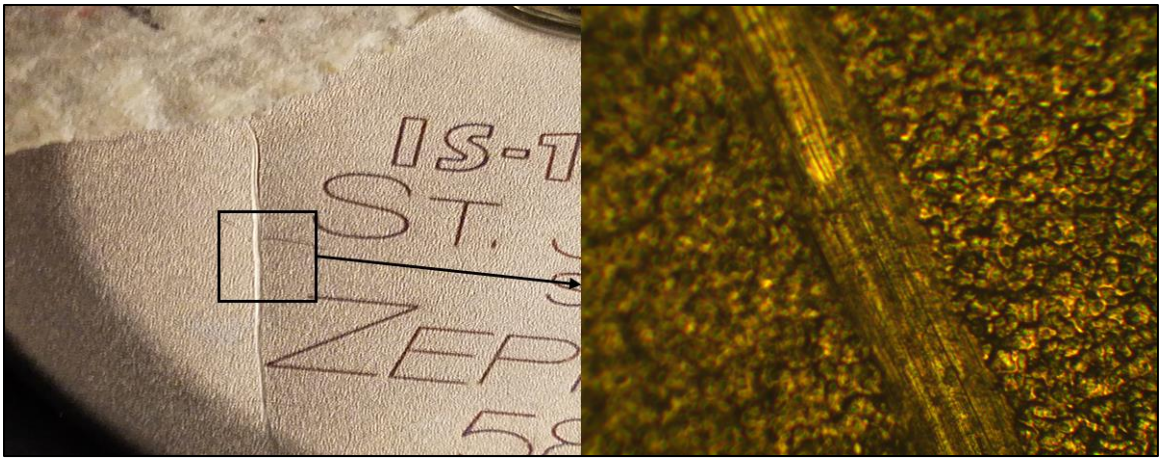

Figure 66 Zephyr XL DR (1294876)

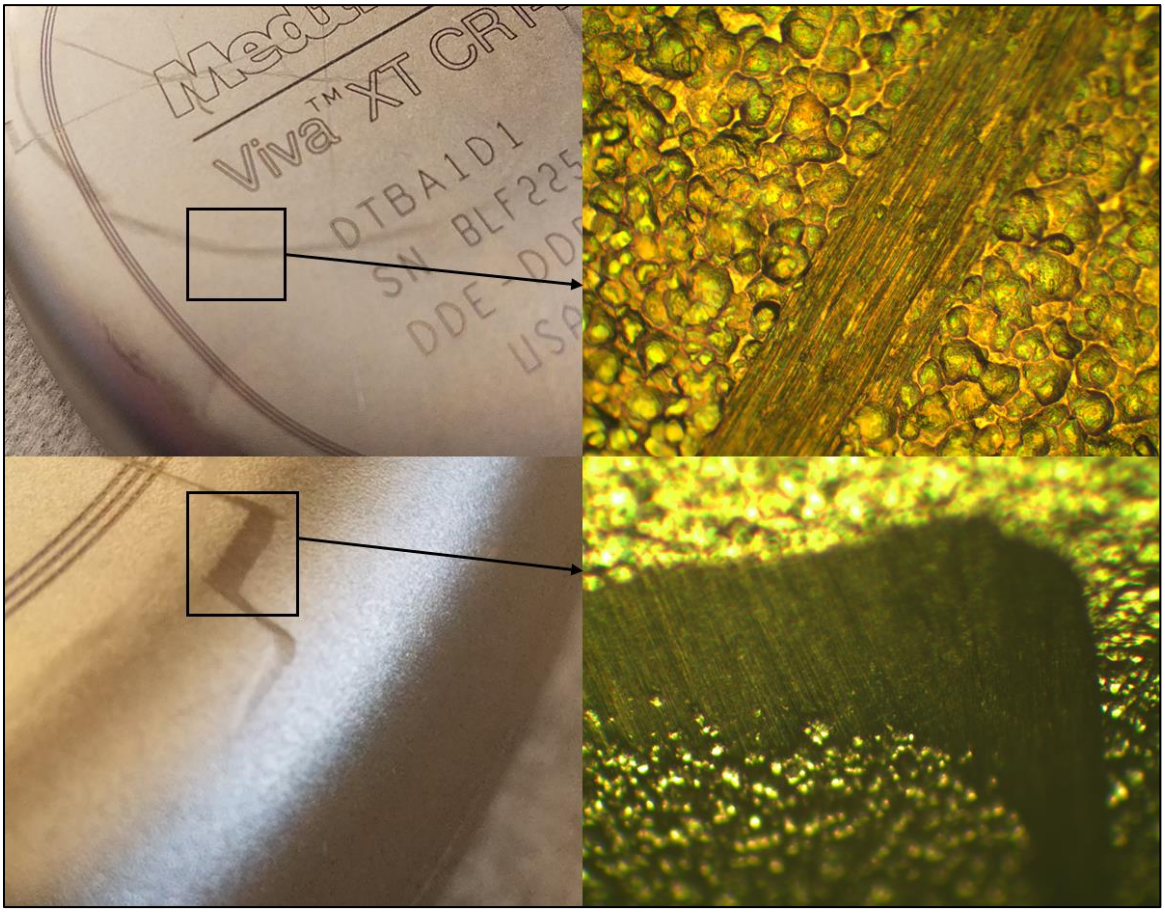

Figure 67 Viva XT CRT-D (BLF225581H)

APPENDIX IV LEAD

Figure 68 INGEVITY Pacing Lead (786132)

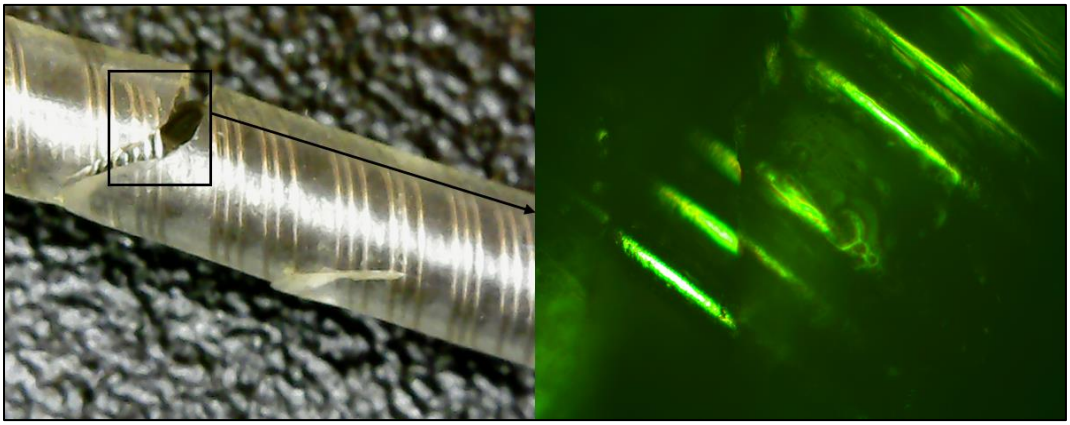

Figure 69 CapSureFix Pacing Lead (PJN1069523)

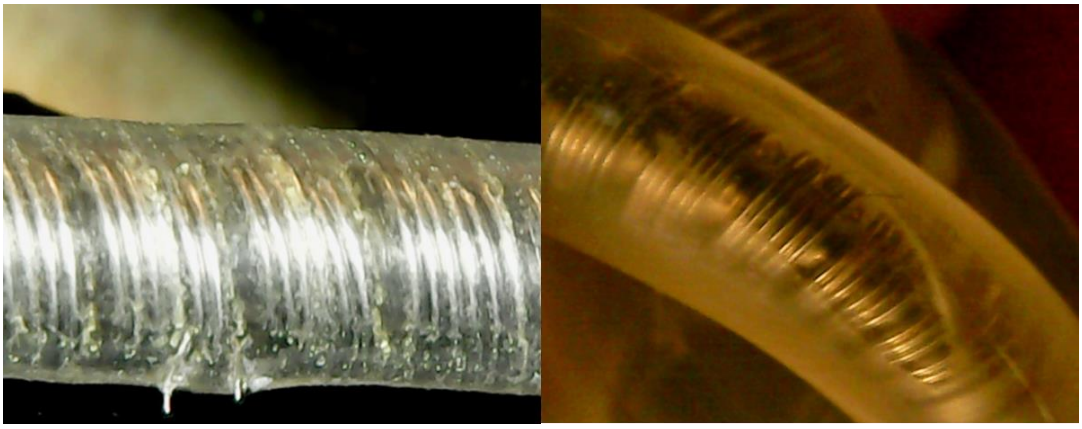

Figure 70 CapSure SP Pacing Lead (LAV070864V) left, Crystalline Pacing Lead (VMR021968V) right

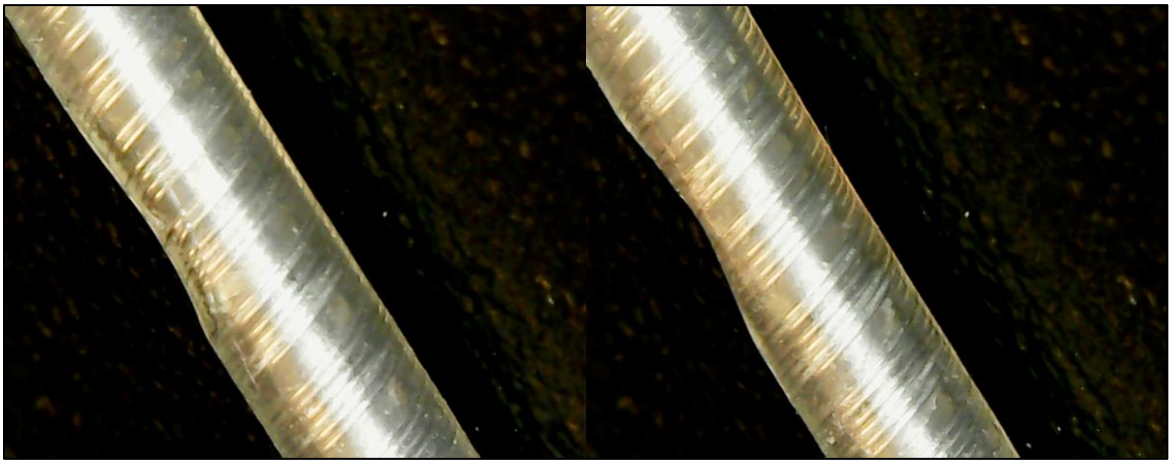

Figure 71 CapSureFix Pacing Lead (PJN2528024)

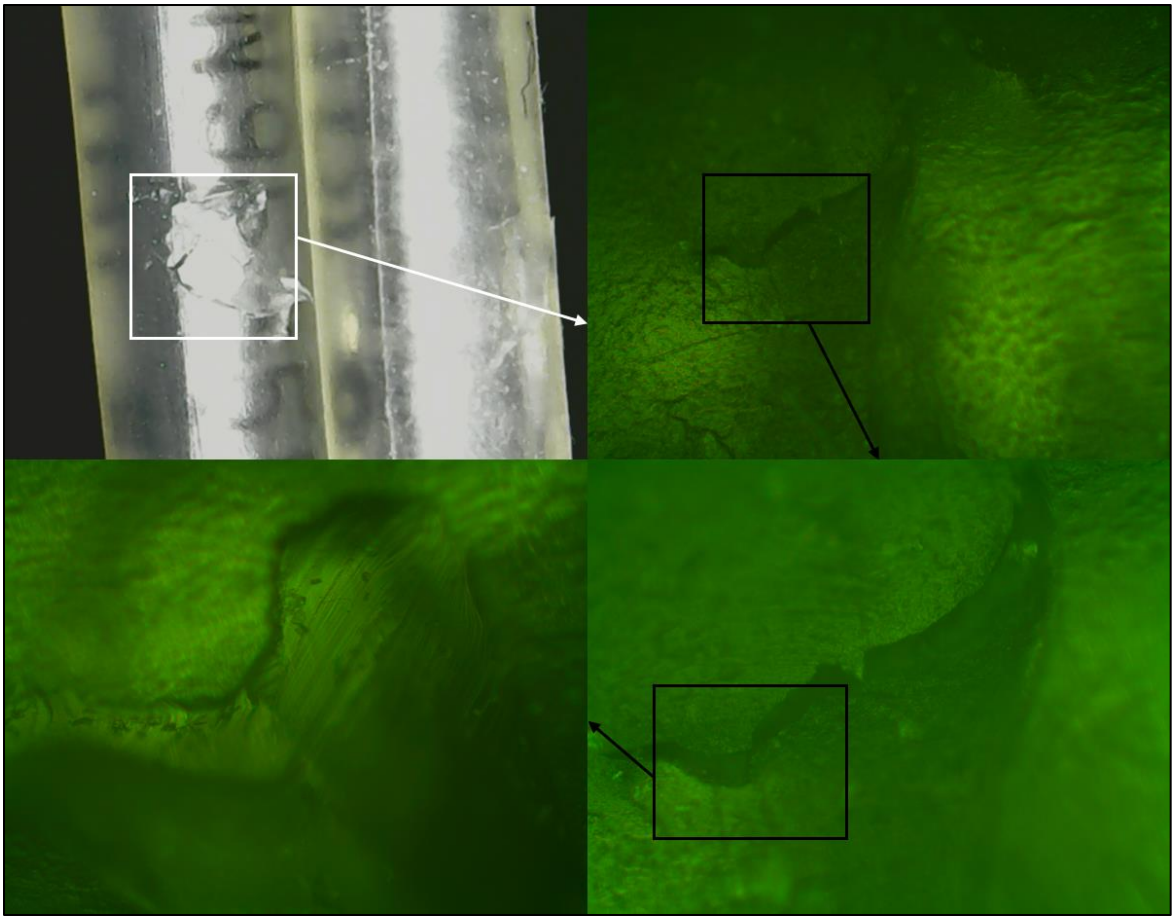

Figure 72 CapSureFix Pacing Lead (PJN956553V)

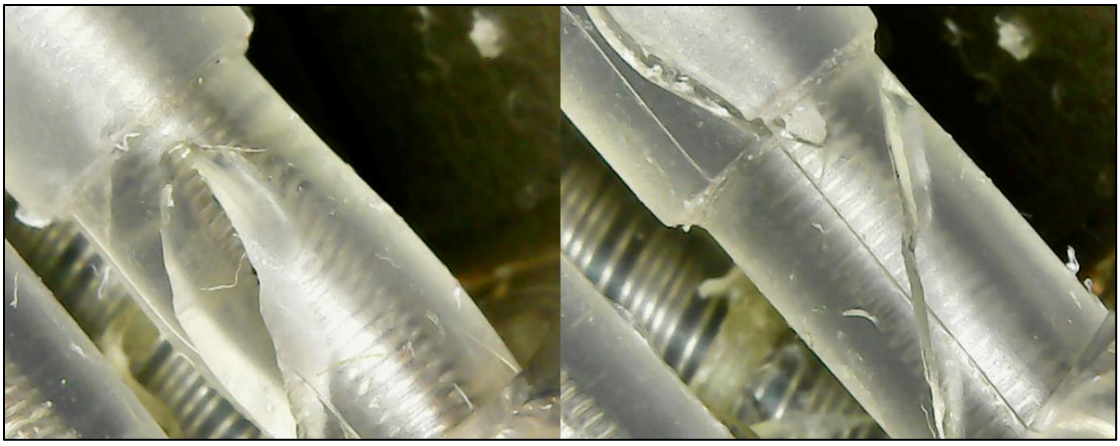

Figure 73 6949 Sprint Fidelis ICD Lead (LFJ217747)

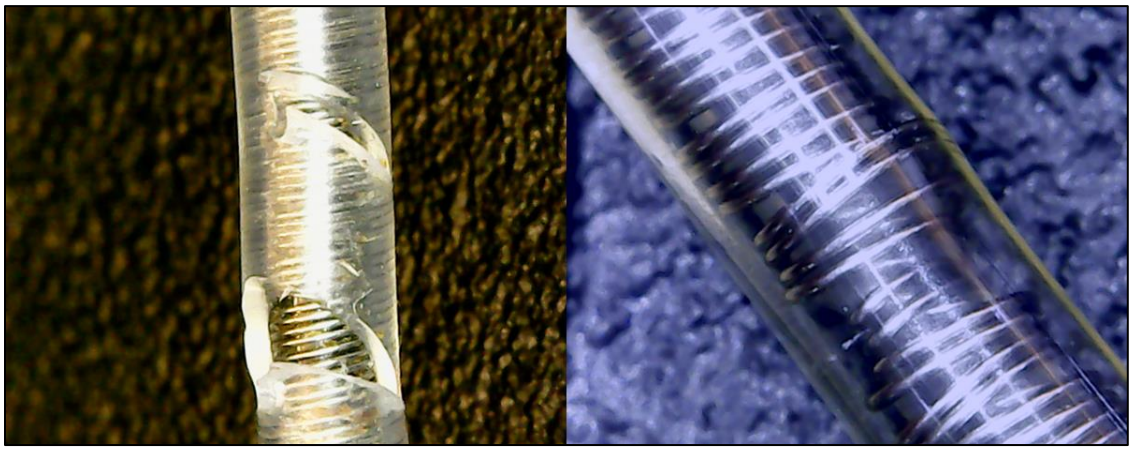

Figure 74 INGEVITY Pacing Lead

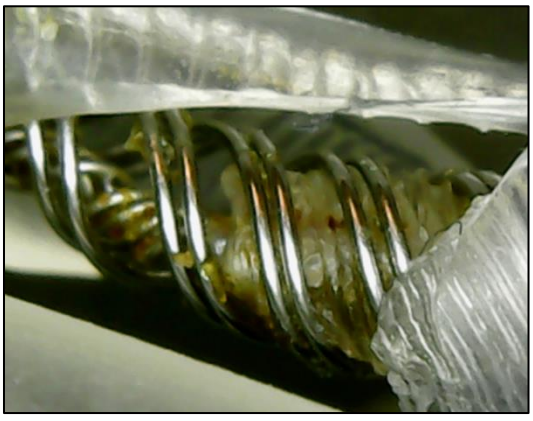

Figure 75 6947 Sprint Quattro Secure (TDG275450V)

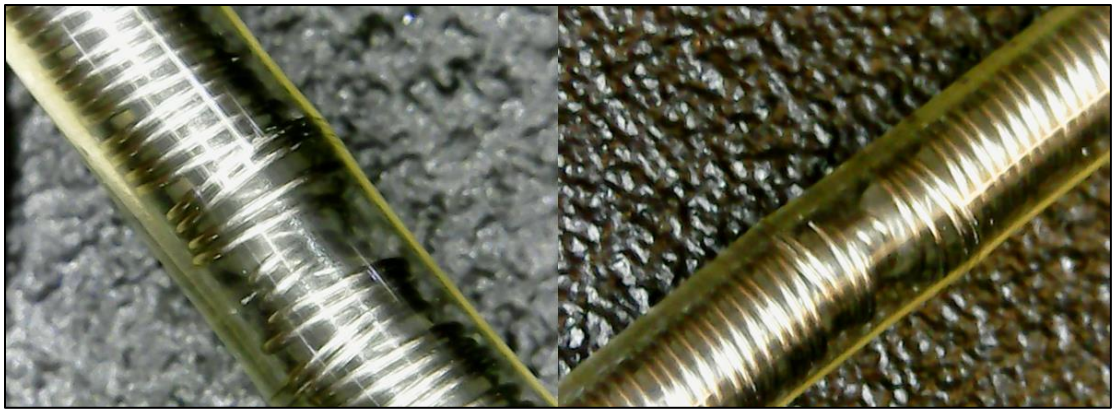

Figure 76 4194 Attain OTW Left-Heart Pacing (LFG204735V)

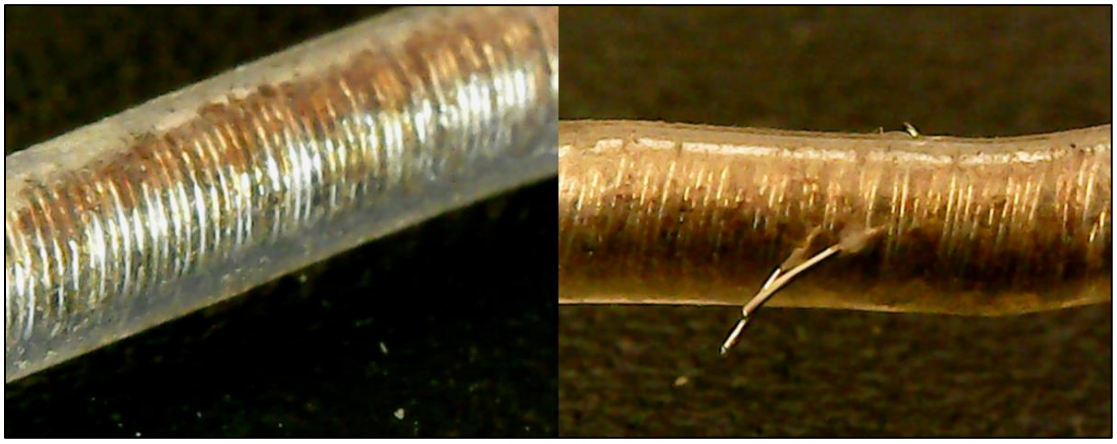

Figure 77 Tendril™ SDX Pacing Lead (DC23385)

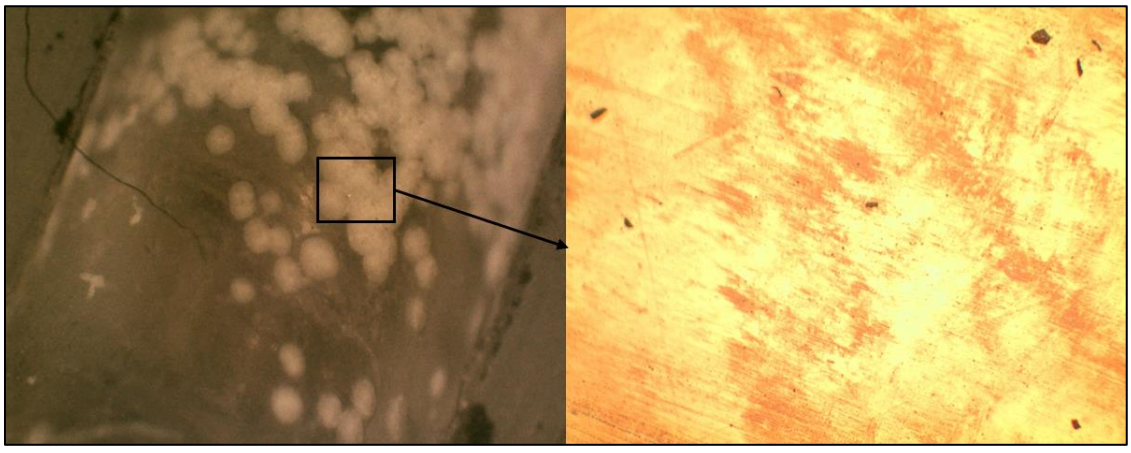

Figure 78 CapSure SP Pacing Lead (LAV091616V)

APPENDIX V MATLAB CODE

```
function createfigure(ZData1, YData1, XData1, VertexNormals1, XData2, YData2,
ZData2)
%CREATEFIGURE(ZDATA1, YDATA1, XDATA1, VERTEXNORMALS1, XDATA2, YDATA2, ZDATA2)
%  ZDATA1:  surface zdata
%  YDATA1:  surface ydata
%  XDATA1:  surface xdata
%  VERTEXNORMALS1:  surface vertexnormals
%  XDATA2:  line xdata
%  YDATA2:  line ydata
%  ZDATA2:  line zdata

%  Auto-generated by MATLAB on 31-May-2018 19:56:07

% Create figure
figure1 = figure('Tag','Print CFTOOL to Figure',...
    'Color',[0.941176470588235 0.941176470588235 0.941176470588235],...
    'OuterPosition',[1 1 1536 467.2]);

% Create axes
axes1 = axes('Parent',figure1,'Tag','sftool surface axes');
hold(axes1,'on');

% Create surface
surface('Parent',axes1,'ZData',ZData1,'YData',YData1,'XData',XData1,...
    'DisplayName','untitled fit 1',...
    'VertexNormals',VertexNormals1,...
    'EdgeAlpha',0.3,...
    'CData',ZData1);

% Create line
line(XData2,YData2,ZData2,'Parent',axes1,...
    'DisplayName','Impedance vs. Sensitivity, PulseWidth',...
    'MarkerFaceColor',[0 0 0],...
    'MarkerEdgeColor',[0 0 0],...
    'MarkerSize',3,...
    'Marker','o',...
    'LineStyle','none');

% Create xlabel
xlabel('Sensitivity');

% Create zlabel
```

```
zlabel('Impedance');

% Create ylabel
ylabel('PulseWidth');

% Uncomment the following line to preserve the X-limits of the axes
% xlim(axes1,[0.035 5.865]);
% Uncomment the following line to preserve the Y-limits of the axes
% ylim(axes1,[0.265 1.035]);
% Uncomment the following line to preserve the Z-limits of the axes
% zlim(axes1,[293.75 981.25]);
view(axes1,[-23.4200000000001 14]);
box(axes1,'on');
grid(axes1,'on');
% Create colorbar
colorbar('peer',axes1);
```

Survival Probability for devices in general

```
function [pd1,pd2] = createFit(BSC,MDT)
%CREATEFIT    Create plot of datasets and fits
%   [PD1,PD2] = CREATEFIT(BSC,MDT)
%   Creates a plot, similar to the plot in the main distribution fitter
%   window, using the data that you provide as input.  You can
%   apply this function to the same data you used with dfittool
%   or with different data.  You may want to edit the function to
%   customize the code and this help message.
%
%   Number of datasets:  2
%   Number of fits:  2
%
%   See also FITDIST.

% This function was automatically generated on 09-Jul-2018 23:21:39

% Output fitted probablility distributions: PD1,PD2

% Data from dataset "BSC data":
%    Y = BSC

% Data from dataset "MDT data":
%    Y = MDT

% Force all inputs to be column vectors
```

```
BSC = BSC(:);
MDT = MDT(:);

% Prepare figure
clf;
hold on;
LegHandles = []; LegText = {};


% --- Plot data originally in dataset "BSC data"
[CdfY,CdfX] = ecdf(BSC,'Function','survivor');  % compute empirical function
hLine = stairs(CdfX,CdfY,'Color',[0.333333 0 0.666667],'LineStyle','-',
'LineWidth',1);
xlabel('Data');
ylabel('Survivor function')
LegHandles(end+1) = hLine;
LegText{end+1} = 'BSC data';

% --- Plot data originally in dataset "MDT data"
[CdfY,CdfX] = ecdf(MDT,'Function','survivor');  % compute empirical function
hLine = stairs(CdfX,CdfY,'Color',[0.333333 0.666667 0],'LineStyle','-',
'LineWidth',1);
xlabel('Data');
ylabel('Survivor function')
LegHandles(end+1) = hLine;
LegText{end+1} = 'MDT data';

% Create grid where function will be computed
XLim = get(gca,'XLim');
XLim = XLim + [-1 1] * 0.01 * diff(XLim);
XGrid = linspace(XLim(1),XLim(2),100);


% --- Create fit "fit 1"

% Fit this distribution to get parameter values
% To use parameter estimates from the original fit:
%     pd1 = ProbDistUnivParam('normal',[ 2.904545454545, 1.993546405963])
pd1 = fitdist(BSC, 'normal');
% This fit does not appear on the plot

% --- Create fit "fit 2"

% Fit this distribution to get parameter values
% To use parameter estimates from the original fit:
```

```
%     pd2 = ProbDistUnivParam('normal',[ 2.433333333333, 1.888042870899])
pd2 = fitdist(MDT, 'normal');
% This fit does not appear on the plot

% Adjust figure
box on;
hold off;

% Create legend from accumulated handles and labels
hLegend = legend(LegHandles,LegText,'Orientation', 'vertical', 'FontSize', 9,
'Location', 'northeast');
set(hLegend,'Interpreter','none');
```

Survival probability for Pacemakers

```
function createfigure1(X1, Y1, X2, Y2)
%CREATEFIGURE1(X1, Y1, X2, Y2)
%  X1:  vector of x data
%  Y1:  vector of y data
%  X2:  vector of x data
%  Y2:  vector of y data

%  Auto-generated by MATLAB on 04-Feb-2019 20:16:19

% Create figure
figure1 = figure;

% Create axes
axes1 = axes('Parent',figure1,...
    'ColorOrder',[1 0 0;0 0 1;0.666666666666667 0.333333333333333
0;0.333333333333333 0.333333333333333 0.333333333333333;1 0 1;1 1 0;1
0.666666666666667 0.333333333333333;0.666666666666667 0.666666666666667
0.666666666666667;0.666666666666667 0.333333333333333 1;0 0.666666666666667
0.333333333333333;0.666666666666667 0 0.333333333333333;1 0.333333333333333
0.666666666666667;0 1 0;0.333333333333333 0.666666666666667 1;0.666666666666667
1 0.333333333333333;0.333333333333333 0 0.666666666666667;0 0.333333333333333
0.666666666666667;0.333333333333333 1 0.666666666666667;0 0 0;0.333333333333333
0.666666666666667 0;0.333333333333333 0 0.666666666666667],...
    'Tag','main');
hold(axes1,'on');

% Create plot
plot(X1,Y1,'DisplayName','BSC Pacemaker (n=8)','Tag','dfdata',...
    'MarkerIndices',[1 2 3 4 5 6 7 8 9 10 11 12 13 14],...
```

```
    'LineWidth',1,...
    'Color',[0 0 1]);

% Create plot
plot(X2,Y2,'ZDataSource','','DisplayName','MDT Pacemaker (n=23)',...
    'Tag','dfdata',...
    'LineWidth',1,...
    'Color',[0 0 0]);

% Create xlabel
xlabel('Data');

% Create ylabel
ylabel('Survivor function');

% Uncomment the following line to preserve the X-limits of the axes
% xlim(axes1,[0.0675 8.4825]);
% Uncomment the following line to preserve the Y-limits of the axes
% ylim(axes1,[0 1]);
% Uncomment the following line to preserve the Z-limits of the axes
% zlim(axes1,[0 1]);
box(axes1,'on');
% Set the remaining axes properties
set(axes1,'OuterPosition',[-0.00178571428571429 -0.00238095238095238 1 1]);
% Create legend
legend1 = legend(axes1,'show');
set(legend1,'Interpreter','none');
```

Survival probability for leads in general

```
function createfigure2(X1, Y1, X2, Y2, X3, Y3)
%CREATEFIGURE2(X1, Y1, X2, Y2, X3, Y3)
%  X1:  vector of x data
%  Y1:  vector of y data
%  X2:  vector of x data
%  Y2:  vector of y data
%  X3:  vector of x data
%  Y3:  vector of y data

%  Auto-generated by MATLAB on 04-Feb-2019 20:22:45

% Create figure
```

```
figure1 = figure;

% Create axes
axes1 = axes('Parent',figure1,...
    'ColorOrder',[1 0 0;0 0 1;0.666666666666667 0.333333333333333
0;0.333333333333333 0.333333333333333 0.333333333333333;1 0 1;1 1 0;1
0.666666666666667 0.333333333333333;0.666666666666667 0.666666666666667
0.666666666666667;0.666666666666667 0.333333333333333 1;0 0.666666666666667
0.333333333333333;0.666666666666667 0 0.333333333333333;1 0.333333333333333
0.666666666666667;0 1 0;0.333333333333333 0.666666666666667 1;0.666666666666667
1 0.333333333333333;0.333333333333333 0 0.666666666666667;0 0.333333333333333
0.666666666666667;0.333333333333333 1 0.666666666666667;0 0 0;0.333333333333333
0.666666666666667 0;0.333333333333333 0 0.666666666666667],...
    'Tag','main');
hold(axes1,'on');

% Create plot
plot(X1,Y1,'DisplayName','BSC Pacing (n=9)','Tag','dfdata',...
    'MarkerIndices',[1 2 3 4 5 6 7 8 9 10 11 12 13 14],...
    'LineWidth',1,...
    'Color',[0 0.333333333333333 0.666666666666667]);

% Create plot
plot(X2,Y2,'DisplayName','MDT ICD (n=12)','Tag','dfdata',...
    'MarkerIndices',[1 2 3 4 5 6 7 8 9 10 11 12 13 14 15 16 17 18 19 20 21 22
23 24],...
    'LineWidth',1,...
    'Color',[0.666666666666667 1 0.333333333333333]);

% Create plot
plot(X3,Y3,'DisplayName','MDT Pacing (n=53)','Tag','dfdata',...
    'MarkerIndices',[1 2 3 4 5 6 7 8 9 10 11 12 13 14 15 16 17 18 19 20 21 22
23 24 25 26 27 28 29 30 31 32 33 34 35 36 37 38 39 40 41 42 43 44 45 46 47 48
49 50 51 52 53 54],...
    'LineWidth',1,...
    'Color',[0.333333333333333 0.666666666666667 1]);

% Create xlabel
xlabel('Data');

% Create ylabel
ylabel('Survivor function');

% Uncomment the following line to preserve the X-limits of the axes
% xlim(axes1,[0.0551999999999999 190.2648]);
```

```
% Uncomment the following line to preserve the Y-limits of the axes
% ylim(axes1,[0 1]);
% Uncomment the following line to preserve the Z-limits of the axes
% zlim(axes1,[0 1]);
box(axes1,'on');
% Set the remaining axes properties
set(axes1,'OuterPosition',[-0.00178571428571429 -0.00238095238095238 1 1]);
% Create legend
legend1 = legend(axes1,'show');
set(legend1,'Interpreter','none');
```

ICD leads survival probability

```
function createfigure4(X1, Y1, X2, Y2)
%CREATEFIGURE4(X1, Y1, X2, Y2)
%  X1:  vector of x data
%  Y1:  vector of y data
%  X2:  vector of x data
%  Y2:  vector of y data

%  Auto-generated by MATLAB on 04-Feb-2019 20:34:24

% Create figure
figure1 = figure;

% Create axes
axes1 = axes('Parent',figure1,...
    'ColorOrder',[1 0 0;0 0 1;0.666666666666667 0.333333333333333
0;0.333333333333333 0.333333333333333 0.333333333333333;1 0 1;1 1 0;1
0.666666666666667 0.333333333333333;0.666666666666667 0.666666666666667
0.666666666666667;0.666666666666667 0.333333333333333 1;0 0.666666666666667
0.333333333333333;0.666666666666667 0 0.333333333333333;1 0.333333333333333
0.666666666666667;0 1 0;0.333333333333333 0.666666666666667 1;0.666666666666667
1 0.333333333333333;0.333333333333333 0 0.666666666666667;0 0.333333333333333
0.666666666666667;0.333333333333333 1 0.666666666666667;0 0 0;0.333333333333333
0.666666666666667 0;0.333333333333333 0 0.666666666666667],...
    'Tag','main');
hold(axes1,'on');

% Create plot
plot(X1,Y1,'DisplayName','MDT ICD Leads (n=12)','Tag','dfdata',...
    'MarkerIndices',[1 2 3 4 5 6 7 8 9 10 11 12 13 14 15 16 17 18 19 20 21 22
23 24],...
    'LineWidth',1,...
```

```
    'Color',[0 0.666666666666667 0.333333333333333]);

% Create plot
plot(X2,Y2,'DisplayName','BSC ICD Leads (n=3)','Tag','dfdata',...
    'MarkerIndices',[1 2 3 4 5 6],...
    'LineWidth',1,...
    'Color',[0.666666666666667 0.333333333333333 1]);

% Create xlabel
xlabel('Months After Implant');

% Create ylabel
ylabel('Survivor function');

% Uncomment the following line to preserve the X-limits of the axes
% xlim(axes1,[4.602 147.198]);
% Uncomment the following line to preserve the Y-limits of the axes
% ylim(axes1,[0 1]);
% Uncomment the following line to preserve the Z-limits of the axes
% zlim(axes1,[0 1]);
box(axes1,'on');
% Set the remaining axes properties
set(axes1,'OuterPosition',[-0.00178571428571429 -0.00238095238095238 1 1]);
% Create legend
legend1 = legend(axes1,'show');
set(legend1,'Interpreter','none');
```

Pacing leads survival probability

```
function createfigure3(X1, Y1, X2, Y2)
%CREATEFIGURE3(X1, Y1, X2, Y2)
%  X1:  vector of x data
%  Y1:  vector of y data
%  X2:  vector of x data
%  Y2:  vector of y data

%  Auto-generated by MATLAB on 04-Feb-2019 20:27:49

% Create figure
figure1 = figure;

% Create axes
axes1 = axes('Parent',figure1,...
```

```
    'ColorOrder',[1 0 0;0 0 1;0.666666666666667 0.333333333333333
0;0.333333333333333 0.333333333333333 0.333333333333333;1 0 1;1 1 0;1
0.666666666666667 0.333333333333333;0.666666666666667 0.666666666666667
0.666666666666667;0.666666666666667 0.333333333333333 1;0 0.666666666666667
0.333333333333333;0.666666666666667 0 0.333333333333333;1 0.333333333333333
0.666666666666667;0 1 0;0.333333333333333 0.666666666666667 1;0.666666666666667
1 0.333333333333333;0.333333333333333 0 0.666666666666667;0 0.333333333333333
0.666666666666667;0.333333333333333 1 0.666666666666667;0 0 0;0.333333333333333
0.666666666666667 0;0.333333333333333 0 0.666666666666667],...
    'Tag','main');
hold(axes1,'on');

% Create plot
plot(X1,Y1,'DisplayName','MDT Pacing (n=53)','Tag','dfdata',...
    'MarkerIndices',[1 2 3 4 5 6 7 8 9 10 11 12 13 14 15 16 17 18 19 20 21 22
23 24 25 26 27 28 29 30 31 32 33 34 35 36 37 38 39 40 41 42 43 44 45 46 47 48
49 50 51 52 53 54],...
    'LineWidth',1,...
    'Color',[0 0 0]);

% Create plot
plot(X2,Y2,'DisplayName','BSC Pacing (n=9)','Tag','dfdata',...
    'MarkerIndices',[1 2 3 4 5 6 7 8 9 10 11 12 13 14],...
    'LineWidth',1,...
    'Color',[0 0.333333333333333 0.666666666666667]);

% Create xlabel
xlabel('Months After Implant');

% Create ylabel
ylabel('Survivor function');

% Uncomment the following line to preserve the X-limits of the axes
% xlim(axes1,[0.0551999999999999 190.2648]);
% Uncomment the following line to preserve the Y-limits of the axes
% ylim(axes1,[0 1]);
% Uncomment the following line to preserve the Z-limits of the axes
% zlim(axes1,[0 1]);
box(axes1,'on');
% Set the remaining axes properties
set(axes1,'OuterPosition',[-0.00178571428571429 -0.00238095238095238 1 1]);
% Create legend
legend1 = legend(axes1,'show');
set(legend1,'Interpreter','none');
```